

© 2015

Joseph Wahler

ALL RIGHTS RESERVED

**INHIBITION OF BREAST CANCER PROGRESSION WITH VITAMIN D
COMPOUNDS**

by

JOSEPH WAHLER

A dissertation submitted to the

Graduate School – New Brunswick

Rutgers, The State University of New Jersey

And

The Graduate School of Biomedical Sciences

in partial fulfillment of the requirements

for the degree of

Doctor of Philosophy

Joint Graduate Program of Cellular and Molecular Pharmacology

written under the direction of

Professor Nanjoo Suh

and approved by

New Brunswick, New Jersey

OCTOBER, 2015

ABSTRACT OF THE DISSERTATION

Inhibition of Breast Cancer Progression with Vitamin D compounds

By: JOSEPH WAHLER

Dissertation Director:

Dr. Nanjoo Suh

Early epidemiological studies have shown an inverse correlation of increased vitamin D₃ to breast cancer. Since this discovery, many studies have linked 1,25-dihydroxyvitamin D₃, the active metabolite of vitamin D, and vitamin D analogs to decreased cell proliferation, invasion, and metastasis. The pharmacological dose of 1,25(OH)₂D₃ required to elicit a response can induce hypercalcemic toxicity. Therefore, non-calcemic vitamin D analogs, such as BXL0124, have been of interest in the inhibition of breast cancer.

Breast cancer is a heterogeneous disease which proceeds through a natural progression, beginning with early hyperplasia and culminating in invasive or metastatic disease. Ductal carcinoma in situ (DCIS) is a non-malignant lesion of the breast with the potential to progress to invasive ductal carcinoma (IDC). Due to the implications of breast cancer stem cells (BCSCs) in breast cancer progression, we investigated the role of vitamin D compounds on these processes.

We showed that BXL0124 inhibited the progression of DCIS to IDC in a model of breast cancer progression by maintaining critical DCIS structures through the modulation of matrix

metalloproteinases transcription. In addition, BXL0124 treatment decreased cell proliferation and maintained vitamin D receptor (VDR) levels in tumors. VDR was expressed in a variety of clinical breast tumors and was lost during malignant transformation of normal mammary cells to pre-malignant histological types, suggesting vitamin D supplementation as a preventative agent due to higher VDR levels in normal breast tissue.

Vitamin D compounds ($1\alpha,25(\text{OH})_2\text{D}_3$ or BXL0124) reduced the growth and self-renewal of mammospheres, an assay which enriches for BCSCs. The putative $\text{CD44}^+/\text{CD24}^{-/\text{low}}$ BCSC population was shifted to a population expressing higher CD24 *in vitro* and *in vivo* by treatment with BXL0124. Pluripotency genes such as *CD44* and *OCT4* were also repressed, contributing to the reduction in cell and tumor growth.

We demonstrated the therapeutic potential of Gemini vitamin D analog BXL0124 on the inhibition of breast cancer progression and the ability of vitamin D compounds to repress the BCSC population *in vitro* and *in vivo*, potentially contributing to the effects on tumor progression.

Acknowledgements

I would first like to thank my supervisor Dr. Nanjoo Suh. She has been a great mentor over the years, and has provided me with the guidance and support necessary for me to be where I am today.

I would like to thank Dr. Suzie Chen, Dr. Wendie Cohick, Dr. Fang Liu, and Dr. Li Cai for serving on my thesis committee and for their valuable suggestions and guidance over the course of my dissertation.

I thank all of the past and present members of Dr. Nanjoo Suh's laboratory, as well as my fellow colleagues in the Susan Lehman Cullman Laboratory for Cancer Research. In particular, I would like to thank the administrative staff, Deborah Stalling, Bobbie Busch, and Erica DiPaola for their help in all day to day tasks and problems encountered over the years.

I want to thank all the friends that I have made during my graduate studies at Rutgers University. Special thanks to Dr. Brian Wall, who has been a close friend and mentor over the past years. I also want to thank my girlfriend, Gabriella Composto, for her patience and support in the decisions that I have made in my career.

I would like to thank my late father, John Wahler, and my mother, Dawn Wahler, for the sacrifices they have made to afford me the opportunity to be where I am today. Finally, I would like to thank my brother, Anthony Wahler, and sister, Nicole Wahler, for their support throughout my life.

Prior Publications

Several sections of the dissertation have been published elsewhere:

Sections of Chapter 2 have been published and have the following citation:

Wahler, J., So, J.Y., Kim, C.Y., Liu, F., Maehr, H., Uskokovic, M., Suh, N. (2014) Inhibition of the Transition of Ductal Carcinoma In Situ to Invasive Ductal Carcinoma by a Gemini Vitamin D Analog. *Cancer Prevention Research*. 7 (6): 617 – 626.

Sections of Chapter 4 have been published and have the following citation:

Wahler, J., So, J.Y., Cheng, L.C., Maehr, H., Uskokovic, M., Suh, N. (2015) Vitamin D compounds reduce mammosphere formation and decrease expression of putative stem cell markers in breast cancer. *J Steroid Biochem Mol Bio*. 148:148-55.

Table of Contents

ABSTRACT OF THE DISSERTATION	ii
Acknowledgements.....	iv
Prior Publications.....	v
Table of Contents	vi
List of Tables	xii
List of Figures	xiii
Chapter 1: Introduction	1
1.1. Breast cancer	1
1.1.1. Luminal breast cancer	1
1.1.2. HER2 enriched.....	3
1.1.3. Triple negative and basal-like	4
1.2. Breast cancer progression.....	5
1.2.1. The microenvironment in DCIS to IDC progression	7
1.3. Breast cancer stem cells (BCSCs).....	9
1.3.1. Stem cell signaling.....	11
1.3.2. Notch signaling	11
1.3.3. Wnt signaling	12
1.3.4. Hedgehog signaling	13
1.3.5. TGF- β signaling.....	14
1.3.6. Mammosphere cell culture system.....	15
1.4. Preclinical models of breast cancer progression	16
1.4.1. Human breast cancer cell lines	16
1.4.2. Xenograft animal model of breast cancer progression	18

1.5. Vitamin D.....	19
1.5.1. Vitamin D Metabolism	19
1.5.2. Biological action of vitamin D.....	20
1.5.3. Vitamin D and breast cancer.....	20
1.5.4. Vitamin D analogs	21
Chapter 2: Inhibition of the transition of ductal carcinoma in situ to invasive ductal carcinoma by a Gemini vitamin D analog.....	26
2.1. Rationale.....	26
2.2. Materials and Methods	27
2.2.1 Reagents and Cell Culture	27
2.2.2. Xenograft Animal Studies.....	27
2.2.3. Determination of Serum Calcium Level	28
2.2.4. Immunohistochemical (IHC) and Immunofluorescence Analysis.....	29
2.2.5. Western Blot Analysis	30
2.2.6. Quantitative Real-Time Polymerase Chain Reaction Analysis	30
2.2.7. DCIS Quantification	31
2.2.8. Statistical analysis.....	31
2.3. Results	31
2.3.1. Optimization of the MCF10DCIS cell line in orthotropic and xenograft injections <i>in vivo</i>	31
2.3.2. BXL0124 inhibits tumor growth without hypercalcemia or hepatotoxicity	32
2.3.3. BXL0124 inhibits tumor progression to invasive ductal carcinoma in MCF10DCIS xenografts.....	33
2.3.4. BXL0124 treatment decreases the cell proliferation of MCF10DCIS tumors at week 4	34
2.3.5. BXL0124 treatment maintains vitamin D receptor levels in MCF10DCIS tumors....	35

2.3.6. Treatment with BXL0124 inhibits progression to IDC by maintaining the myoepithelial cell layer.....	36
2.3.7. Treatment with BXL0124 maintains the basement membrane.....	37
2.3.8. BXL0124 inhibits the mRNA expression of the matrix metalloproteinases during DCIS to IDC progression.....	37
2.4. Discussion	38
2.5 Conclusion.....	41
Chapter 3: Vitamin D receptor is differentially expressed in from normal to malignant tissue ...	60
3.1 Rationale.....	60
3.2 Materials and Methods	60
3.2.1 Patient Samples	60
3.2.2. Immunohistochemical (IHC) Analysis	61
3.2.3. Western Blot Analysis	61
3.2.4. Statistical analysis	62
3.3 Results	62
3.3.1 The vitamin D receptor is expressed in clinical breast cancer samples at different stages of progression.....	62
3.3.2 The vitamin D receptor was not differentially expressed in DCIS or IDC from the same patient	63
3.3.3. Vitamin D receptor levels were lower in tumor tissue compared to normal adjacent breast tissue	63
3.4 Discussion	64
3.5 Conclusion.....	65
Chapter 4: Vitamin D compounds repress mammosphere formation and decrease expression of stem cell markers in breast cancer	72
4.1. Rationale.....	72

4.2. Materials and Methods	73
4.2.1. Reagents and Cell Culture	73
4.2.2. Mammosphere Forming Assay	74
4.2.3. Flow Cytometry	75
4.2.4. Quantitative Real-Time Polymerase Chain Reaction Analysis	76
4.2.5. Annexin-FITC Apoptosis Assay	76
4.2.6. Western Blot Analysis	77
4.2.7. Xenograft studies	77
4.2.8. Statistical analysis	78
4.3. Results	78
4.3.1. Mammosphere cell culture enriches for putative breast cancer stem cell populations and markers of pluripotency in the MCF10DCIS cell line	78
4.3.2. $1\alpha 25(\text{OH})_2\text{D}_3$ and BXL0124 reduce the mammosphere forming efficiency and alter the mammosphere phenotype of MCF10DCIS cells	80
4.3.3. $1\alpha 25(\text{OH})_2\text{D}_3$ and BXL0124 inhibit the proliferation and decrease the expression of putative stem cell markers in MCF10DCIS mammospheres.....	81
4.3.4. $1\alpha 25(\text{OH})_2\text{D}_3$ and BXL0124 inhibits the self-renewal of MCF10DCIS mammospheres	83
4.3.5. Mammosphere cell culture enriches for putative breast cancer stem cell populations and markers of pluripotency in SUM159 and MCF-7 cell lines.....	84
4.3.6. $1\alpha 25(\text{OH})_2\text{D}_3$ and BXL0124 inhibits the mammosphere forming efficiency in SUM159 and MCF-7 cell lines	85
4.3.7. $1\alpha 25(\text{OH})_2\text{D}_3$ and BXL0124 decrease the self-renewal of SUM159 mammospheres	85
4.3.8. $1\alpha 25(\text{OH})_2\text{D}_3$ and BXL0124 decrease the self-renewal of MCF-7 mammospheres ..	86
4.3.9. $1\alpha 25(\text{OH})_2\text{D}_3$ and BXL0124 decrease the self-renewal of MCF-7 mammospheres supplemented with estradiol	87

4.4. Discussion	89
4.5. Conclusion.....	92
Chapter 5: Inhibition of the breast cancer stem cell subpopulation by vitamin D and a Gemini vitamin D analog.....	112
5.1. Rationale.....	112
5.2. Materials and Methods	112
5.2.1. Reagents and Cell Culture	113
5.2.2. Flow Cytometry and FACS	113
5.2.3. Aldefluor Assay	114
5.2.4. Quantitative Real-Time Polymerase Chain Reaction Analysis	114
5.2.5. Mammosphere Forming Assay	115
5.2.6. Xenograft Animal Studies and Tumor Dissociation	115
5.2.7. Statistical analysis	117
5.3. Results	117
5.3.1 CD44 and CD24 are markers for putative breast cancer stem cell subpopulations in MCF10DCIS cells.....	117
5.3.2. $1\alpha 25(\text{OH})_2\text{D}_3$ and BXL0124 decrease the breast cancer stem cell population in MCF10DCIS cells.....	118
5.3.3. Fluorescently activated cell sorting (FACS) was used to sort the MCF10DCIS cells using CD44 and CD24	119
5.3.4. The $\text{CD44}^+/\text{CD24}^{\text{low}}$ putative breast cancer stem cell population has higher expression of notch signaling ligands, Jag1 and Jag2.....	119
5.3.5. Vitamin D compounds repress the mammosphere formation of putative breast cancer stem cell subpopulations	121
5.3.6. BXL0124 treatment of MCF10DCIS xenografts shifts the CD44/CD24 population to a $\text{CD24}^{\text{high}}$ expressing population	121

5.3.7. BXL0124 reduces the expression of stem cell markers and markers of pluripotency in MCF10DCIS xenografts	123
5.3.8. Effects of BXL0124 on re-established MCF10DCIS xenograft model.....	123
5.3.9. Secondary xenografts from BXL0124 treated primary xenografts do not show a reduction of stem cell markers or markers of pluripotency	125
5.4. Discussion	125
5.5 Conclusion.....	129
Chapter 6: Conclusion.....	144
Chapter 7: Future Directions.....	147
Appendix.....	151
References.....	154

List of Tables

Table 1.1 Markers used in the identification of breast cancer stem cells	22
Table 1.2 Pathways involved in stem cell self-renewal	23
Table 1.3 Markers used for analysis of pluripotency and differentiated cells	24
Table 3.1 Pathological analysis of clinical breast cancer samples.....	67

List of Figures

Figure 1.1 The structures of $1\alpha,25(\text{OH})_2\text{D}_3$ and the Gemini vitamin D analog, BXL0124	25
Figure 2.1 Comparison of the progression of untreated MCF10DCIS subcutaneous and mammary fat pad xenografts	43
Figure 2.2 Comparison of the progression of MCF10DCIS subcutaneous and mammary fat pad xenografts treated with BXL0124.....	45
Figure 2.3 BXL0124 inhibits tumor growth in MCF10DCIS xenografts without hypercalcemia or hepatotoxicity.....	46
Figure 2.4 BXL0124 inhibits tumor progression to invasive ductal carcinoma in MCF10DCIS subcutaneous xenografts	48
Figure 2.5 BXL0124 inhibits tumor progression to invasive ductal carcinoma in MCF10DCIS mammary fat pad xenografts.	49
Figure 2.6 Treatment with BXL0124 decreases the proliferation of MCF10DCIS tumors at week 4.....	50
Figure 2.7 BXL0124 treatment inhibits the loss of vitamin D receptor (VDR) in MCF10DCIS tumors	51
Figure 2.8 Immunofluorescence staining of vitamin D receptor (VDR) does not co-localize with smooth muscle actin (SMA) in MCF10DCIS xenografts.....	53
Figure 2.9 The expression of vitamin D receptor (VDR), and metabolizing enzymes, CYP24A1 (catabolism) and CYP27B1 (synthesis), in MCF10DCIS subcutaneous xenografts treated with BXL0124 at weeks 3 and 4.....	54
Figure 2.10 Treatment with BXL0124 inhibits progression to invasive ductal carcinoma by maintaining the myoepithelial cell layer.....	55
Figure 2.11 Treatment with BXL0124 maintains the basement membrane in ductal carcinoma in situ structures.	56
Figure 2.12 BXL0124 inhibits the mRNA expression levels of the matrix metalloproteinases during DCIS to IDC progression	57

Figure 2.13 Summary of the effects of BXL0124 treatment on MCF10DCIS xenografts.....	58
Figure 3.1 Vitamin D receptor is expressed in clinical breast cancer samples at different stages of progression.....	68
Figure 3.2 Vitamin D receptor is expressed to varying degrees in clinical breast cancer samples.	69
Figure 3.3 Vitamin D receptor was not differentially expressed in DCIS or IDC lesions from the same patient.	70
Figure 3.4 Vitamin D receptor (VDR) levels were lower in tumor tissue compared to normal adjacent breast tissue from the same patient.	71
Figure 4.1 Mammosphere cell culture enriches for putative breast cancer stem cell subpopulations and markers of pluripotency in the MCF10DCIS cell line.....	94
Figure 4.2 Dose optimization for the inhibition of mammosphere forming efficiency by $1\alpha 25(\text{OH})_2\text{D}_3$ and BXL0124 in MCF10DCIS cells.....	95
Figure 4.3 Repression of the mammosphere forming efficiency by $1\alpha 25(\text{OH})_2\text{D}_3$ and BXL0124 in MCF10DCIS cells.....	96
Figure 4.4 $1\alpha 25(\text{OH})_2\text{D}_3$ and BXL0124 decrease proliferation but do not affect apoptosis in MCF10DCIS mammospheres.	98
Figure 4.5 $1\alpha 25(\text{OH})_2\text{D}_3$ and BXL0124 decrease the level of stem cell markers in MCF10DCIS mammospheres.	99
Figure 4.6 Repression of stem cell genes and markers of pluripotency by $1\alpha 25(\text{OH})_2\text{D}_3$ and BXL0124 in MCF10DCIS mammospheres.....	100
Figure 4.7 $1\alpha 25(\text{OH})_2\text{D}_3$ and BXL0124 inhibit the self-renewal of MCF10DCIS mammospheres.	101
Figure 4.8 Mammosphere cell culture enriches for putative breast cancer stem cell subpopulations in SUM159 and MCF-7 breast cancer cell lines.....	103
Figure 4.9 Dose optimization for the inhibition of mammosphere forming efficiency by $1\alpha 25(\text{OH})_2\text{D}_3$ and BXL0124 in SUM159 and MCF-7 breast cancer cell lines.	104

Figure 4.10 Inhibition of mammosphere self-renewal by $1\alpha 25(\text{OH})_2\text{D}_3$ and BXL0124 in SUM159 mammospheres.....	105
Figure 4.11 $1\alpha 25(\text{OH})_2\text{D}_3$ and BXL0124 inhibit the self-renewal of MCF-7 mammospheres..	107
Figure 4.12 $1\alpha 25(\text{OH})_2\text{D}_3$ and BXL0124 inhibit the self-renewal of MCF-7 mammospheres supplemented with Estradiol.....	109
Figure 4.13 Comparison of xenograft growth from MCF10DCIS monolayer and mammosphere cell culture.....	111
Figure 5.1 Levels of putative breast cancer stem cell markers in the MCF10DCIS cell line. MCF10DCIS cells were grown in monolayer cell culture for 24h without treatment.....	131
Figure 5.2 $1\alpha 25(\text{OH})_2\text{D}_3$ and BXL0124 repress the breast cancer stem cell subpopulations in MCF10DCIS cells.....	132
Figure 5.3 Flow cytometry verification of FACS sorted subpopulations of MCF10DCIS cells based on CD44 and CD24 cell sorting.....	133
Figure 5.4 Gene expression of breast cancer stem cell markers in MCF10DCIS subpopulations	134
Figure 5.5 Vitamin D compounds repress the formation of putative breast cancer stem cell subpopulations in mammosphere cell culture.....	135
Figure 5.6 BXL0124 treatment of MCF10DCIS xenografts shifts the CD44+/CD24- subpopulation to a population that is more CD24high	136
Figure 5.7 BXL0124 treatment of MCF10DCIS xenografts shifts the CD44+/CD24- subpopulation to a population that is more CD24high	137
Figure 5.8 BXL0124 represses markers of pluripotency and cancer stem cell genes in MCF10DCIS xenografts	139
Figure 5.9 Schematic of MCF10DCIS xenograft tumorigenicity assay in nu/nu mice after BXL0124 treatment in primary xenografts and secondary xenografts.....	140
Figure 5.10 BXL0124 treatment does not result in long term effects on tumor growth in secondary MCF10DCIS xenografts relative to untreated mice.	141

Figure 5.11 Secondary MCF10DCIS xenografts from BXL0124 treated primary xenografts do not show reductions in pluripotency genes	143
---	-----

Chapter 1: Introduction

1.1. Breast cancer

Breast cancer is one of the most commonly diagnosed cancers. An estimated 234,000 new cases will be diagnosed in 2015 in North America alone with another 40,000 existing cases resulting in death (1). Breast cancer is also the second leading cause of cancer-related death with a 5-year survival rate of 24% for late stage disease (1). Regardless of its high prevalence in society, the etiology and pathogenesis of breast cancer have yet to be elucidated (2-5). Genetic, hormonal and environmental factors have been suggested as causes of breast cancer (6, 7). Breast cancer is a heterogeneous disease clinically subdivided into three major subtypes based upon the receptor expression; the luminal subtype, human epidermal growth factor receptor 2 (HER2-amplified) and triple-negative breast cancer (TNBC) (8). Other characteristics such as hormone receptor status, histological origin, proliferation rate, and gene expression profile are used to define the major subtypes of breast cancer.

1.1.1. Luminal breast cancer

The most common type of breast cancers are estrogen receptor (ER) positive tumors which fall into the “luminal” subtypes, so-called because they have a gene expression pattern reminiscent of the luminal epithelial component of the breast (9). Tumors of the luminal subtypes are characterized by expression of ER, progesterone

receptor (PR) and genes associated with ER activation such as LIV1, TFF1/pS2 and Cyclin D1 (9, 10). The Luminal A subtype, constituting approximately 40% of cases of breast cancer, are typically ER positive, PR positive, and have low expression of HER2 as well as low expression of proliferation-associated genes including Ki-67 (10, 11). As such, they are slow growing and less aggressive than other subtypes. Luminal A tumors are associated with the most favorable, short-term prognosis of all breast cancer subtypes, with relatively high survival rates and fairly low recurrence rates (12-14). This could be partially attributed to the fact that less than 15% of Luminal A tumors contain loss of function mutations in tumor suppressor p53 (15-17). Since Luminal A tumors are typically ER+, these tumors have been the prime example of cancer amenable to targeted drug therapy. Treatment for these tumors have been estrogen-focused with endocrine disrupting therapies such as the ER modulator, tamoxifen, improving survival in women with early as well as advanced breast cancer (18, 19). Adjuvant endocrine modalities such as aromatase inhibitors (AIs) and the ER-degrading agent, fulvestrant, have improved prognosis; however, their long-term efficacy is limited by relapse of the disease and development of resistance (18, 20, 21).

Of the luminal breast cancer cases approximately 10-20% are of the Luminal B subtype. Luminal B tumors are a more aggressive luminal subtype compared to Luminal A. Luminal B tumors tend to be ER+, PR+, have increased expression of HER2, contain loss-of-function mutations in p53 and have an increased proliferation rate. Luminal B tumors tend to have a poorer prognosis compared to Luminal A due to poor tumor grade, overall larger tumor size, and lymph node status (12, 14). This is due, in part, to tumors

that are both HER2 and ER over-expressing, HER2 signaling is dominant and endocrine therapy alone gives rise to poor response.

1.1.2. HER2 enriched

Human epidermal growth factor receptor 2 (HER2) amplification has been implicated in approximately 20-30% of human breast cancer cases (22). HER2+ tumors carry a poor prognosis and are prone to high rates of recurrence and metastases (23-25). HER2, also known as ErbB2 or *neu*, is a 185-kDa transmembrane glycoprotein receptor tyrosine kinase. HER2 is part of the epidermal growth factor receptor (EGFR/ErbB/HER1) family of growth factor receptors. Four members of the ErbB family, HER1 (EGFR), HER2 (ErbB2/*neu*), HER3 (ErbB3) and HER4 (ErbB4) dimerize in various combinations resulting in auto-phosphorylation of the receptor and transduction of downstream intracellular signaling pathways which regulate a variety of cellular processes including cell growth, proliferation, survival, and differentiation, invasion and angiogenesis (26, 27). Two major pathways that regulate these cellular processes are the Ras/Raf/MEK/ MAPK cascade as well as induction of the phosphatidylinositol 3-kinase (PI3K)/Akt pathway which in turn activates the NF-kB pathway (27, 28). The combination of these signaling cascades allows HER2+ breast cancer to continue to proliferate as well as evade apoptosis (29, 30).

Currently there are several treatment options specific to HER2+ breast cancer such as the monoclonal antibodies, trastuzumab (Herceptin) and pertuzumab, and the dual tyrosine kinase inhibitor, lapatinib (31-33). Trastuzumab is a monoclonal antibody

that directly targets the HER2 protein and has become standard first-line chemotherapy for early stage HER2-positive breast cancers. Patients whose tumors have the HER2-overexpressing phenotype receiving trastuzumab in combination with adjuvant chemotherapeutics have shown reductions in the risk of recurrence and death by 52% and 33%, respectfully (34). Despite these more targeted therapies; resistance to these drugs has been a major challenge to effectively treat HER2+ breast cancer (35, 36). Resistance to therapy can occur as a result of cross-talk between the ER and HER2 or between signaling cascades downstream of the receptors such as the presence of activating PI3K mutations or loss of function of the phosphatase PTEN (37, 38). In preclinical models, the addition of PI3K and mTOR inhibitors was able to restore sensitivity to anti-HER2 agents (39). In a Phase III study the mTOR inhibitor, everolimus, combined with paclitaxel and trastuzumab was used in patients with HER2 overexpressing metastatic breast cancer. The combination showed antitumor activity with an overall response rate of 44% for at least six months in 74% of patients treated. The relative resistance occurs due to the fact that HER2 overexpression confers resistance to hormone-based therapy regardless of the presence of hormone receptors (40). Indeed, with increased efforts, new approaches and chemopreventive strategies targeting HER2 breast cancer are emerging and preclinical and clinical research is underway to validate these new approaches.

1.1.3. Triple negative and basal-like

Triple negative breast cancer (TNBC) is an aggressive disease lacking a historical therapeutic target. TNBC is defined by the lack of expression of both ER and PR, as well

as lack of expression of HER2 (41, 42). TNBC represents approximately 15% of breast cancer cases and is the most aggressive subtype of breast cancer, accountable for higher rates of recurrence and metastasis (11, 12, 15). The peak risk of recurrence is within the first 3 years after initial treatment with the majority of deaths occurring within the first 5 years (43, 44). The metastasis of TNBC is linked to significantly shorter survival compared to other breast subtypes (44). Basal-like breast cancer, a subset of triple negative breast cancer, has features similar to that of basal cells, or the cells that surround the mammary ducts. Basal-like breast tumors also contain a high frequency of *TP53* gene mutations (45). Additionally, a large majority of breast cancers with BRCA1 mutations are related to the triple-negative phenotype (46). Since triple negative tumors do not express receptors commonly used in therapy, such as ER and HER2, patients are unlikely to benefit from currently available targeted systemic therapy. Currently surgical resection, radiation, and chemotherapy are the only options for patients with TNBC.

1.2. Breast cancer progression

Early development of ductal breast cancer begins with atypical ductal hyperplasia (ADH), progressing to ductal carcinoma *in situ* (DCIS), culminating in invasive ductal carcinoma (IDC) (47). The earliest detectable form of breast cancer consists of non-invasive lesions such as DCIS, and approximately 25% of breast abnormalities detected during screening are DCIS (48). The human breast ductal structure is made up of an inner layer of luminal epithelial cells, surrounded by an outer layer of myoepithelial cells and is separated from the breast stroma by the basement membrane (49). DCIS is defined by

enhanced proliferation of intraductal luminal epithelial cells, and is separated from the stroma by an intact layer of myoepithelial cells and a basement membrane (50). The disappearance and breakdown of the semi-continuous myoepithelial cell layer and basement membrane in DCIS have been identified as major events in the progression from DCIS to invasive ductal carcinoma (IDC) (51). In order for tumor cells to invade and metastasize, they must penetrate these two protective layers (52). DCIS has indeed become a clinical challenge due to its increasing incidence with approximately 50,000 diagnoses expected in 2015 according to the American Cancer Society (2015). This rapid increase in the incidence of DCIS tightly parallels the introduction of mammography screening (53). Despite the high number of diagnoses of DCIS and the risk of progression to a more aggressive disease, current treatment modalities remain limited.

Currently, treatment of DCIS typically consists of surgery, radiation, and when applicable, hormonal therapy. Despite the effective treatment regimen and initial response to therapy, approximately 15% of patients with DCIS will develop relapse within the first decade following surgical lumpectomy (54). DCIS is a pre-cancerous lesion and if left untreated, approximately 30 to 50% of cases will progress to invasive disease (55-57). Currently there are no reliable tests to determine which DCIS cases will progress to IDC and which will remain confined to the mammary ducts (58, 59). Preliminary studies have shown that image analysis of DCIS in addition to histological evaluation and nuclear features could help provide a prognostic evaluation on the progression of DCIS to IDC; however these studies need further validation (60, 61).

Patients diagnosed with DCIS often opt for breast-conserving surgery such as lumpectomy with or without adjuvant treatment such as radiation therapy, hormones or

chemotherapy. A small number of women diagnosed with DCIS choose to conservatively monitor the premalignant lesions. Breast-conserving surgery alone is associated with higher rates of ipsilateral breast tumor recurrence for most women with 50% of lesions advancing to invasive disease. Patients with DCIS who have full mastectomy have reduced rates of chest wall and distal recurrence, however there is no survival advantage (62). In specific cases, such as in patients with larger DCIS lesions or patients with DCIS expressing ER, mastectomy or hormonal therapy is preferred. There is a particular dilemma to balance the risk of causing unnecessary overtreatment since the majority of DCIS lesions are not associated with subsequent invasive tumors. However, even with treatment, some initially observed DCIS lesions will progress to invasive carcinomas. This clinical obstacle of identifying high risk *in situ* lesions has sparked efforts to try and identify characteristics of DCIS and prognostic molecular markers to gain a better understanding as to the factors that play a role in breast cancer progression.

1.2.1. The microenvironment in DCIS to IDC progression

A prevalent theory in progression from DCIS to IDC is that the microenvironment or tumor stroma drives tumor progression. The tumor microenvironment consists of various cell types including mesenchymal stem cells, adipocytes, fibroblasts, as well as endothelial and immune cells which interact with tumor cells via direct interaction and cytokine networks (63). Epithelial-mesenchymal interactions between the cells composing the microenvironment and the molecules of the extracellular matrix (ECM) modulate tissue specificity of the normal breast as well as the survival, growth, and

invasive behavior of breast cancer cells (64, 65). It has been postulated that somatic mutations in myoepithelial cells render them unable to aid in the polarization and organization of the normal duct. This leads to an increase in the number of fibroblasts and infiltrated leukocytes in the stroma, elevating the secretion of growth factors, cytokines, chemokines and matrix metalloproteinases (MMPS) resulting in enhanced angiogenesis and tumor progression (63). The increased loss of integrity of the myoepithelial layer and basement membrane surrounding the ductal lumen leads to transition from *in situ* to invasive ductal carcinoma characterized by degradation of basement membrane, loss of myoepithelial cells and invasion of epithelial cells into the stroma and vasculature (66).

Several studies have linked the pro-invasive nature of the ECM to effects on DCIS. For example post-pregnancy-induced remodeling of the ECM has been attributed to the progression of DCIS. MCF10DCIS cells that were implanted into the involution microenvironment formed larger tumors with increased collagen deposition and higher expression of cyclooxygenase-2 (COX-2) (67). In another study it was observed that stromal fibroblasts increased the invasive capacity of MCF10DIS xenografts through the up-regulation of COX-2 in tumor epithelial cells (68). Other studies have also linked enzymes, such as lysyl oxidases, secreted from stromal cells, to ECM modification, invasion and metastasis (69, 70).

Gene expression analysis has proven that there are significant changes that occur in cells of the tumor microenvironment, such as fibroblasts, myoepithelial cells and leukocytes, during the DCIS to IDC progression (66, 71). Hu and colleagues also found that co-transplantation of fibroblasts enhanced the tumor growth and invasion in MCF10DCIS xenografts (51). Studies have identified a paracrine interaction involving

stromal derived factor-1 (SDF-1), a ligand produced by the activated stroma, binding to and activating the CXCR4 receptor on tumor epithelial cells (72). This interaction can activate AKT, EGFR, JAK2/STAT3, which leads to enhanced survival and inhibition of apoptosis (73-75). SDF-1 signaling can also induce production of matrix metalloproteinases, MMP-2, MMP-9, and MMP-13, which break down the myoepithelial cell layer and basement membrane (76, 77). These studies provide evidence that the tumor microenvironment plays a major role in the progression of DCIS to IDC, and can be utilized as a target in cancer prevention.

1.3. Breast cancer stem cells (BCSCs)

Over the past decades several theories have been proposed as to explain how breast tumors form and progress from DCIS to IDC such as clonal selection and cancer stem cells (CSCs) (78). CSCs are a subpopulation of cells within tumors or premalignant lesions which have the ability to self-renew through symmetrical division or differentiate through asymmetrical division (79, 80). Evidence supports the notion that self-renewing cancer cells are responsible for tumor initiation, growth, and maintenance and hence are known as tumor initiating cells, cancer stem cells or tumor propagating cells (81-83). A tumor can be viewed as a heterogeneous mass of cells comprised of cells at various stages of the differentiation process, all originating from an initial BCSC, or TIC (84). CSCs are also believed to compose a subpopulation in tumors which are responsible for drug resistance, tumor recurrence, and metastasis (85-88). Studies have shown that cells

that remain after chemotherapy are more aggressive and enriched for putative BCSCs (89, 90).

Initial studies identified the $CD44^{\text{high}}/CD24^{\text{low}}$ subpopulation of breast cancer cells from breast tumors to be enriched in cells with an increased tumor initiating capacity (82). Since this time a number of cell surface markers have been utilized to identify breast cancer stem cells (Table 1.1). The $CD44^{\text{high}}/CD24^{\text{low}}$ subpopulation in breast cancers expresses a phenotype which is enriched for tumor initiating cells (81, 82). These populations have been reported to be higher in TNBC compared to other breast cancer subtypes partially explaining the higher rates of relapse observed in TNBC (91).

Evidence suggests that breast cancer stem cells (BCSCs) interact with the surrounding tumor microenvironment via cell adhesion molecules and receptors (92). The interaction of BCSCs with the microenvironment results in crosstalk of signaling and regulation of BCSCs via growth factors and cytokines from the microenvironment (93). However, it is unclear how BCSC signaling can interact with the surrounding microenvironment, such as the stroma, to influence breast cancer progression. Signaling crosstalk with surrounding cells along with other emerging biological properties of BCSC provide strategies and targets to effectively develop therapies against the BCSC population. Elimination of the BCSC population may improve the treatment outcomes for breast cancer patients. Therefore CSCs and the signaling pathways associated with them are novel targets to prevent cancer initiation, tumor growth, resistance, recurrence, and metastasis.

1.3.1. Stem cell signaling

The identification of breast cancer stem cells and progenitor cells has led to investigation of pathways that drive these subpopulations. A number of molecular pathways have been proposed to play a role in the maintenance of the BCSC phenotype. BCSCs have been shown to preferentially rely on embryonal signaling pathways, such as Notch, Wnt, Hedgehog, and bone morphogenetic protein (BMP) (94). It is unlikely that a single pathway will be the driving force of all BCSCs in a given tumor; therefore it is important to target multiple pathways in order to effectively eliminate the BCSC population in a tumor. Another limitation to this BCSC targeted approach is that these pathways are not exclusive to CSCs so these treatments may not be specific to BCSCs.

1.3.2. Notch signaling

The Notch signaling pathway is required for normal mammary gland development and plays a key role in regulating multiple cellular processes including the cellular fate of mammary, stem and progenitor cells (95). Deregulation of Notch has been implicated in the development of mammary carcinoma, particularly the triple negative subtype (96). There are four known Notch receptors (Notch 1-4) which are activated in trans by a variety of ligands (JAG1, JAG2, DLL1, DLL2, DLL3) excreted from adjacent cells (Table 1.2) (95). Binding of Notch ligands to Notch receptors initiates a proteolytic cascade via a disintegrin, a metalloproteinase (ADAM), and γ -secretase to give the activated Notch intracellular domain (NICD), or cleaved Notch (95). The NICD translocates to the nucleus to interact with Cbf-1/Rbp-Jk to affect transcription and

regulation of target genes such as *HEY1*, *HES1*, and *MYC* (95, 97). Recently Notch activation has been implicated in breast, lung, pancreatic, and ovarian cancers through up-regulation of the receptor or associated ligands (98-102). More specifically Notch has been implicated in the self-renewal and maintenance of cancer stem cells (95). These studies have prompted the development of several investigational Notch inhibitors, including Notch targeting antibodies and γ -secretase inhibitors (103, 104). These inhibitors have shown promise in decreasing the number of CSCs and tumorigenic potential in preclinical models of breast and brain cancer (103, 105, 106).

The role of the Notch pathway during early stages of mammary development and stem/progenitor cell restriction has important implications for understanding how dysregulated Notch signaling leads to mammary tumorigenesis (107, 108). Both Notch 1 and 4 have been shown to induce mammary tumors when over expressed in transgenic mice (107). Additionally, the ligand Wnt appears to elicit oncogenesis via a Notch-dependent mechanism in human breast epithelial cells and over expression of NOTCH1 has been correlated with poor overall survival in breast cancer patients (109, 110).

1.3.3. Wnt signaling

The first implication that the Wnt/ β -catenin signaling played a role in mammary tumorigenesis began when the *Int-1* integration site of the mouse mammary tumor virus (MMTV) was identified as the mammalian homolog of the *Drosophila* Wingless polarity morphogen (111). *Int-1* was renamed to Wnt-1 and its overexpression was found to be sufficient to induce mammary tumorigenesis (112). The WNT proteins are a family of

secreted, glycosylated and palmitoylated peptides which regulate cell fate during embryonic development and play important roles in adult tissue homeostasis by regulating stem cells and their niches (113). The Wnt proteins are ligands that activate several intracellular pathways upon binding to transmembrane frizzled (FZD) receptors or a frizzled and LDL-receptor related protein (LRP) complex (Table 1.2) (114). Activation of the pathway occurs when Wnt binds to and activates FZD, leading to further activation of the intracellular cytoplasmic phosphoprotein, disheveled (Dsh). The association of Dsh with axin prevents the phosphorylation and degradation of β -catenin by the glycogen synthase kinase 3 β (GSK3 β)/APC/axin destruction complex. Unphosphorylated β -catenin then escapes recognition by β -TRCP, a component of an E3 ubiquitin ligase, then translocates and accumulates in the nucleus where it binds to TCF and LEF transcription factors resulting in the regulation of target genes governing proliferation, survival and matrix remodeling (115, 116). Aberrant activation of the canonical Wnt pathway leads to enhanced cell proliferation and regulation of the CSC self-renewal program during tumor development (113). Developments of therapeutics to target Wnt signaling have focused on the FZD receptor as a target and have showed promise in reducing tumor growth in breast and pancreatic cancer cells (117).

1.3.4. Hedgehog signaling

Hedgehog signaling is involved in stem cell maintenance and organ development during embryogenesis (118, 119). Inappropriate activation of the Hedgehog pathway has been implicated in several human cancers including skin, brain, colon, lung, breast and

prostate (120). Hedgehog was first identified in *Drosophila*, the three corresponding mammalian homologs were later identified as Sonic hedgehog (SHH), Desert hedgehog (DHH), and Indian hedgehog (IHH) (Table 1.2) (121). These ligands bind to the receptor Patched1 (PTCH1), a 12-transmembrane domain protein that is then internalized. This stops the export of endogenous agonist molecules out of the cell, causing them to accumulate intracellularly. This leads to activation of the G-protein coupled receptor-like protein, Smoothened (SMO) which translocates to the plasma membrane and leads to activation of Gli2 transcription factors in the cytoplasm (119). This transcription factor translocates to the nucleus and regulates the transcription of target genes such as Gli1 and Patched1 (119, 122).

It is not surprising that a pathway that regulates both cell proliferation and differentiation could contribute to the onset of neoplastic transformation or acceleration of tumor growth. Hedgehog activity has been implicated in various human cancers and has shown to be a strong determinant of an increased risk for metastasis and increased understanding of this morphogenic pathway in development and cancer provides opportunities for future cancer therapeutics (123, 124).

1.3.5. TGF- β signaling

The transforming growth factor- β (TGF- β) superfamily has 42 known ligands and plays a role in the regulation of cell growth, differentiation, and development (Table 1.2) (125). TGF- β signaling can be divided into two major signaling cascades based upon activation and intermediate signaling molecules involved. Activation of TGF- β occurs by

proteolytic cleavage, interaction with integrins or pH changes in the local environment. Signaling is initiated by the binding of TGF- β to specific receptors which are transmembrane serine/threonine kinases. TGF- β binds to TGF- β receptor type II (T β RII) which is an active kinase. TGF- β receptor type I (T β RI) is recruited into the complex and phosphorylated by T β RII. This then leads to T β RI-phosphorylation of cytoplasmic signaling molecules, Smad2 and Smad3 for the TGF- β /activin pathway, and Smad 1/5/8 for the bone morphogenetic protein (BMP) pathway (126) (127). Activated Smads then complex with Smad 4 and the resulting heteromeric Smad complexes translocate to the nucleus to regulate gene transcription in a variety of cellular processes such as differentiation, proliferation, migration, EMT and cancer stem cell maintenance including MAP kinase pathways, phosphoinositol-3-kinase, and PP2A (126, 127). TGF- β signaling can have a tumor-suppressive or tumor-promoting effect depending on the type of cancer and the combination of ligand/receptor activation and downstream gene transcription (127). TGF- β signaling can become a promoter of cancer progression in later stages by inducing EMT in cancer cells, promoting CSC maintenance, stimulation of angiogenesis leading to tumor progression, and induction of extracellular matrix degradation resulting in metastasis (128). Because TGF- β is a hormonally regulated growth factor, targeting TGF- β signaling as a therapeutic strategy can reduce the number of CSCs in breast cancer and inhibit bone metastasis, and is therefore a promising route for further investigation (129).

1.3.6. Mammosphere cell culture system

Due to an increased interest in the cancer stem cell field, new *in vitro* methods were necessary to study the characteristics and potential therapeutics for CSCs. From this demand, a non-adherent cell culture system was optimized for the *in vitro* growth of CSC-enriched colonies in suspension. This assay was first developed by Reynolds et al. for the quantification of neural stem cells (130). It was later adapted for mammary tissue and demonstrated the presence of a stem cell population by Dontu and termed the mammosphere assay (131). The mammosphere assay has been used to quantify stem and progenitor cells as well as self-renewal in normal mammary, DCIS and IDC breast cancer cell lines (99, 132, 133). Primary mammosphere formation is a measure of stem cell and early progenitor activity based on the idea that undifferentiated cells will survive in suspension culture with other cell types dying of anoikis (134). To assess the self-renewal of cancer stem cells, primary mammospheres can be harvested, dissociated to single cells and passaged to secondary, tertiary, and subsequent passages for the quantification of self-renewal (134). The ability to form several generations of mammospheres in serial non-adherent passage is related to the self-renewal ability of the stem cells which can give rise to colonies in subsequent culture passages (134). This *in vitro* culture system has also been used for the selection of tumorigenic breast cancer cells from primary tumors, metastatic tumors, and as a tool to screen for new CSC targeting drugs (132, 135, 136)

1.4. Preclinical models of breast cancer progression

1.4.1. Human breast cancer cell lines

Cell lines have been widely used for decades in the study of cancer. The MCF10 cell series is a unique model of breast cancer progression that originated from the normal, non-malignant human MCF10A breast epithelial cells which are (137). This series of cell lines consists of four cell lines with increasing malignancy including MCF10A, MCF10AT1, MCF10DCIS, and MCF10CA1a. MCF10A was transfected with constitutively activated HRAS forming a pre-malignant cell line, MCF10AT1 (137, 138). This cell line forms pre-malignant lesions *in vivo* which resemble human ADH and DCIS when transplanted into immunodeficient mice (139). Approximately 25% of these lesions will slowly progress to IDC (137). MCF10DCIS is a cell line derived by way of serial passage of the cells from MCF10AT1 xenografts. MCF10DCIS cells reproducibly form DCIS-like comedo lesions that spontaneously progress to IDC as xenografts in immunodeficient mice (140). MCF10CA1a is the most aggressive cell line from the MCF10 series, forming large tumors without evidence of a precursor stage. MCF10CA1a was derived from the MCF10AT1 cells by multiple passages in immunodeficient mice (141). MCF10CA1a cells also produce tumors in the lungs of immunodeficient mice, showing the metastatic potential of this cell line (142).

MCF10A, MCF10AT1, MCF10DCIS, and MCF10CA1a cell lines are ER- (data unpublished). Two gene copies of HER2 are present in the MCF10AT1, MCF10DCIS.com and MCF10CA1 cell lines (143). Previous studies by our laboratory show the gradual increase of HER2 expression from MCF10AT1 to MCF10CA1a cells (141). We have shown that VDR is expressed at low levels in MCF10A with increasing levels in MCF10DCIS. Highest levels of VDR are expressed in MCF10AT1 and MCF10CA1a (data unpublished). The MCF10 series of cell lines provides the ability to

analyze the progression of breast cancer at different stages of cancer progression from normal tissue to metastatic IDC (51, 144-146).

1.4.2. Xenograft animal model of breast cancer progression

Of the MCF10 series of cells lines, the MCF10DCIS cell line is unique in the fact that it is representative of breast cancer progression *in vitro* and *in vivo* (140, 141). The MCF10DCIS cell line consistently produces comedo DCIS-like lesions in animal xenografts, which highly resemble the histopathology of human DCIS in xenograft models. The DCIS-like lesions have been shown to reproducibly progress to invasive tumors, providing a unique *in vivo* model to investigate the transition for DCIS to IDC (140, 147). Clinically DCIS is defined as the proliferation of malignant epithelial cells confined to the mammary ducts. The MCF10DCIS xenograft model forms histology that resembles human DCIS, however these lesions are not contained within the ductalobular system of the mouse mammary tissue and hence is not by definition classical DCIS. In addition, Hu *et al.* showed similarities of cell type specific expression profiles between human DCIS samples and MCF10DCIS xenografts by comparing myoepithelial and epithelial cell gene expression profiles (51). The study showed a statistically significant enrichment of genes involved in the extracellular matrix, basement membrane structure, and development in the myoepithelial cell populations of both the human DCIS samples and MCF10DCIS xenografts. Since the enrichment patterns of genes were highly similar from human to the MCF10DCIS xenograft tumors, this is an excellent model to test the

effects of chemopreventive agents on the structural, molecular, and phenotypic changes during the progression of DCIS to IDC.

1.5. Vitamin D

1.5.1. Vitamin D Metabolism

Vitamin D, also known as cholecalciferol, is the precursor to the steroid hormone calcitriol. Vitamin D is derived from the diet or the energy from UV radiation converts 7-dehydrocholesterol to vitamin D₃ in the skin (148). Vitamin D₃ is then converted to the active form of vitamin D in the body, calcitriol, via two cytochrome P450 mediated steps (149). The first hydroxylation step in this process occurs in the liver and is mediated by the enzyme vitamin D-25-hydroxylase (25-OHase; *CYP2R1*) forming 25-hydroxyvitamin D₃ or 25-hydroxycholecalciferol (25(OH)D₃) (150). Circulating 25(OH)D₃ is further hydroxylated in the kidney by 25-hydroxyvitamin D₃-1 α -hydroxylase (1 α -OHase; *CYP27B1*) producing the biologically activate form of vitamin D, 1 α ,25(OH)₂D₃ or calcitriol (149, 151). Although these enzymes are primarily found in the liver and kidney, they have also been detected locally in other tissues, including the mammary glands and in cancer cells (152, 153). This can induce the local production of 1 α ,25(OH)₂D₃, leading to various tissue specific biological effects (152, 154, 155). Calcitriol then exerts its action by binding to an intracellular receptor, the vitamin D receptor (VDR), which belongs to the superfamily of nuclear receptors for steroid hormones and regulates gene expression by acting as a ligand-activated transcription factor (156). Activation of VDR influences

several hundred genes that are responsible for cellular growth, differentiation and apoptosis (157).

1.5.2. Biological action of vitamin D

Calcitriol primarily functions by binding to and activating the vitamin D receptor (VDR), thereby causing its dimerization with the retinoid X receptor (RXR) (158). Binding of this complex to vitamin D response elements (VDREs) in multiple regulatory regions causes the activation or repression of genes which are responsible for the biological action of vitamin D (152, 155). In addition to the genomic action of vitamin D, vitamin D can also exert more rapid responses that are independent of transcriptional regulation (159-161). This rapid response is typically mediated through a membrane bound form of VDR which activates PKC signaling and increases the levels of intracellular Ca^{2+} (160, 161). This increase in intracellular Ca^{2+} activates the Raf/MAPK/ERK signaling pathway (160, 161).

1.5.3. Vitamin D and breast cancer

Vitamin D is classically involved in calcium and phosphate homeostasis and is essential for bone mineralization (158). However many preclinical studies have demonstrated beneficial effects of vitamin D in association with various diseases, including cancer (155). Exposure to sunlight has shown an inverse relationship to breast cancer risk (162). This was eventually linked to the increased production of vitamin D_3

upon exposure to ultraviolet light (163-166). Since this discovery, many studies have linked 1,25-dihydroxyvitamin D₃ (1,25(OH)₂D₃), the active metabolite of vitamin D, and vitamin D analogs to the suppression of cancer cell invasion, proliferation, and metastasis (167-170). In certain breast cancer cell lines, 1,25(OH)₂D₃ has been shown to increase the expression of E-cadherin resulting in prevention of invasion and metastasis (171). Additionally, 1,25(OH)₂D₃ has antiangiogenic properties that decrease activity of MMPs and urokinase plasminogen and tissue-type plasminogen activators which play important roles in invasion and metastasis (172). 1,25(OH)₂D₃ has been shown to suppress the estrogen pathway via downregulation of aromatase which is responsible for the conversion of androgens to estrogens (173). Additionally, 1,25(OH)₂D₃ reduces transcription of *ESR1* resulting in decreased expression of ER- α and its downstream effector pathways (174, 175).

1.5.4. Vitamin D analogs

The pharmacological dose of vitamin D required to reduce cancer and other diseases is typically higher than that needed to support bone health. The side effects of the administration of supra-physiological concentrations of calcitriol are hypercalcemia, which is an increase of circulating calcium in the blood (170, 176-178). These effects are primarily due to calcitriol's effects on calcium absorption in the intestine. For this reason structural analogs of vitamin D have been developed to reduce the calcemic effects and increase the efficacy of traditionally used forms of vitamin D (179). These analogs have been of particular interest in the inhibition of breast cancer (167, 176, 180, 181).

Table 1.1 Markers used in the identification of breast cancer stem cells

Marker	Characteristics	Reference(s)
CD44	A cell surface marker involved in invasion, cancer stem cell maintenance The CD44 ⁺ /CD24 ^{-/low} population has been used to isolate stem cells from the normal mammary epithelium	(82, 182, 183)
CD49f	An integrin (Integrin $\alpha 6$) involved in invasion and enrichment displays increased tumorigenic potential; Has been shown to regulate stem cell properties in basal-like breast cancer	(184-186)
CD24	A cell surface marker; Low levels correspond to cells with increased tumorigenic capacity the ability to self-renew and differentiate	(82)
ESA	Epithelial specific antigen; High expression of ESA is typically used in combination with CD44, CD49f, and CD24 for breast cancer stem cell identification	(82, 187)
ALDH1	Association to the cancer stem like phenotype is based on the enzymatic activity of the detoxifying enzyme Aldehyde Dehydrogenase 1. High levels are associated with worse clinical outcome, increased tumorigenic capacity, and stem and progenitor cells.	(188-191)
CD133	Associated with the luminal compartment in breast cancer, and high expression correlates with the CD44 ⁺ /CD24 ^{-/low} breast cancer stem cell phenotype	(192)
CD29	An integrin ($\beta 1$ -integrin) which plays a role in luminal cell fate among CD24 ⁺ cells. Mammary stem cells (CD29 ^{high}) and luminal progenitors (CD29 ^{low})	(193)

Table 1.2 Pathways involved in stem cell self-renewal

Pathway	Receptors	Ligands	Genes activated	Reference(s)
Notch	Notch 1, 2, 3, 4	JAG1, JAG2, DLL-1, DLL-3, DLL-4	HES1/3/5, HEY1/2, MYC, Cyclin D1, p21, NF- κ B	(194-196)
Hedgehog	Patched-1, 2	SHH, DHH, IHH	Patched, Gli1, Wnt, BMPs, MYC, Cyclin D1, Cyclin E, JAG2	(194, 197)
Wnt	Frizzled-1, 2, Ror2, RYK	Wnt (19 ligands)	MYC, Cyclin D1, CD44, TGF-1, Axin, MMP-7, DKK1	(194)
TGF- β /SMAD	TGF β RI, TGF β RII, Activin Receptors (ALK-1, 2, 4, 7, RII, RIIB), BMPRIA, BMPRII, BMPRI	TGF- β (TGF- β 1, 2, 3), Activins, Nodal, BMPs (BMP 2-7, 8A, 8B, 10,15), GDF (GDF1-3, 5-11, 15)	SLUG, p21, BIM, MMP1, ITGB4, ITGA2, LAMA3, FZD1, FZD7, JAG1, HES1, GATA2, SOX9, SOX4	(198, 199)

Table 1.3 Markers used for analysis of pluripotency and differentiated cells

Markers used in differentiation	
Basal/Myoepithelial markers	SMA, CD10, p63, CK14, CK5/6, CK17, CD44, CD49f (ITGA6), ITGB4, ITGB6
Luminal Markers	MUC1, GATA3, CK18, CD24, EpCAM (ESA), E-Cadherin, CK19, ESR1
Stem/Progenitor Markers	CD44, ALDH1, CD24, CD49f, CD29 (ITGB1), Notch1, Vimentin, CK19, CD133
Pluripotency genes	<i>OCT4 (POU5F1), SOX2, NANOG, KLF4, MYC</i>
EMT markers	Mesenchymal: Vimentin, N-Cadherin, Fibronectin Epithelial: E-cadherin, Slug, Snail, Zeb1, Zeb2, Twist, p63

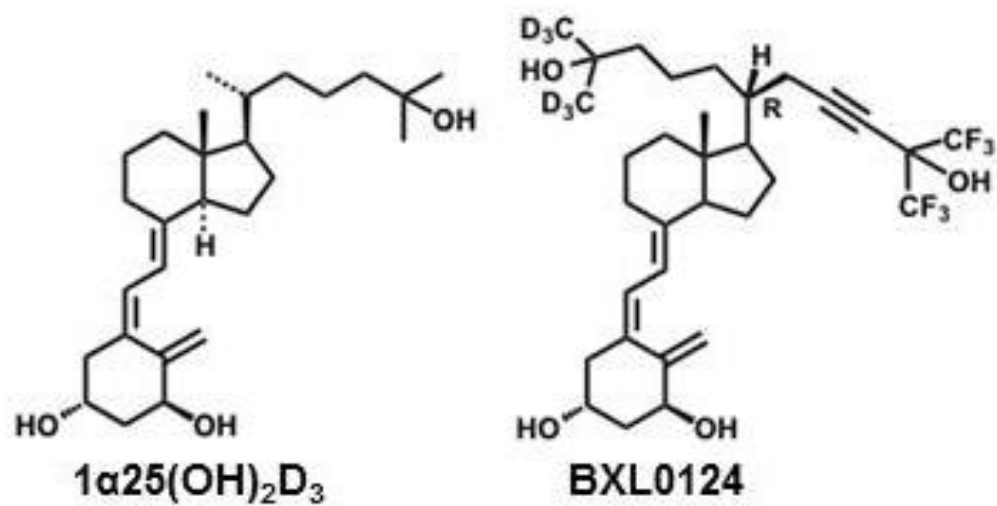


Figure 1.1 The structures of 1α₂₅(OH)₂D₃ and the Gemini vitamin D analog, BXL0124

Chapter 2: Inhibition of the transition of ductal carcinoma in situ to invasive ductal carcinoma by a Gemini vitamin D analog

Note: Sections of this chapter have been reproduced from the following publication: Wahler, J., So, J.Y., Kim, C.Y., Liu, F., Maehr, H., Uskokovic, M., Suh, N. (2014) Inhibition of the Transition of Ductal Carcinoma In Situ to Invasive Ductal Carcinoma by a Gemini Vitamin D Analog. *Cancer Prevention Research*. 7 (6): 617 – 626.

2.1. Rationale

Due to the unpredictable behavior of ductal carcinoma in situ (DCIS) and lack of established therapy for patients diagnosed with DCIS, the need for more effective chemopreventive agents targeting early stages of breast cancer is of utmost importance. Previous studies have shown that the Gemini vitamin D analog, BXL0124 has an inhibitory effect on the growth of MCF10DCIS xenograft mammary tumors when treated for five weeks from the time of cell injection (147, 176). We have also shown that vitamin D BXL0124 can delay mammary tumor incidence in the MMTV-ErbB2/neu transgenic model of HER-2 overexpressing breast cancer when used as a chemopreventive agent (180). However, the effects of BXL0124 on DCIS progression to invasive ductal carcinoma (IDC) have not been elucidated, and are critical to the mechanistic understanding of vitamin D inhibition of breast oncogenesis. The early stage of breast cancer development, specifically the transition from DCIS to IDC, is a crucial event in the advancement of breast carcinogenesis, and is of utmost importance from a

prevention standpoint. Therefore, in the present study, we evaluated whether BXL0124 blocks or delays the early transition of DCIS to IDC *in vivo*.

2.2. Materials and Methods

2.2.1 Reagents and Cell Culture

$1\alpha,25(\text{OH})_2\text{D}_3$ and a Gemini vitamin D analog [BXL0124; $1\alpha,25$ -dihydroxy-20R-21(3-hydroxy-3-deuteromethyl-4,4,4-trideuterobutyl)-23-yne-26,27-hexafluoro-cholecalciferol, >95% purity] (Figure 1.1) were provided by BioXell, Inc. (Nutley, NJ) and dissolved in dimethyl sulfoxide (DMSO). For *in vivo* animal experiments, BXL0124 was diluted in Cremophor EL: PBS (1:8, v/v) for intraperitoneal (i.p.) injection. The MCF10DCIS human breast cell line was provided by Dr. Fred Miller at the Barbara Ann Karmanos Cancer Institute (Detroit, MI). The MCF10DCIS cell line was authenticated by short tandem repeat profiling at American Type Culture Collection (ATCC, Manassas, VA). MCF10DCIS human breast cancer cells were maintained in Dulbecco's Modified Eagle's Medium (DMEM)/F12 medium supplemented with 5% horse serum, 1% penicillin/streptomycin, and 1% HEPES solution at 37°C, 5% CO₂.

2.2.2. Xenograft Animal Studies

All animal studies were approved by the Institutional Review Board for the Animal Care and Facilities Committee of Rutgers University. Female nude mice (5-6 weeks old) were purchased from Charles River Laboratories (Wilmington, MA). They were allowed to

acclimate to the facilities for two weeks at which time they were injected (7-8 weeks old) with human MCF10DCIS cells into the mammary fat pad or dorsal area at 10^6 cells per site and treatment began the following day. Mice were treated with DMSO control or BXL0124 (0.1 $\mu\text{g/kg}$ body weight) by i.p. injection six times per week for until the end of the experiment. Tumors were palpated twice per week and total body weights were measured weekly. Tumors were measured with a vernier caliper and tumor volume (V; cubed centimeters) was calculated using the equation $V = (D \cdot d^2)/2$ where D (centimeters) and d (centimeters) are the largest and smallest perpendicular diameters. Animals were sacrificed by CO_2 exposure 1, 2, 3, 4, and 5 weeks after injection at which time tumors were excised and blood was drawn by cardiac puncture for further analysis. Tumors from 1, 2, 3, 4, and 5 weeks were cut into two pieces either fixed in 10% formalin for 15 hours for immunohistochemical analysis or were snap frozen in liquid nitrogen for qPCR analysis. Livers from mice treated for 5 weeks were fixed in 10% formalin for 15 hours for immunohistochemical analysis.

2.2.3. Determination of Serum Calcium Level

The determination of calcium concentration in serum was carried out by using the calcium reagent set from Pointe Scientific, Inc. (Canton, MI) following the manufacturer's protocol. Briefly, serum (4 μL) was mixed with the diluted reagent (200 μL) in the wells of a 96-well plate and incubated at room temperature for 1 minute and absorbance read at 570 nm using a Tecan infinite M200 plate reader (Tecan, Durham,

NC). The calcium concentrations were calculated from calcium standards provided by the manufacturer.

2.2.4. Immunohistochemical (IHC) and Immunofluorescence Analysis

Subcutaneous tumors were fixed, embedded in paraffin and sectioned at 5 μ m thickness. Individual tumors were analyzed histopathologically by hematoxylin and eosin (H&E) staining. Livers were fixed, and embedded in paraffin and sectioned at 5 μ m thickness. Liver sections were analyzed by the Rutgers Histopathology Core facility for the following criteria: lymphocyte infiltrates, neutrophilic infiltrates, glycogen stores, and mitotic figures. For immunohistochemistry, sections were stained as previously described (200) with antibodies to smooth muscle actin (SMA) (1:200, Abcam, ab5694, Cambridge, MA), proliferating cell nuclear antigen (PCNA) (1:8000, Dako, M0879, Carpinteria, CA) and vitamin D receptor (VDR) (1:200, Santa Cruz Biotechnology, sc-13133, Santa Cruz, CA). The sections were counterstained with Harris hematoxylin (Sigma Aldrich, St. Louis, MO). The PCNA nuclear intensity and VDR total pixel intensity were quantified by blinding the samples and having a third party carry out the analysis using a Scan Scope (Aperio, Vista, CA). For immunofluorescence staining, the slides were blocked in 10% goat serum, and then incubated overnight at 4°C with the combination of primary antibodies to smooth muscle actin (SMA) (1:200, Abcam, ab5694, Cambridge, MA), laminin 5 (1:50, Santa Cruz Biotechnology, sc13587, Santa Cruz, CA), pancytokeratin (panCK) (1:50, Dako, M3515, Carpinteria, CA), vitamin D receptor (VDR) (1:200, Santa Cruz Biotechnology, sc-13133, Santa Cruz, CA), and TO-PRO-3 iodide nuclear antibody

(Invitrogen, 1 μ M). Fluorophore-conjugated secondary antibodies (Alexa Fluor 488 or 546, 1:100, Invitrogen, Carlsbad, CA) were incubated at room temperature for 30 minutes. The images were taken using confocal microscopy with lasers at 488 nm, 546 nm, and 633nm (TO-PRO-3). Immunofluorescence was visualized using a Nikon Eclipse C1 Plus confocal microscope system.

2.2.5. Western Blot Analysis

The procedures have been described previously (200). Five tumor samples from each group were homogenized and pooled for analysis. Primary antibodies against VDR (1:200, Thermoscientific, MA1-710, Waltham, MA) and β -actin (1:2000, Sigma-Aldrich, A1978, St. Louis, MO) were used for analysis. Secondary antibodies were from Santa Cruz Biotechnology. Western Blots were quantified by using ImageJ software (US National Institutes of Health, Bethesda, MD) and calculating the relative density of the bands using the gel analyzer command.

2.2.6. Quantitative Real-Time Polymerase Chain Reaction Analysis

These procedures have been reported previously (201, 202). The Taqman® probe-based gene expression system from Applied Biosystems (Foster City, CA) was used to detect the genes of interest. Labeled primers for *GAPDH* (Hs02758991), *VDR* (Hs00172113), *CYP24A1* (Hs00167999), *CYP27B1* (Hs01096154), *MMP2* (Hs00234422), *MMP9* (Hs00234579), *MMP14* (Hs01037009), *MMP15* (Hs00233997), *MMP16* (Hs00234676),

TIMP1 (Hs00171558), *TIMP2* (Hs00234278), *TIMP3* (Hs00165949), *TIMP4* (Hs00162784) were used in analysis.

2.2.7. DCIS Quantification

Hematoxylin and eosin and smooth muscle actin IHC stained images of MCFDCIS xenografts were quantified using ImageJ software (US National Institutes of Health, Bethesda, MD). The total tumor area was selected, and then the areas of DCIS within the tumor were calculated. DCIS-like lesions were identified by luminal cells contained within a continuous myoepithelial cell layer. Invasive areas were identified by luminal tumor cells that had no distinct outer myoepithelial cell layer. The percentage of DCIS within each tumor was presented as the area of DCIS divided by the total tumor area.

2.2.8. Statistical analysis

Statistical significance was evaluated using the Student's t-test.

2.3. Results

2.3.1. Optimization of the MCF10DCIS cell line in orthotopic and xenograft injections *in vivo*

In our preliminary studies, we first compared the DCIS progression of MCF10DCIS xenografts between the mammary fat pad and subcutaneous injections. The

subcutaneous xenografts formed a higher number of comedo DCIS lesions and more consistently produced DCIS lesions compared to the mammary fat pad xenografts (Fig. 2.1 and Fig 2.2), in agreement with a previous report by Hu *et al* (51). Comparison of four separate lesions from subcutaneous or mammary fat pad at week 3 shows that subcutaneous xenografts reproducibly form a higher number of DCIS lesions compared to the mammary fat pad xenografts (Fig. 2.1). The subcutaneous xenografts show a clear point of DCIS to IDC transition so it is easy to determine whether pharmacological agents, such as BXL0124, inhibits this transition (Fig. 2.2A), whereas with the mammary fat pad xenografts it is not clear when or if the transition is blocked, and quantification of DCIS structures is difficult without further IHC analysis (Fig. 2.2B). Therefore, we proceeded with the MCF10DCIS subcutaneous xenograft model for the clarity of studying the effects of pharmacological agents on DCIS progression to IDC.

2.3.2. BXL0124 inhibits tumor growth without hypercalcemia or hepatotoxicity

Animals treated with BXL0124 showed a reduction in average tumor volume over the first 3 weeks and significant repression was observed by week 4 with a 43% reduction in tumor size ($p < 0.05$) ($n=5$ per group) (Fig. 2.3A). BXL0124 treatment did not cause any significant changes in body weight or serum calcium levels, indicating that there was no observed hypercalcemic toxicity associated with the given dose over four weeks of treatment ($n=4$ per group) (Fig. 2.3B-C). Histopathological analysis of livers from mice treated with BXL0124 six times per week for did not show significant pathologic processes ($n=4$ per group) (Fig. 2.3D). There was variability within the range of normal

for the following criteria: lymphocyte infiltrates, neutrophilic infiltrates, glycogen stores, and mitotic figures.

2.3.3. BXL0124 inhibits tumor progression to invasive ductal carcinoma in MCF10DCIS xenografts

Using MCF10DCIS subcutaneous xenografts, we investigated the histopathological and molecular changes that occurred during the growth of tumors in nu/nu mice over the course of 4 weeks. H&E staining showed that MCF10DCIS cells subcutaneously xenografted into nu/nu mice formed lesions histologically resembling that of human DCIS. In the control group, DCIS lesions started to escape to an invasive-like stage at week 3 and the tumors advanced to IDC rapidly by week 4, at which time the tumors were 80% invasive (Fig. 2.4B). The tumors treated with BXL0124 formed DCIS lesions by week 3 and unlike control tumors, maintained these DCIS lesions through week 4, showing approximately 30% invasive histology ($p < 0.05$) (Fig. 2.4B).

These results prompted the investigation at a further time point of 5 weeks to assess whether DCIS-like lesions from BXL0124 treated tumors would progress to IDC (Fig. 2.4C). H&E staining reconfirmed the initial study, which showed that lesions started to escape to an invasive-like stage at week 3 and progressively advanced to IDC at week 4 in the control group (Fig. 2.4C). BXL0124 treated tumors showed invasive areas at week 3, however these lesions did not rapidly progress as was observed in the control group. Progression was delayed and by week 5 BXL0124 treated xenografts were still primarily DCIS-like lesions (Fig. 2.4C).

The inhibition of MCF10DCIS progression with BXL0124 was confirmed in mammary fat pad xenografts. Difficulty in analyzing H&E staining for DCIS-like lesions in the mammary fat pad, due to increased stromal composition and microenvironment, prompted the use of alternative staining which directly stains the myoepithelial cell layer. Immunohistochemical staining of the myoepithelial cell layer with smooth muscle actin (SMA) was used to stain for DCIS-like lesions (Fig. 2.5A). As previously shown, the formation of DCIS lesions in the mammary fat pad was less consistent and the sheer number of DCIS lesions was less compared to the subcutaneous lesions (Fig 2.1, Fig 2.5A). Despite this, in the control group, the percentage of DCIS-like lesions slowly progressed to an invasive-like state starting at 30% DCIS in week 1 and progressing to 5% DCIS by week 4 in the control group (Fig. 2.5B). Similar to the control group, tumors treated with BXL0124 formed 31% DCIS histology in week 1, however, these levels of DCIS were maintained through week 4, exhibiting 34% DCIS histology at the time the experiment was terminated (Fig. 2.5B).

2.3.4. BXL0124 treatment decreases the cell proliferation of MCF10DCIS tumors at week 4

Cell proliferation was determined by measuring proliferating cell nuclear antigen (PCNA) by immunohistochemistry staining. The cell proliferation in MCF10DCIS tumors remained relatively low through week 3. As control tumors progressed to an invasive phenotype at week 4, there was a marked increase in the level of PCNA expression compared to previous weeks. Treatment with BXL0124 showed a significant

decrease in PCNA levels compared to the control at week 4 (Fig. 2.6A). For subjective analysis, four tumors from each group were blinded and were analyzed for PCNA staining intensity. The intensities were scored from 0+ (negative staining) to 3+ (strongest staining) for each individual cell. The sum of all positive staining including 1+, 2+, and 3+ was used to calculate the percentage of PCNA-positive cells. Quantification showed that 52% of the cells were PCNA-positive in the control group at week 4, whereas only 32% of cells were positive in the BXL0124-treated group at week 4 ($p < 0.05$) (Fig. 2.6B).

2.3.5. BXL0124 treatment maintains vitamin D receptor levels in MCF10DCIS tumors

MCF10DCIS xenograft tumors express vitamin D receptor (VDR). From weeks 1 to 3, VDR levels were similar between control and BXL0124 treatment groups. VDR was lost upon the rapid progression from DCIS to invasive tumors in the control group in week 4. However, treatment with BXL0124 not only maintained DCIS histology but also retained VDR levels at week 4 (Fig. 2.7A). It is interesting to note that VDR expression is lost where epithelial and stromal cells come in contact, suggesting that this cell-to-cell interaction could potentially reduce VDR levels. Four tumors from each group were blinded and analyzed for VDR staining intensity. The intensities were scored from 0+ (negative staining) to 3+ (strongest staining) based on pixel intensity of staining. The sum of all positive staining including 1+, 2+, and 3+ was used to calculate the percentage of VDR-positive cells. Quantification showed 66% VDR-positive staining in the control

tumors, compared to 81% positive staining in the BXL0124 group at week 4 ($p < 0.05$) (Fig. 2.7B). VDR levels were also analyzed in xenograft tumors by western blot, showing a 60% increase in the xenografts from BXL0124 treated mice compared to the control xenograft tumors (Fig. 2.7C).

Interestingly, despite the changes in protein levels of VDR we did not see a significant change in mRNA expression of the *VDR* gene at weeks 3 or 4 upon BXL0124 treatment (Fig. 2.9). We did not detect significant biological changes in the vitamin D metabolizing genes *CYP24A1* (catabolism) or *CYP27B1* (synthesis) in week 3 and 4 xenograft tumors (Fig. 2.9). In order to determine if VDR is expressed in myoepithelial cells, we assessed the immunofluorescence staining of VDR together with the myoepithelial marker, smooth muscle actin (SMA). VDR staining did not co-localize with SMA staining in any of the samples that were analyzed, indicating that VDR expression was confined in luminal cells (Fig. 2.8). In addition, the loss of VDR was evident in week 4 control xenografts, whereas the maintenance of VDR levels upon BXL0124 treatment was shown at week 4 (Fig. 2.8).

2.3.6. Treatment with BXL0124 inhibits progression to IDC by maintaining the myoepithelial cell layer

The main diagnostic feature which distinguishes DCIS from invasive lesions is the loss of the critical myoepithelial cell layer and basement membrane (51). To investigate the integrity of the cell layers throughout progression, we analyzed the myoepithelial marker smooth muscle actin (SMA) and the epithelial marker

pancytokeratin (panCK) in xenograft tumors. Tumors at weeks 1 and 2 were composed primarily of epithelial cells as noted by panCK staining. There was a gradual establishment of the myoepithelial cell layer starting at week 2, fully forming around the epithelial cells in both the control and BXL0124 treated group by week 3 (Fig. 2.10). In the control group tumors, the myoepithelial cell layer spontaneously dissociated from its organized structure by week 4 as the tumors progressed to IDC. However, the course of BXL0124 treatment showed the formation of the myoepithelial cell layer in week 3 and maintained organization of the myoepithelial cell layer at week 4 (Fig. 2.10).

2.3.7. Treatment with BXL0124 maintains the basement membrane

To assess the effects of BXL0124 on the integrity of the basement membrane, co-immunofluorescence staining was carried out with a basement membrane marker, laminin 5, and a myoepithelial marker, SMA. The basement membrane formed by week 2, and was maintained in week 3 in both the control and BXL0124 treated groups. At week 4, the basement membrane was disrupted in the invasive-like tumors of the control group, as indicated by reduced and fragmented staining of laminin 5. This structure remained intact in the BXL0124 treated tumors at week 4 (Fig. 2.11).

2.3.8. BXL0124 inhibits the mRNA expression of the matrix metalloproteinases during DCIS to IDC progression

Matrix metalloproteinases (MMPs) have been implicated in increased tumor growth, invasion, and metastasis (202, 203). These effects are largely due to the enzymatic activity of MMPs, which allows them to remodel the extracellular matrix leading to cell invasion (204, 205). Additionally growth factors and cytokines secreted by inflammatory and stromal cells have been shown to modulate MMP expression (206). Consequently, we assessed the mRNA levels of specific MMPs in MCF10DCIS tumor xenografts at weeks 3 and 4. Analysis of MCF10DCIS tumors showed a significant decrease in the mRNA levels of *MMP2*, *9*, *14*, and *15* upon BXL0124 treatment at week 3 while *MMP16* did not change (Fig. 2.12A). The modulation of *MMP2* and *MMP14* expression by BXL0124 treatment persisted to week 4. Tissue inhibitors of metalloproteinases (TIMPs) are endogenous inhibitors of these MMPs (207). We did not detect significant biological changes in *TIMP1*, *2*, *3*, or *4* in week 3 and 4 xenograft tumors (Fig. 2.12B). These observations suggest that reduction of MMP expression by BXL0124 contributes to the inhibition of transition from DCIS to invasive carcinomas.

2.4. Discussion

DCIS progression to IDC is defined by the escape of inner luminal epithelial cells through the outer layer of myoepithelial cells and the basement membrane, ultimately coming in contact with the stromal cell population (49). Previous reports have shown that myoepithelial cells can arise from the luminal cell population, but not vice versa (49, 187, 208, 209). In our study, the MCF10DCIS xenografts show growth of the epithelial cells in the early weeks followed by the formation of the myoepithelial cell layer which is

consistent with those reports. BXL0124 does not seem to affect the rate of formation of the myoepithelial layer (Fig. 2.10, Weeks 1, 2, and 3), however it does significantly reduce the rate at which the myoepithelial cell layer is broken down (Fig. 2.10, Week 4), suggesting that BXL0124 inhibits the transition from DCIS to invasive carcinoma. When the staining of laminin 5 in the DCIS and IDC lesions are examined histologically, it is clear that BXL0124 treatment helps to maintain an intact, organized structure of the critical basement membrane (Fig. 2.11, Week 4). It is also interesting to note that the basement membrane forms first in week 2 followed by the myoepithelial cell layer at week 3. This suggests that the basement membrane might act as a scaffold for the formation of the myoepithelial cell layer, and the loss of this scaffold through enzymatic degradation could partially account for the disorganization of the myoepithelial cell layer observed in week 4 control tumors. Analyzing the effects of BXL0124 on the progression of DCIS to IDC (Fig. 2.4A, 2.5A), we found that the treatment sustains DCIS lesions and prevents progression to IDC through maintenance of the critical myoepithelial cell layer and the basement membrane.

The progression from DCIS to IDC is believed to be provoked largely by the production of proteolytic enzymes (210). MMPs degrade proteins involved in extracellular matrix structure and molecules involved in cell-cell adhesion, which release epithelial cells from their ordered layers and deregulate cell signaling, ultimately leading to extensive changes in gene transcription (211). MMP2 and MMP9, the gelatinases, are responsible for the degradation of type IV collagen as well as laminin 5, components of the basement membrane (210, 212). MMP2 is secreted in a latent form and requires activation by MMP14 to its pro-MMP2 form (213). Aside from its activating function,

MMP14 as well as MMP15 and MMP16 have been shown to directly affect cell invasion by remodeling the basement membrane *in vivo* (214). Thus, reduction of *MMP2*, *MMP9*, *MMP14* and *MMP15* by BXL0124 in week 3 prior to the transition of DCIS to IDC likely contributes to the maintenance of the basement membrane in the tumor xenografts. This suggests that the down-regulation of MMPs by BXL0124 treatment could play a major role in the preservation of DCIS histology.

As tumors progress to IDC, there is a significant increase in cell proliferation which is consistent with previous findings that stromal and tumor epithelial cell interactions can enhance proliferation (215). The significant reduction of the proliferation rate in tumors from BXL0124 treated animals at week 4 demonstrates the potential of BXL0124 to slow the growth of DCIS epithelial cells. Since the effects of BXL0124 are known to be dependent on VDR (147, 202), we analyzed VDR levels over the course of tumor progression. It was previously shown that a decrease in protein levels of VDR have been correlated with the progression from benign to malignant breast lesions (153). In our study, the BXL0124 treatment not only maintained the integrity of the DCIS structure, but also retained VDR levels in the epithelial cells (Fig. 2.7A, Week 4). VDR protein levels were increased in week 4 BXL0124 treated xenografts, however mRNA expression was unchanged in weeks 3 or 4, suggesting that loss of VDR in week 4 control tumors is likely due to protein degradation or possible post-translational regulation. Interestingly, loss of DCIS architecture seems to be a determining factor in the loss of VDR expression, suggesting that the interaction with the surrounding stromal cells could play a major role in the down-regulation of VDR. Whether adjacent stromal-to-epithelial cell contact or factors secreted from stromal cells contribute to the loss of VDR needs to be further

investigated. Analysis of VDR and SMA co-localization studies show that VDR is not expressed in the myoepithelial cell layer or stroma but within the luminal cells. In invasive tumors, VDR negative cells include both tumor and stroma cells. Taken together, it appears that VDR is expressed in the luminal cell population and this expression is lost upon progression to IDC. This further suggests that BXL0124 does not act directly on the myoepithelial cell layer but may exert its anti-tumor effects through a paracrine mechanism from the luminal cells. The analysis of DCIS revealed increased VDR levels and decreased cell proliferation, providing a prevention strategy to inhibit the early progression of DCIS to IDC with the treatment of vitamin D or its analogs (Fig. 2.13, 2.14). These data suggest a novel mechanism in which down-regulation of VDR is synchronized with the loss of the critical myoepithelial cell layer and basement membrane.

2.5 Conclusion

Breast cancer progression is indicated by the loss of normal tissue architecture allowing invasion into surrounding tissue (47). In the present study, BXL0124 inhibited the progression of DCIS to IDC by maintaining the integrity of the myoepithelial cell layer and basement membrane. The inhibitory activity of BXL0124 on MMP mRNA expression is likely a contributor to the maintenance of DCIS organization and inhibition of tumor progression. Finally the tumor cell proliferation was reduced by BXL0124, likely due to the presence and maintenance of VDR in luminal cells as tumors progressed. This study with a novel Gemini vitamin D analog BXL0124 in the

MCF10DCIS model suggests a unique treatment modality preventing the progression of DCIS to an aggressive, invasive-like disease.

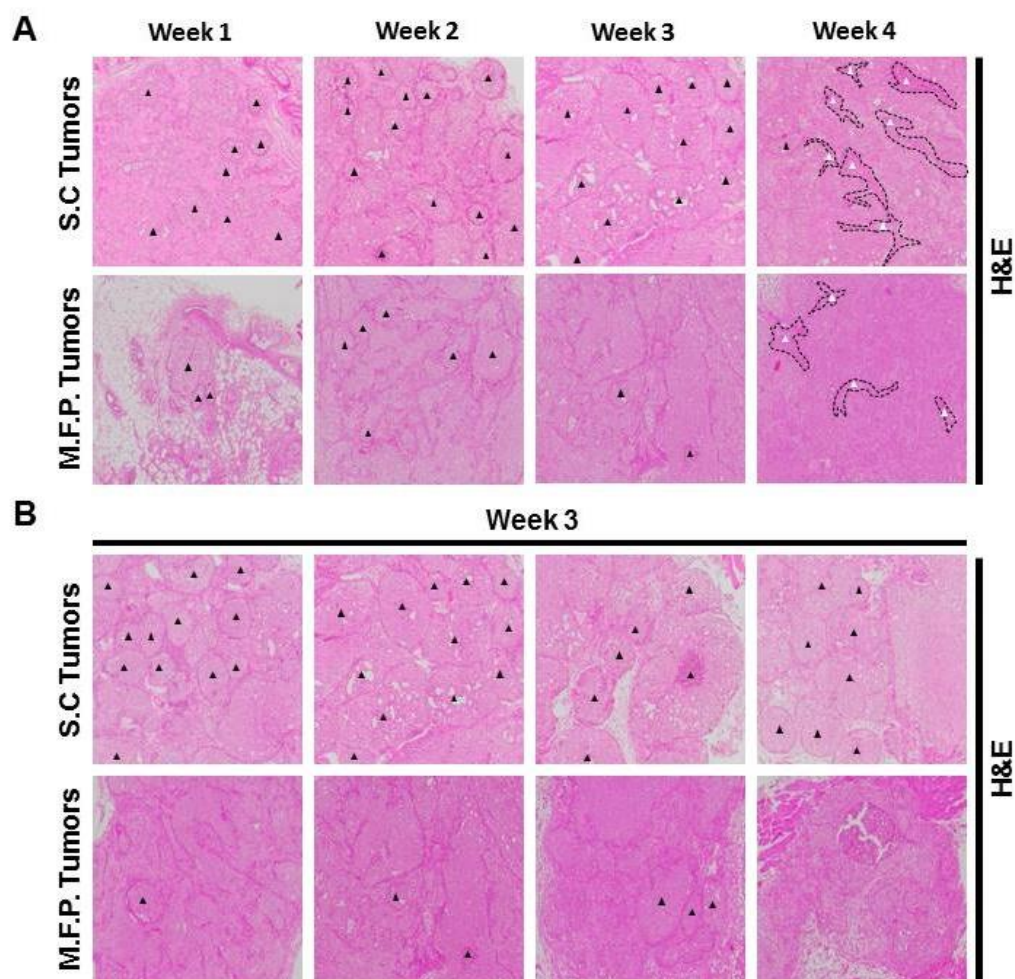


Figure 2.1 Comparison of the progression of untreated MCF10DCIS subcutaneous and mammary fat pad xenografts

(A) Representative hematoxylin and eosin (H&E) staining comparing the progression of MCF10DCIS subcutaneous and mammary fat pad untreated xenografts from one to four weeks. Black triangles mark centers of DCIS lesions within xenografts. White triangles inside dotted outlines mark areas of stromal invasion in week 4 tumors. (B) Comparison between subcutaneous and mammary fat pad xenografts at week 3. Each section

represents a tumor from a different mouse, exhibiting the higher number of DCIS lesions formed and the consistency in DCIS formation in the subcutaneous xenograft model compared to the orthotopic xenograft model. Black triangles mark centers of DCIS lesions within xenografts.

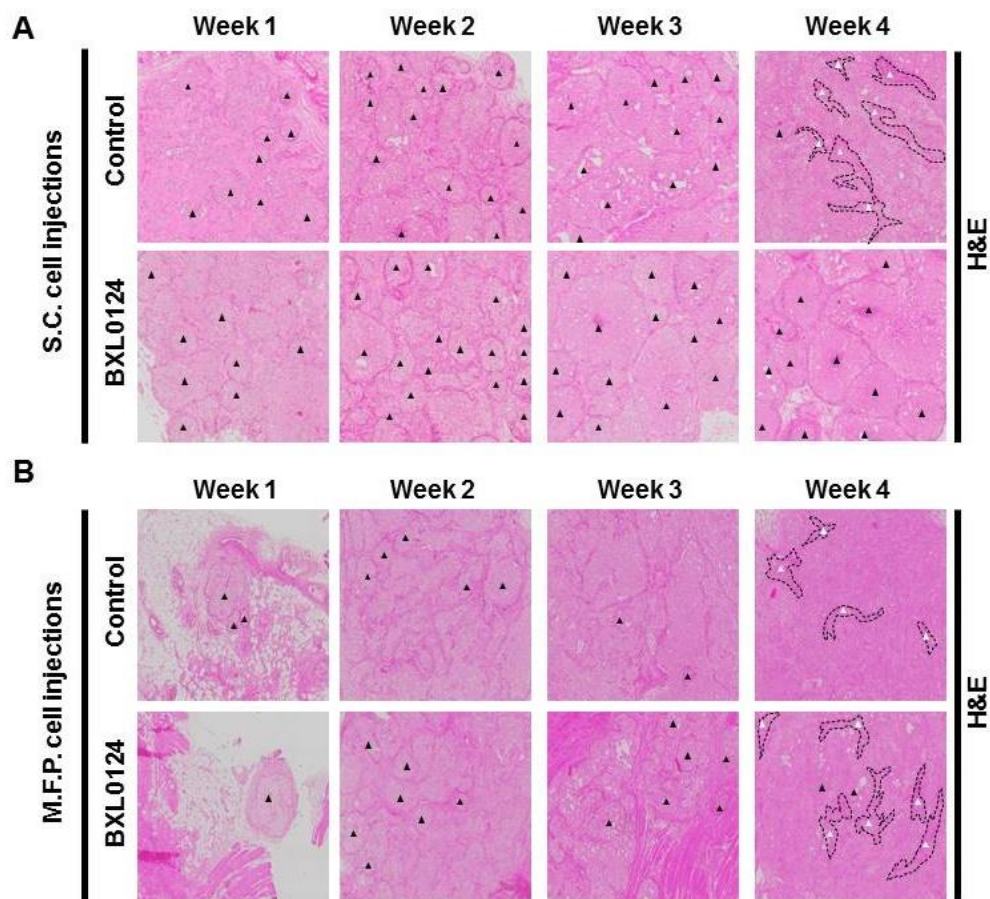


Figure 2.2 Comparison of the progression of MCF10DCIS subcutaneous and mammary fat pad xenografts treated with BXL0124

Representative hematoxylin and eosin (H&E) staining showing the progression of MCF10DCIS subcutaneous (**A**) and mammary fat pad xenografts (**B**) in nu/nu mice from weeks 1, 2, 3, and 4 (400x). Black triangles mark centers of DCIS lesions within xenografts. White triangles inside dotted outlines mark areas of stromal invasion in week 4 tumors.

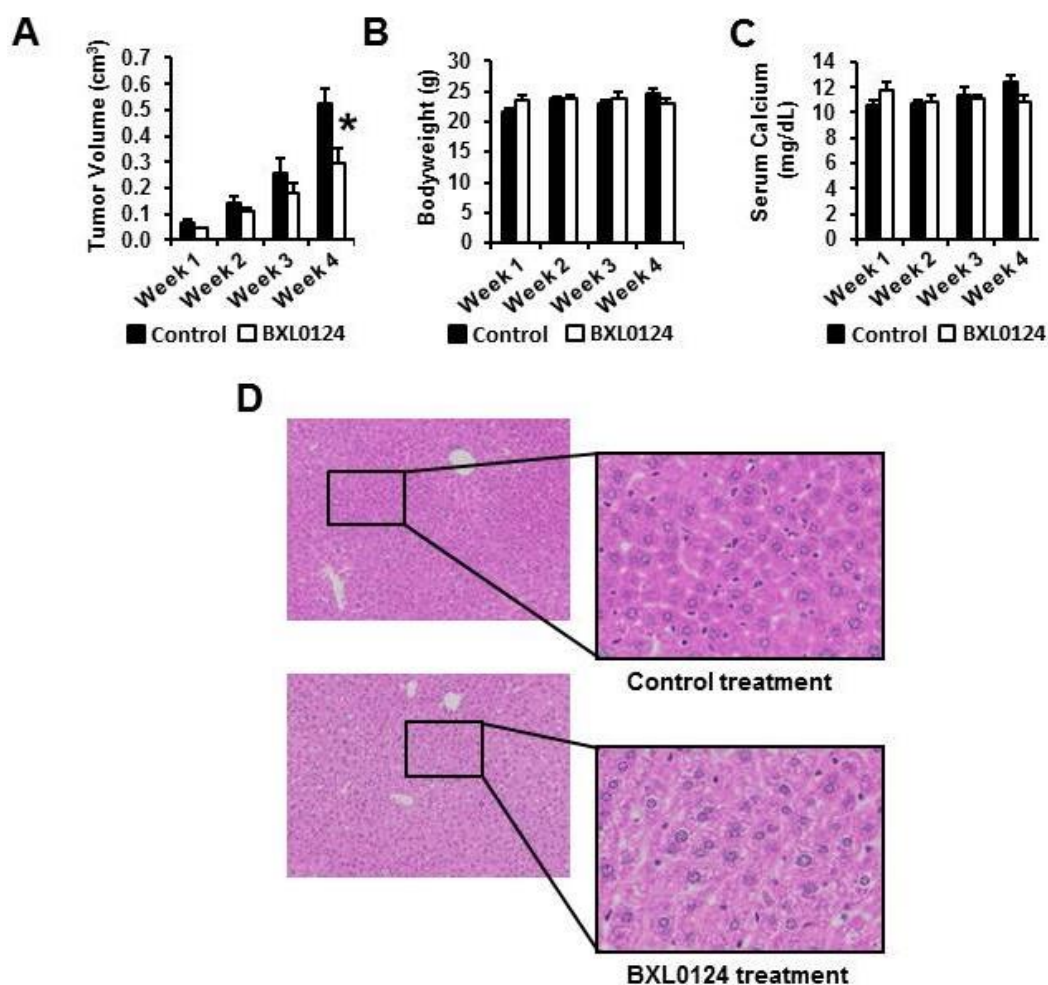


Figure 2.3 BXL0124 inhibits tumor growth in MCF10DCIS xenografts without hypercalcemia or hepatotoxicity

(A) Average tumor volume of MCF10DCIS subcutaneous xenografts at weekly time points is shown, * $p < 0.05$ ($n=5$ per group). Tumor volume (V ; cubed centimeters) was calculated using the equation $V = D \cdot d^2 / 2$ where D (centimeters) and d (centimeters) are the largest and smallest perpendicular diameters. (B) Average final bodyweight at necropsy is shown ($n=5$ per group) (C) Serum calcium determination to assess

hypercalcemic toxicity is shown (n=5 per group) **(D)** A representative hematoxylin and eosin (H&E) staining showing the histology of liver sections (5µm) from mice treated with BXL0124 and with vehicle control for 5 weeks, 100x magnification is shown, expanded magnification (400x) is shown for an enhanced view of cells.

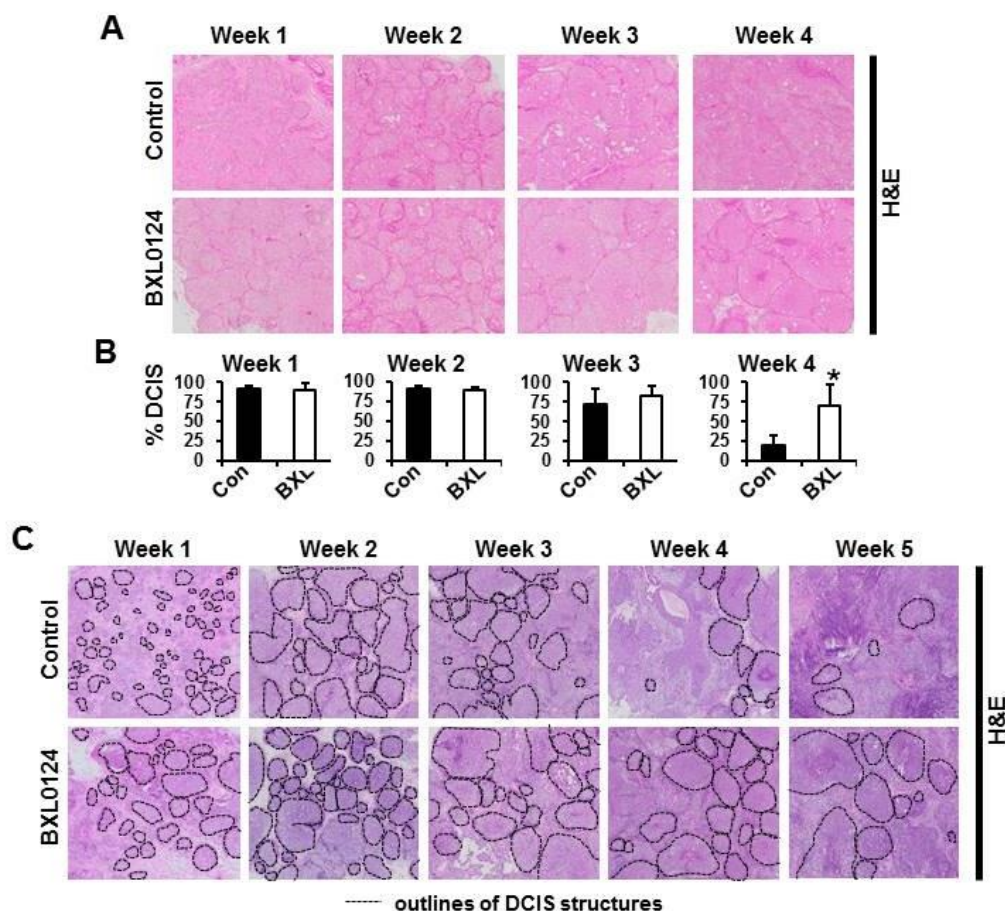


Figure 2.4 BXL0124 inhibits tumor progression to invasive ductal carcinoma in MCF10DCIS subcutaneous xenografts

(A) A representative hematoxylin and eosin (H&E) staining showing the progression of MCF10DCIS subcutaneous xenografts in nu/nu mice from weeks 1, 2, 3, and 4 (40x). (B) DCIS quantification, * $p < 0.05$ ($n=4$ per group) (C) A representative hematoxylin and eosin (H&E) staining showing the progression of MCF10DCIS subcutaneous xenografts in nu/nu mice from weeks 1, 2, 3, 4, and 5 (40x). Dotted lines represent the outlines of individual DCIS lesions for a visualization of the amount of DCIS in each H&E section.

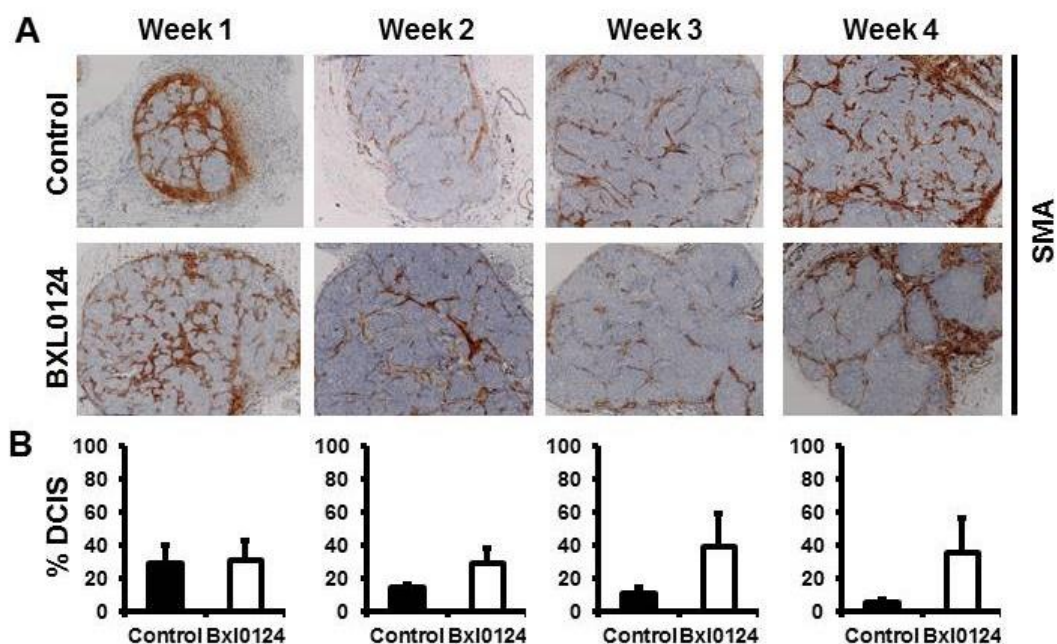


Figure 2.5 BXL0124 inhibits tumor progression to invasive ductal carcinoma in MCF10DCIS mammary fat pad xenografts.

(A) A representative immunohistochemical analysis of SMA in mammary fat pad tumor samples from weeks 1, 2, 3, and 4 is shown (100x). **(B)** DCIS quantification, (n=4 per group).

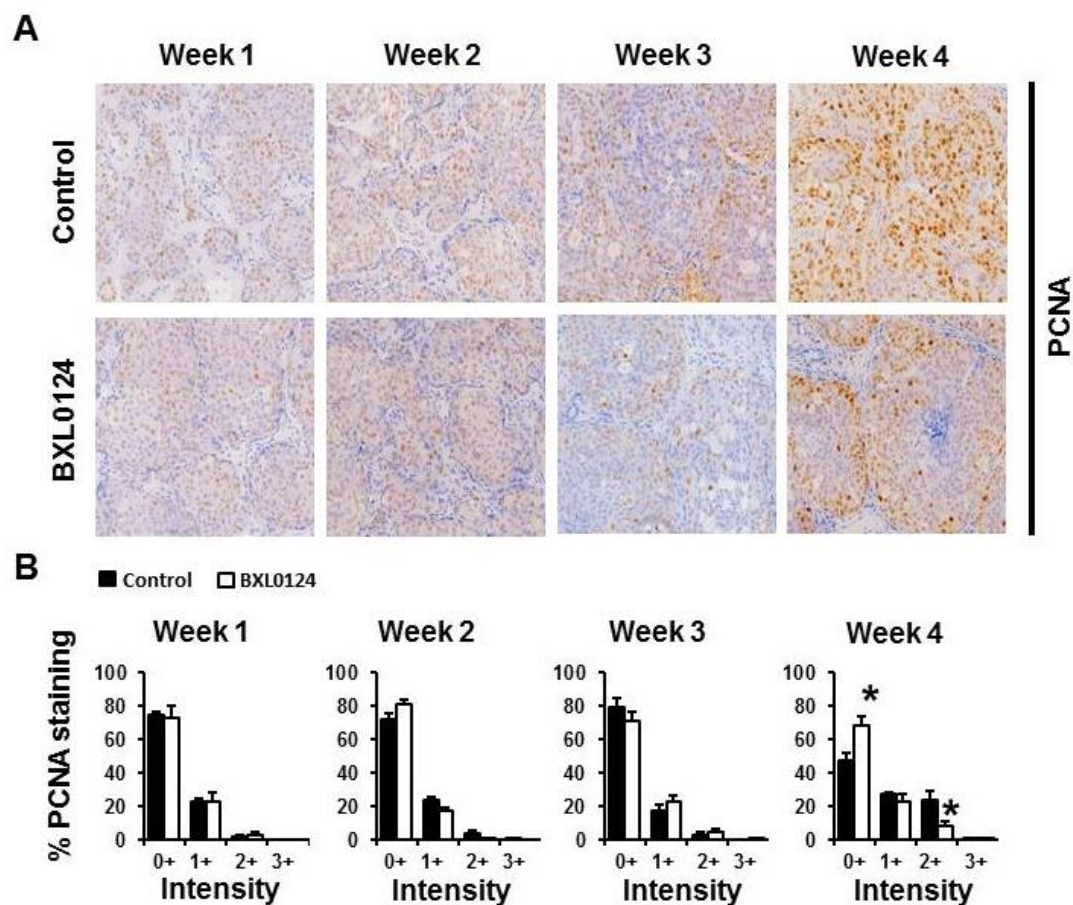


Figure 2.6 Treatment with BXL0124 decreases the proliferation of MCF10DCIS tumors at week 4

(A) A representative immunohistochemical analysis of PCNA in tumors from weeks 1, 2, 3, and 4 is shown (100x). PCNA-positive staining is found in the nucleus of the cells. (B) Four tumors from each group were blinded and quantified, three representative areas from each tumor were quantified for the intensity of PCNA staining, mean \pm S.E.M. The staining intensities were scored from 0+ (negative staining) to 3+ (the strongest staining), * $p < 0.05$.

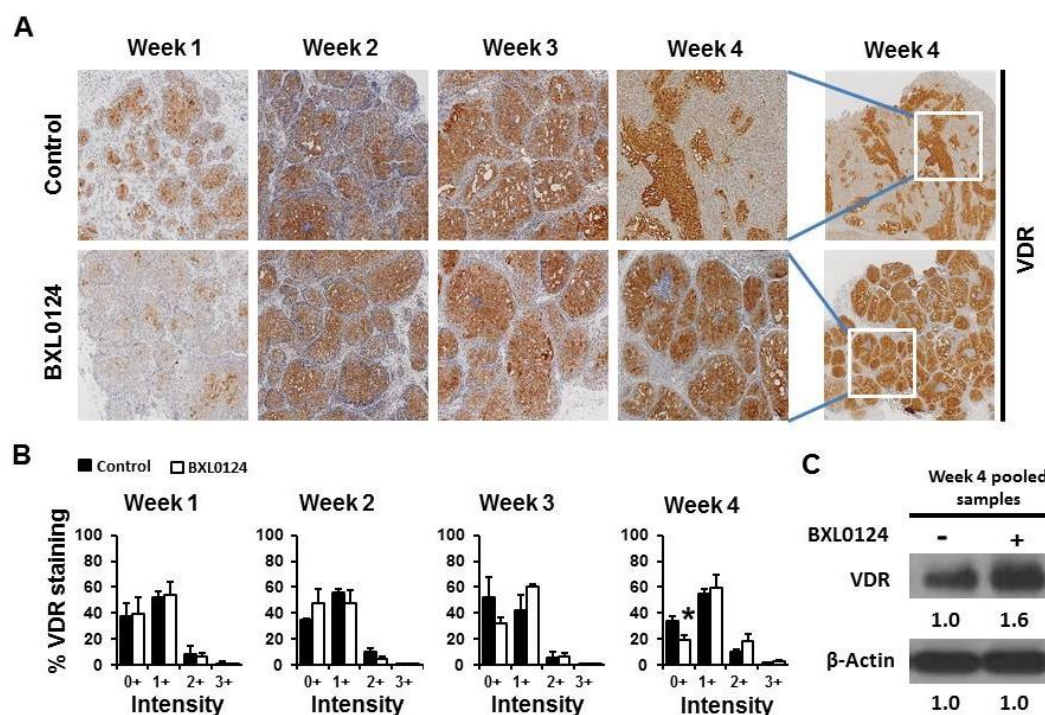


Figure 2.7 BXL0124 treatment inhibits the loss of vitamin D receptor (VDR) in MCF10DCIS tumors

(A) A representative immunohistochemical analysis for VDR from weeks 1, 2, 3, and 4 is shown (40x). VDR-positive staining is found in the cytoplasm and nucleus of the cells. Whole tumor mounts of VDR expression from week 4 is shown as a contracted view (10x). (B) Four tumors from each group were blinded and quantified and three representative areas from each tumor were quantified for the intensity of VDR staining, mean \pm S.E.M. The staining intensities were scored from 0+ (negative staining) to 3+ (the strongest staining), * $p < 0.05$. (C) The protein level of VDR was increased in the tumors of week 4 BXL0124 treated mice as shown by western blot analysis. Five

xenograft tumors from each group were combined for pooled samples. β -actin was used as a loading control.

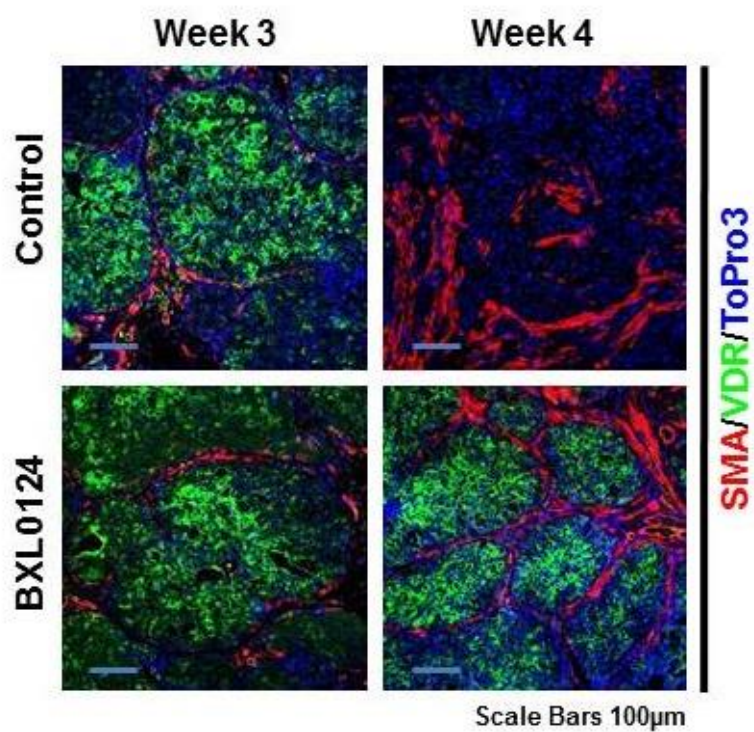


Figure 2.8 Immunofluorescence staining of vitamin D receptor (VDR) does not co-localize with smooth muscle actin (SMA) in MCF10DCIS xenografts.

A representative immunofluorescence staining with the myoepithelial cell marker, SMA (shown in red), and VDR (shown in green) on tumors from weeks 3 and 4 are shown (200x). Nuclei were stained with TO-PRO-3 (blue). Scale bars represent 100 μm.

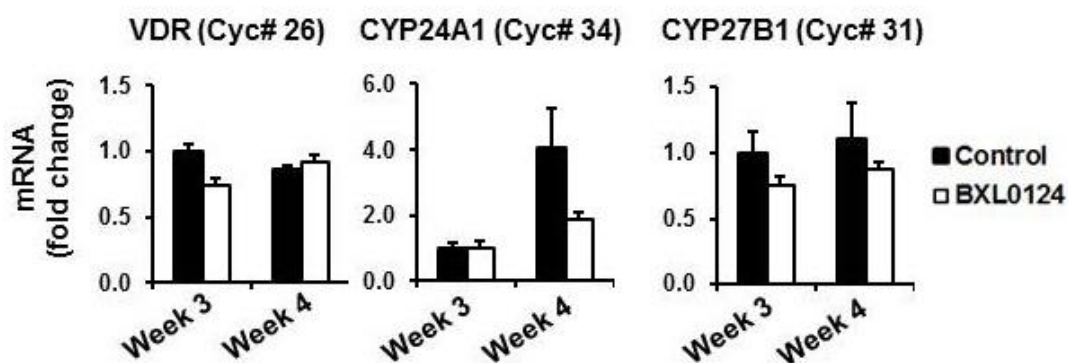


Figure 2.9 The expression of vitamin D receptor (*VDR*), and metabolizing enzymes, *CYP24A1* (catabolism) and *CYP27B1* (synthesis), in MCF10DCIS subcutaneous xenografts treated with BXL0124 at weeks 3 and 4

qPCR analysis of mRNA expression of the vitamin D receptor (*VDR*) and vitamin D metabolizing enzymes, *CYP24A1* (catabolism) and *CYP27B1* (synthesis), is shown from MCF10DCIS subcutaneous xenograft samples from weeks 3 and 4, mean \pm S.E.M (n=5 per group). The cycle number is provided in parenthesis.

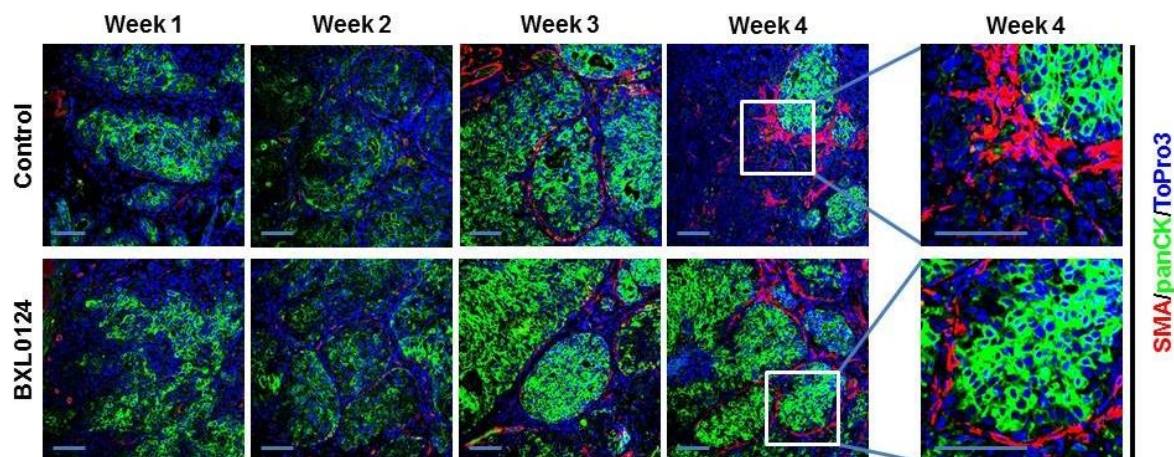


Figure 2.10 Treatment with BXL0124 inhibits progression to invasive ductal carcinoma by maintaining the myoepithelial cell layer.

Treatment with BXL0124 inhibits DCIS progression to IDC by maintaining the myoepithelial cell layer. A representative immunofluorescence staining for tumor samples from weeks 1, 2, 3, and 4 with the myoepithelial cell marker smooth muscle actin (SMA, shown in red) and the epithelial cell marker pancytokeratin (panCK, shown in green) is shown (200x). Nuclei were stained with TO-PRO-3 (blue). Expanded magnification is shown for specific areas from week 4 tumors. Scale bars represent 100 μm.

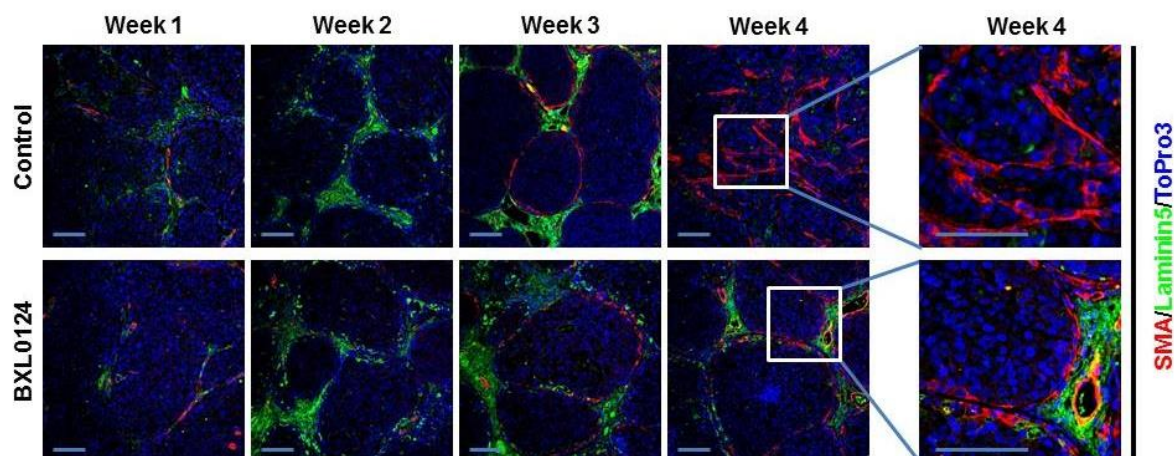


Figure 2.11 Treatment with BXL0124 maintains the basement membrane in ductal carcinoma in situ structures.

Treatment with BXL0124 maintains the basement membrane. A representative immunofluorescence staining with the myoepithelial cell marker SMA (shown in red) and the basal membrane marker laminin 5 (shown in green) on tumors from weeks 1, 2, 3, and 4 is shown (200x). Nuclei were stained with TO-PRO-3 (blue). Expanded magnification is shown for specific areas from week 4 tumors. Scale bars represent 100 μm.

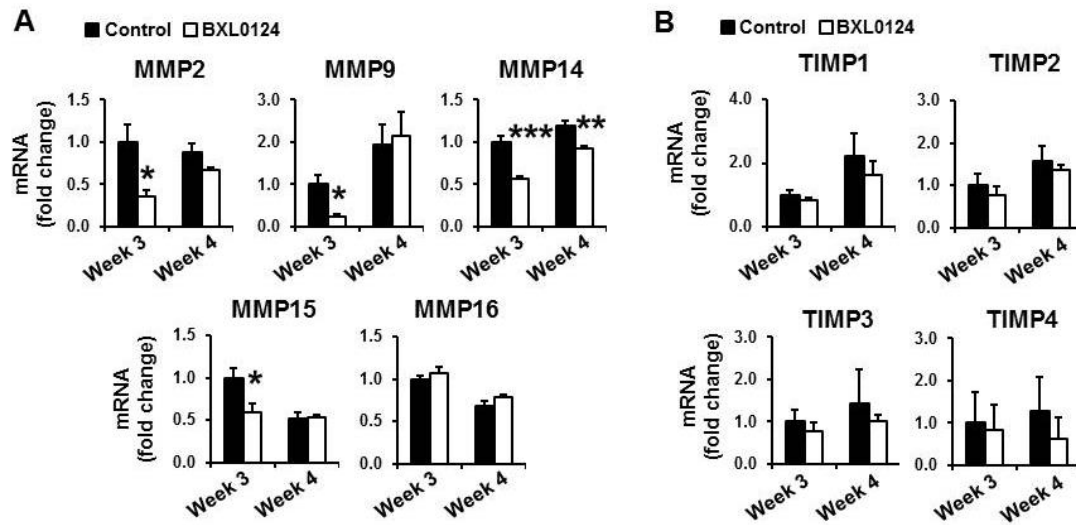


Figure 2.12 BXL0124 inhibits the mRNA expression levels of the matrix metalloproteinases during DCIS to IDC progression

(A) qPCR analysis of MMP mRNA levels in MCF10DCIS tumors from weeks 3 and 4 is shown, mean \pm S.E.M., Cycle numbers are shown in parenthesis: *MMP2* (25), *MMP9* (28), *MMP14* (23), *MMP15* (28), and *MMP16* (25). Statistical significance refers to the respective week control, * $p < 0.05$, ** $p < 0.01$, *** $p < 0.001$ ($n=3-5$ per group). (B) qPCR analysis of tissue inhibitor of matrix metalloproteinases (TIMP) mRNA levels in MCF10DCIS tumors from weeks 3 and 4 is shown, mean \pm S.E.M., Cycle numbers are shown in parenthesis: *TIMP1* (30), *TIMP2* (26), *TIMP3* (24), *TIMP4* (33), ($n=3-5$ per group).

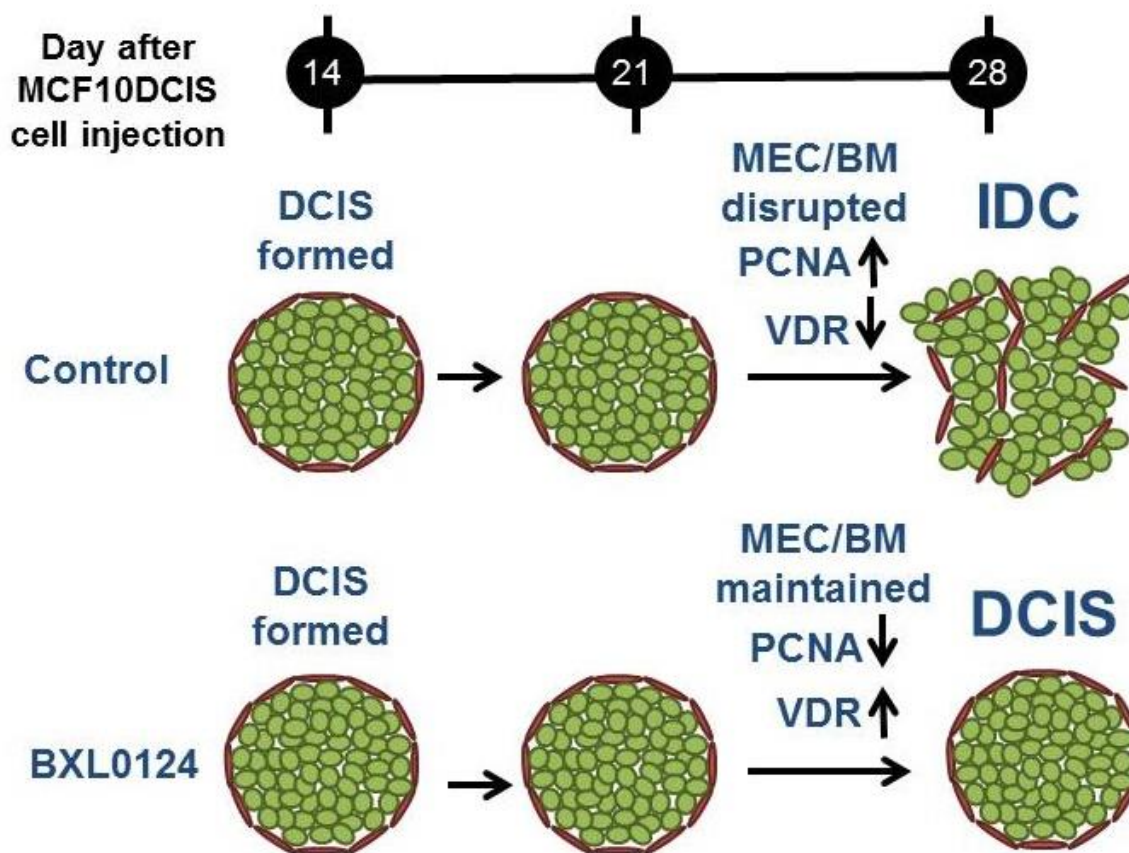


Figure 2.13 Summary of the effects of BXL0124 treatment on MCF10DCIS xenografts.

Abbreviations: DCIS – ductal carcinoma *in situ*; IDC – invasive ductal carcinoma;

MEC – myoepithelial cell layer; BM- basement membrane; PCNA – proliferating cell nuclear antigen; VDR – vitamin D receptor

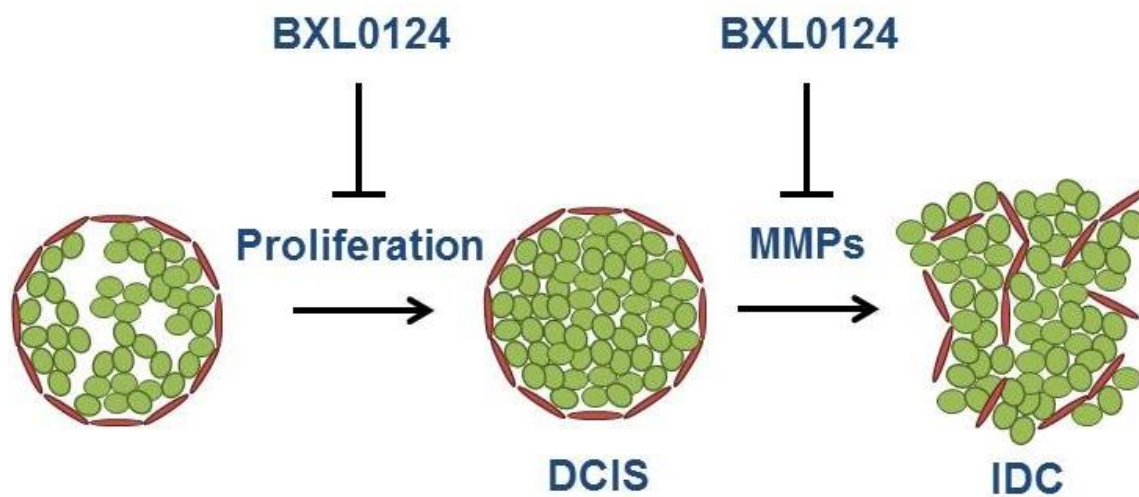


Figure 2.14 Summary of BXL0124 effects on breast cancer progression

Abbreviations: DCIS – ductal carcinoma *in situ*; IDC – invasive ductal carcinoma;

MMPs – matrix metalloproteinases

Chapter 3: Vitamin D receptor is differentially expressed in from normal to malignant tissue

3.1 Rationale

Vitamin D receptor (VDR) is expressed in various cell types of the mammary gland. Vitamin D treatment inhibits breast cancer cell proliferation, induces cell apoptosis, and prevents carcinogenesis in models of breast cancer (216, 217). We have previously demonstrated that a Gemini Vitamin D analog inhibits breast cancer tumor growth *in vivo* and works in a VDR-dependent manner (147, 218). We observed that the VDR is expressed in early stages of an *in vivo* model of breast cancer progression, but is sequentially lost as DCIS-like lesions progress to invasive disease (218). There is limited data on VDR levels during the clinical progression of breast cancer from premalignant lesions to advanced disease. Due to the necessity of VDR in breast cancer to utilize endogenous vitamin D as well as exogenous forms of the compound, such as BXL0124, as a preventative or treatment option, we assessed VDR levels in samples of breast tissue from patients having various stages of the disease.

3.2 Materials and Methods

3.2.1 Patient Samples

Patient samples were acquired from the Biospecimen Repository Service tissue bank, under the administrative control of The Cancer Institute of New Jersey (CINJ). The

study was approved by the UMDNJ institutional review board and CINJ Scientific Review Board. We randomly identified 11 patient samples from the available breast cancer samples containing ductal carcinoma *in situ* or invasive disease. These breast tissues were obtained from women who had undergone mastectomy to remove their breast cancer. Frozen samples of tumors and normal tissue, and unstained cut slides from paraffin embedded tumors were acquired. The tissue sample (tumor and normal adjacent breast tissue) was collected and snap frozen in liquid nitrogen or fixed in formalin for 24 hours, and then embedded in paraffin. These samples were assessed by a pathologist at the facilities to establish clinicopathologic features (Table 3.1).

3.2.2. Immunohistochemical (IHC) Analysis

Tumor sections were received from the Biospecimen Repository Service at The Cancer Institute of New Jersey (CINJ) cut at 5 μ m thickness and mounted on slides. Sections were stained as previously described with antibodies to vitamin D receptor (VDR) (1:200, Santa Cruz Biotechnology, sc-13133, Santa Cruz, CA) (200). The sections were counterstained with Harris hematoxylin (Sigma Aldrich, St. Louis, MO).

3.2.3. Western Blot Analysis

The procedures have been described previously (200). Five tumor samples from each group were homogenized and pooled for analysis. Primary antibodies against VDR (1:200, Thermoscientific, MA1-710, Waltham, MA) and β -actin (1:2000, Sigma-Aldrich,

A1978, St. Louis, MO) were used for analysis. Secondary antibodies were from Santa Cruz Biotechnology. Western Blots were quantified by using ImageJ software (US National Institutes of Health, Bethesda, MD) and calculating the relative density of the bands using the gel analyzer command. Bands from VDR levels were normalized to the loading control, β -actin.

3.2.4. Statistical analysis

Statistical significance was evaluated using the Student's t-test.

3.3 Results

3.3.1 The vitamin D receptor is expressed in clinical breast cancer samples at different stages of progression

VDR was assessed in clinical tumor samples by immunohistochemistry staining. VDR was expressed in tumor samples at different stages of progression. VDR was expressed but did not show localization to a specific cell type or region within tumors (Fig. 3.1). Western blot analysis was performed to attain more quantifiable measurements of VDR levels in the tumors. Normalized quantification of VDR western blots is labelled below the VDR blot and gave relative density values ranging from 0.2 to 1.1 (Fig. 3.2). These western blot results reconfirmed VDR expression in all tumor samples and that expression varied between tumors. We did not observe significant correlations of VDR

levels with histological type (DCIS/IDC) or receptor status of the tumors, however it is important to note that the small sample size may not portray a full picture (Table 3.1).

3.3.2 The vitamin D receptor was not differentially expressed in DCIS or IDC from the same patient

In the two samples that contained lesions of DCIS and invasive disease, VDR was analyzed by immunohistochemistry staining against the different histological areas within the same patient. The areas consisting of both DCIS and IDC expressed VDR. VDR was found not to be differentially expressed between these two tumor types in the same individual (Fig. 3.3).

3.3.3. Vitamin D receptor levels were lower in tumor tissue compared to normal adjacent breast tissue

VDR levels from the clinical samples were analyzed by western blot. Breast cancer samples (labeled with T) were compared to adjacent normal breast tissue (labelled with N) for VDR protein levels. Quantification of VDR normalized to β -actin as loading control is labelled under the VDR blots. The results consistently show that expression of VDR in normal tissue was higher than that in the tumor-containing tissue (Fig 3.4). The quantification of western blots is represented in a bar graph normalized to VDR expression in corresponding normal tissue. From these results we show that tumor

containing tissue showed 64% lower levels of VDR compared to the normal adjacent breast tissue from the same patients ($p < 0.01$), (Fig. 3.4).

3.4 Discussion

Breast cancer is a heterogeneous disease associated with various outcomes and responses to therapies. Vitamin D and its analogs have been suggested as prevention and treatment methods for breast cancer (179). They act through the vitamin D receptor (VDR), hence making clinical VDR expression essential for the utilization of vitamin D and its analogs in the treatment of breast cancer (147, 179, 219). We investigated the expression of VDR in 11 clinical samples comprising normal breast, carcinomas *in situ*, and invasive carcinoma.

The VDR is expressed in clinical breast cancer samples at different stages of progression from normal mammary tissue to invasive disease. We observed that VDR was expressed in normal adjacent breast tissue and its levels were diminished in tumor containing tissue from the same patient. This suggests that the malignant transformation of normal cells could induce the down-regulation of VDR leading to reduced expression observed in *in situ* and invasive carcinomas. Consistent with our results, immunohistochemical studies on human tissue have shown that VDR is expressed in normal breast tissues (153, 220). Lopes et al. demonstrated that the normal mammary gland expressed VDR in 100% of cases assessed and a reduction in the percentage of positive cases was observed in carcinomas *in situ* (47.3%) and in invasive carcinomas (56.2%) (153). These results are also consistent with our study which showed that VDR

was not differentially expressed in *in situ* and invasive carcinomas from the same patient. The molecular composition of DCIS and invasive cancer from the same patients are frequently found to be closely related on the basis of their gene expression profiles (221-223). Therefore it is not surprising that the VDR levels are similar between DCIS and IDC in the same patient in the samples that were analyzed. It is important to note that normal and malignant tissues were derived from different patients in the Lopes study and our study assessed normal and malignant tissues within the same patient. This design was to gain a better understanding of how VDR progresses within individual patients.

These results show that VDR is differentially expressed from normal mammary tissue to early lesions of breast cancer, suggesting that vitamin D or its analogs could have an added benefit during different stages of breast cancer progression. Clinically, vitamin D can be utilized in a variety of breast cancer cases but would be most effective in a preventative setting due to higher levels of VDR expression in normal breast tissues.

3.5 Conclusion

From these studies we conclude that during the malignant transformation of mammary cells, tumor cells lose their ability to maintain their VDR levels and in turn might have a lower response rate to the active form of vitamin D. These studies also show the presence of VDR in normal mammary tissue and in tumors from clinical samples, suggesting the potential of vitamin D supplementation as a preventative or treatment strategy. Despite these results and consistencies with the literature, it is

important to note that this is a small sample set, and in order to verify these results it is necessary to analyze a much larger sample size.

Table 3.1 Pathological analysis of clinical breast cancer samples

	Clinical Sample	Pathological Analysis	Receptor Status	Relative VDR levels from western quantification
Ductal	4301	Ductal hyperplasia (recurrent)	N/A	0.3
	3417	High grade comedo DCIS	N/A	1.0
	3988	DCIS	ER- PR+ Her2+	0.3
	4285	Intracystic/intraductal papillary carcinoma (IPC)	ER+ PR+	0.6
Mixed	4110	DCIS and IDC	ER+ PR+ Her2-	0.6
	4021	DCIS and IDC	ER+ PR+ Her2+	0.5
Invasive	3353	IDC	ER- PR- Her2-	0.5
	3940	IDC	ER+ PR-	0.9
	4005	IDC	ER+ PR- Her2-	0.2
	4039	Infiltrating lobular carcinoma (ILC)	ER+ PR+ Her2+	1.1
	4247	Invasive micropapillary carcinoma (IMPC)	ER+ PR+ Her2+	0.5

DCIS - ductal carcinoma *in situ*; IDC - Infiltrating/Invasive ductal carcinoma

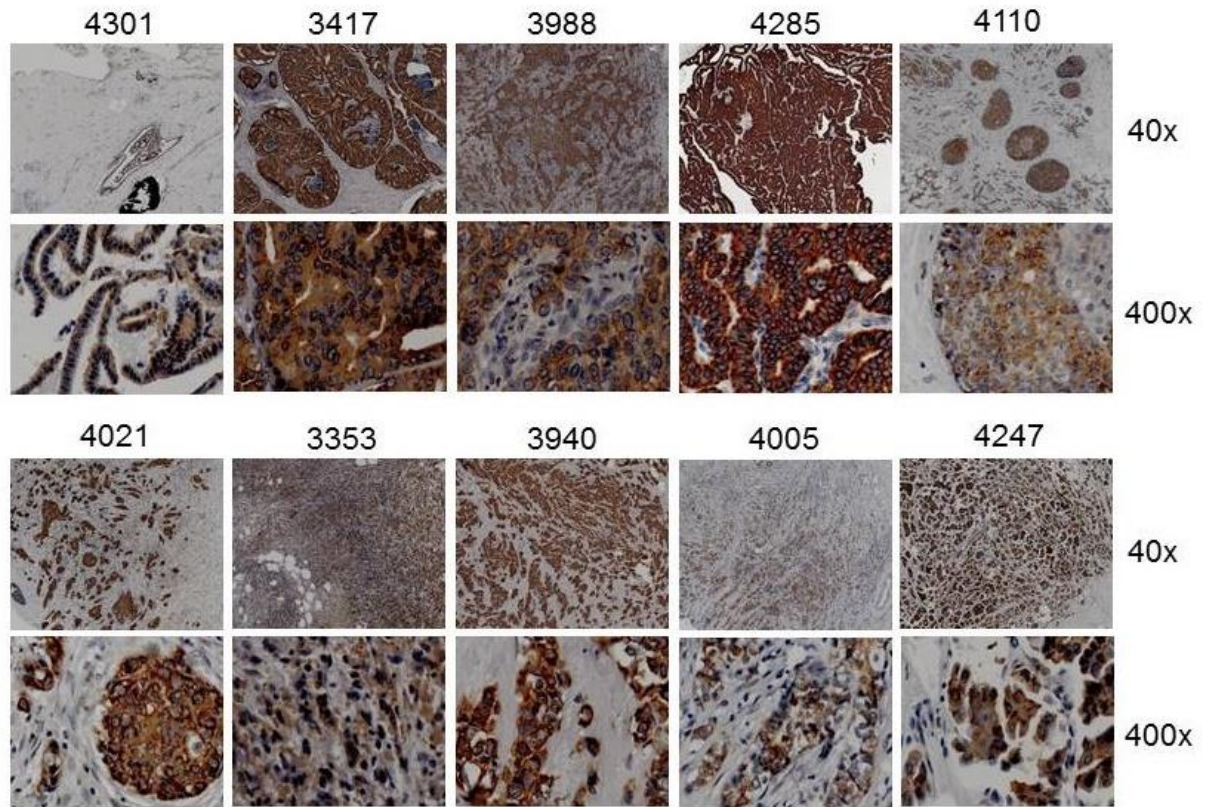


Figure 3.1 Vitamin D receptor is expressed in clinical breast cancer samples at different stages of progression.

Immunohistochemistry for VDR in individual tumors samples from patients with pre-malignant lesions or invasive disease. Panels are 40x and 400x magnifications. Numbers indicate patient sample ID numbers; each number represents a tumor from a different patient.

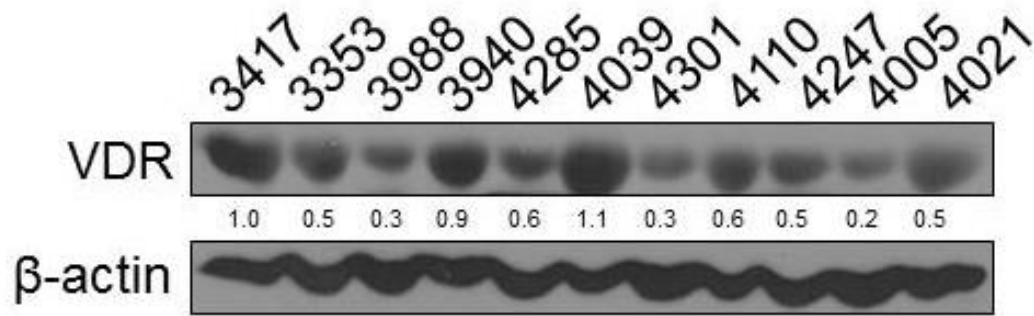


Figure 3.2 Vitamin D receptor is expressed to varying degrees in clinical breast cancer samples.

Western blot analysis of vitamin D receptor levels is shown. Numbers above western blot indicate patient sample ID numbers; each number represents a tumor from a different patient. Numbers below the western blot represent quantification of western blot by densitometric analysis using ImageJ software. The VDR quantification was normalized to the β -actin loading control.

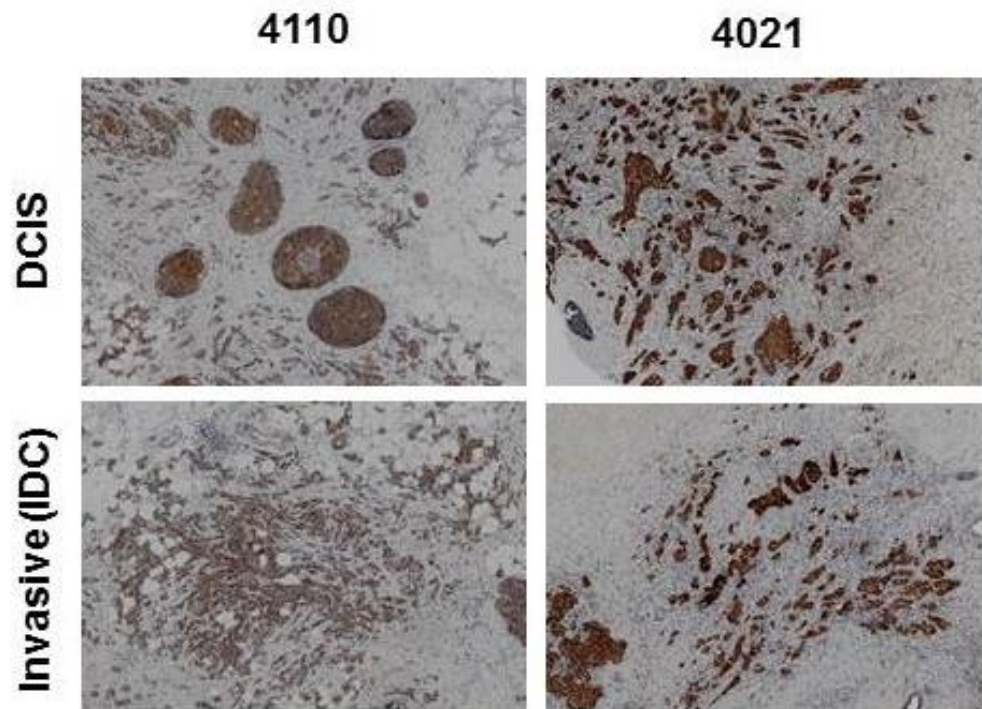


Figure 3.3 Vitamin D receptor was not differentially expressed in DCIS or IDC lesions from the same patient.

Immunohistochemistry for VDR in clinical samples containing both lesions of ductal carcinoma in situ (DCIS) and invasive ductal carcinoma (IDC). Panels are 40x magnification. Numbers above panels represent patient sample numbers: each number represents a tumor from a different patient.

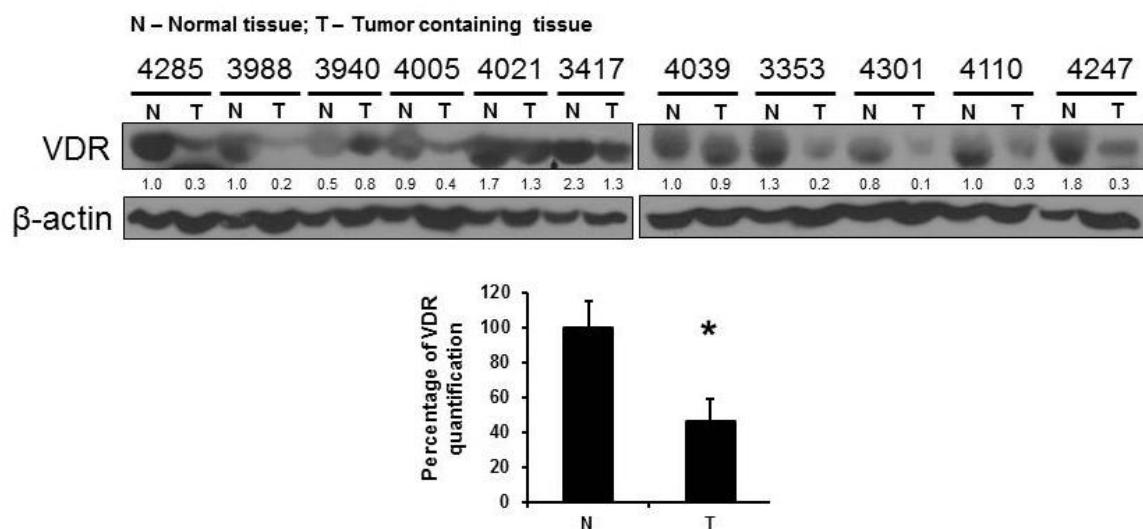


Figure 3.4 Vitamin D receptor (VDR) levels were lower in tumor tissue compared to normal adjacent breast tissue from the same patient.

Western blot analysis of vitamin receptor (VDR) is shown. Tissues were analyzed for VDR levels in tumor containing tissue (designated as T) and normal tissue (designated as N). The normal adjacent breast tissue was acquired from the same patient as the tumor containing tissue. Quantification of the VDR western blot was performed by densitometry and normalized to the β -actin loading control. This was represented as a bar graph with the normal tissue samples set to 100% and tumor tissue represented as a percentage of the VDR levels in normal tissue, mean \pm S.E.M., * $p < 0.01$.

Chapter 4: Vitamin D compounds repress mammosphere formation and decrease expression of stem cell markers in breast cancer

Note: Sections of this chapter have been reproduced from the following publication:

Wahler, J., So, J.Y., Cheng, L.C., Maehr, H., Uskokovic, M., Suh, N. (2015) Vitamin D compounds reduce mammosphere formation and decrease expression of putative stem cell markers in breast cancer. *J Steroid Biochem Mol Bio.* 148:148-55.

4.1. Rationale

Based on the results presented in Chapter 2, BXL0124 maintained the integrity of critical structures related to non-cancerous breast lesions which are typically lost during the progression to malignant disease, suggesting that BXL0124 slows the progression of breast cancer in the MCF10DCIS xenograft model of breast cancer. Recent studies demonstrated that a cancer stem cell-like population identified within basal-like DCIS has the capacity to drive malignant progression to IDC (224). We previously showed that the vitamin D analog, BXL0124, repressed CD44, a key surface marker in cancer stem cells, suggesting that it could be a potential agent to target breast cancer stem cells (BCSCs) (147).

Since BCSCs have been implicated in DCIS progression, we investigated the effects of vitamin D compounds on the breast cancer stem cell-like population and stem cell properties. A hallmark of breast cancer stem cells is their ability to form anchorage-

independent spherical colonies *in vitro* known as mammospheres. In order to study BCSCs, we utilized breast cancer cell lines in mammospheres-forming assays. These assays have been used in various tissue types for the quantification of stem cell activity and self-renewal (132). The formation of primary mammospheres is a measure of stem cell and early progenitor activity (225). The ability to specifically target the BCSC subpopulation has important implications in the treatment and prevention of breast cancer with vitamin D compounds.

4.2. Materials and Methods

4.2.1. Reagents and Cell Culture

$1\alpha,25(\text{OH})_2\text{D}_3$ and a Gemini vitamin D analog [BXL0124; $1\alpha,25$ -dihydroxy-20R-21(3-hydroxy-3-deuteromethyl-4,4,4-trideuterobutyl)-23-yne-26,27-hexafluoro-cholecalciferol, >95% purity] (Figure 1) were provided by BioXell, Inc. (Nutley, NJ) and dissolved in dimethyl sulfoxide (DMSO). The MCF10DCIS human breast cell line was provided by Dr. Fred Miller at the Barbara Ann Karmanos Cancer Institute (Detroit, MI). The MCF10DCIS cell line was authenticated by short tandem repeat profiling at American Type Culture Collection (ATCC, Manassas, VA). MCF10DCIS human breast cancer cells were maintained in Dulbecco's Modified Eagle's Medium (DMEM)/F12 medium supplemented with 5% horse serum, 1% penicillin/streptomycin, and 1% HEPES solution at 37°C, 5% CO₂. MCF10A (normal breast epithelial cells) and MCF-7 cells were acquired from ATCC. MCF10A cells were grown in DMEM/F12 medium, 5% horse serum, 1% penicillin/streptomycin, 10 mM HEPES solution, 500 ng/ml

hydrocortisone (Stemcell Technologies, Vancouver, BC), 20 ng/ml epidermal growth factor (EGF) (Sigma Aldrich, St. Louis, MO), 10 µg/ml insulin (Life Technologies, Carlsbad, CA) and 100 ng/ml cholera toxin (Sigma Aldrich, St. Louis, MO). MCF-7 cells were maintained in DMEM/F-12 supplemented with 10% fetal bovine serum and 1% penicillin/streptomycin at 37°C and 5% CO₂. 17-β estradiol was purchased from Sigma Aldrich (E2758, St. Louis, MO) and dissolved in ethanol. SUM159 breast cancer cells were purchased from Asterand (Detroit, MI). SUM159 cells were grown in Ham's F-12 culture medium supplemented with 5% fetal bovine serum, 1% penicillin/streptomycin, 1 µg/ml hydrocortisone and 5 µg/ml insulin at 37°C and 5% CO₂.

4.2.2. Mammosphere Forming Assay

MCF10A or MCF10DCIS cells were grown to 50-70% confluence and cells were detached with StemPro Accutase (Life Technologies). MCF10A and MCF10DCIS cells were plated at 10,000 cells/mL in 6-well ultra-low attachment plates (Corning Inc., Corning, NY). MCF-7 and SUM159 cells were plated at 2,000 cells/mL in 24-well ultra-low attachment plates. Mammosphere colonies were maintained in MammoCult serum-free medium supplemented with hydrocortisone and 0.2% heparin (Stem Cell Technologies). For MCF-7 cells supplemented with 17-β estradiol (E2758, Sigma Aldrich, St. Louis, MO) cells were grown in phenol red free, serum free mammary epithelial basal medium (CC-3153, MEBM, Lonza, Walkersville, MD), supplemented with 2% B27 supplement (17504-044, Gibco ThermoFisher Scientific, Grand Island, NY), 20 ng/ml epidermal growth factor (EGF) (E9644, Sigma Aldrich, St. Louis, MO),

20 ng/ml basic fibroblast growth factor (PHG0264, Gibco ThermoFisher Scientific, Grand Island, NY), 0.5 µg/ml hydrocortisone (07904, Stem Cell Technologies), and 5 µg/ml bovine insulin (I6634, Sigma Aldrich, St. Louis, MO). Cells were treated with $1\alpha25(\text{OH})_2\text{D}_3$ (100 nM) or BXL0124 (10 nM). For secondary and tertiary mammosphere culture, primary mammospheres were collected and enzymatically dissociated using StemPro Accutase (Life Technologies). Then, cells were re-plated at a density of 5,000 cells/mL (MCF10DCIS) or 2,000 cells/mL (MCF-7 and SUM159) for subsequent passages. Images of mammospheres were taken using an overhead light microscope, and the number of mammospheres per well was counted using the lowest magnification (20x) to determine the mammosphere forming efficiency (MFE). The MFE was calculated by dividing the number of mammospheres (≥ 100 µm) formed by the number of single cells seeded. Roundness of spheres was obtained by analysis of photos with ImageJ software (US National Institutes of Health, Bethesda, MD). The formula used to calculate roundness is $4 \times ([\text{area}]/\pi[\text{major axis}]^2)$. A value of 1.0 represents an object that is uniformly rounded. A value of 0.0 represents an object that is formless. Experiments were repeated in triplicates.

4.2.3. Flow Cytometry

In monolayer cell culture, MCF10DCIS, SUM159, or MCF-7 cells were grown for 48 h. In mammosphere cell culture cells were plated at concentrations of 5,000 cells/mL (MCF10DCIS) or 2,000 cells/mL (MCF-7 and SUM159) and grown for 5 days. Cells were harvested and processed for further analysis. The detailed procedure was

described previously (147). MCF10DCIS cells were stained with antibodies against CD44-FITC (Cat. 555478), CD49f-FITC (Cat. 561893) ESA-PE (Cat. 347198), and CD24-PE (Cat. 555428) from BD Biosciences (San Jose, CA) and ESA-FITC (Cat. MCA1870F) from AbD Serotec (Raleigh, NC). The stained cells were analyzed by flow cytometry using an FC500 Analyzer (Beckman Coulter) to determine the percentage of different CD44/CD24, CD49f/CD24, ESA/CD49f, and CD24/ESA subpopulations. The acquisition of $\geq 10,000$ cells per treatment was analyzed.

4.2.4. Quantitative Real-Time Polymerase Chain Reaction Analysis

These procedures have been reported previously (201, 202). The Taqman® probe-based gene expression system from Applied Biosystems (Foster City, CA) was used to detect the genes of interest. Labeled primers for *GAPDH* (Hs02758991), *CD44* (Hs01075861), *ITGA6* (Hs01041011), *ITGB6* (Hs00168458), *LAMA5* (Hs00966585), *CD24* (Hs03044178), *NOTCH1* (Hs01062014), *JAG1* (Hs01070032), *JAG2* (Hs00171432), *NFKB1* (Hs00765730), *OCT4* (*POU5F1*) (Hs00999634), *GATA3* (Hs00231122), *KLF4* (Hs00358836), *SOX2* (Hs01053049), and *MYC* (Hs00153108) were used in analysis.

4.2.5. Annexin-FITC Apoptosis Assay

The procedures have been described previously (226). The apoptosis assay was performed using an apoptosis kit (BD Biosciences, San Jose, CA) according to the

manufacturer's instructions. MCF10DCIS cells were plated at 5,000 cells/mL in 6-well ultra-low attachment plates and treated with $1\alpha 25(\text{OH})_2\text{D}_3$ (100 nM) or BXL0124 (10 nM) for 5 days. Mammospheres were then trypsinized to form a single cell suspension. Cells were resuspended in binding buffer at a density of 10^6 cells/mL. Cells were stained with Annexin V-FITC and propidium iodide, and analyzed by flow cytometry.

4.2.6. Western Blot Analysis

The procedures have been described previously (200). Whole-cell lysates (15 $\mu\text{g}/\text{lane}$) were resolved in 4% to 20% SDS-PAGE from Bio-Rad (Hercules, CA). Blots were then probed with the indicated antibodies. Primary antibodies against CD44 (sc-7297, 1:200), which recognizes both CD44s (standard form) and CD44v (variant form), NF κ B (sc-372, 1:200) and cyclin D1 (sc-718, 1:200) were from Santa Cruz Biotechnology (Santa Cruz, CA); CD49f (3750, 1:1000), Notch1 (4380, 1:1000), c-Notch1 (4147, 1:1000), and pNF κ B (3031, 1:1000) were from Cell Signaling Technology (Beverly, MA); CD24 (555426, 1:200) was from BD Biosciences (San Jose, CA), proliferating cell nuclear antigen (PCNA) (M0879, 1:400) was from Dako (Carpinteria, CA), and β -actin (A1978, 1:2000) was from Sigma-Aldrich (St. Louis, MO). Secondary antibodies were from Santa Cruz Biotechnology.

4.2.7. Xenograft studies

All animal studies were approved by the Institutional Review Board for the Animal Care and Facilities Committee of Rutgers University. Female nude mice (5-6 weeks old) were purchased from Charles River Laboratories (Wilmington, MA). They were allowed to acclimate to the facility for two weeks at which time they were injected (7-8 weeks old) with human MCF10DCIS cells (10^5 cells) from monolayer or mammosphere cell culture into the mammary fat pad. Tumors were palpated twice per week and total body weights were measured weekly. Tumors were measured with a vernier caliper and tumor volume (V; cubed centimeters) was calculated using the equation $V = D \cdot d^2 / 2$ where D (centimeters) and d (centimeters) are the largest and smallest perpendicular diameters. Animals were sacrificed 45 days after injection at which time tumors were excised and weighed.

4.2.8. Statistical analysis

Statistical significance was evaluated using the Student's t-test.

4.3. Results

4.3.1. Mammosphere cell culture enriches for putative breast cancer stem cell populations and markers of pluripotency in the MCF10DCIS cell line

To validate the use of mammosphere cell culture as a method that enriches for breast cancer stem cells (BCSCs), we assessed markers of cancer stem cells in monolayer cell culture and compared this to mammosphere cell culture. Flow cytometry analysis of

CD44/CD24 was first examined. We observed an increase in the putative CD44⁺/CD24^{-/low} breast cancer stem cell population in mammosphere cell culture compared to monolayer cell culture (Fig. 4.1A). This was confirmed with an increase in the CD49f⁺/CD24^{-/low} subpopulation in mammosphere cell culture (Fig. 4.1A). Mammosphere cell culture did not enrich for the putative CD49f⁺/ESA⁺ stem cell subpopulation since monolayer cell culture was already 100% CD49f⁺/ESA⁺ (Fig. 4.1A). This also suggests that ESA may not be an effective marker in MCF10DCIS to enrich for the breast cancer stem cell population since cells are already 100% ESA⁺.

Genes involved in pluripotency and maintenance of the stem cell population were also enriched in mammosphere cell culture. These included the transcription factor *OCT4* which increased by 2-fold in mammosphere cell culture ($p < 0.05$), (Fig. 4.1B). Expression of *GATA3*, a transcription factor regulating luminal-epithelial differentiation, was also increased 5-fold in mammosphere cell culture ($p < 0.05$), (Fig. 4.1B). Transcription factor *KLF4* (Kruppel-like factor 4) expression was increased 8-fold ($p < 0.05$), (Fig. 4.1B). The expression of transcription factor *SOX2* demonstrated a 9.5-fold increase in mammosphere cell culture over monolayer culture ($p < 0.05$), (Fig. 4.1B). Transcription factor *MYC* was decreased by 64% in mammosphere cell culture ($p < 0.05$), (Fig. 4.1B). The increased expression of these genes in mammospheres cell culture suggests the enrichment of a cell population that is capable of increased self-renewal and differentiation to multiple cell lineages.

4.3.2. $1\alpha 25(\text{OH})_2\text{D}_3$ and BXL0124 reduce the mammosphere forming efficiency and alter the mammosphere phenotype of MCF10DCIS cells

Initially a dose range finding assay was performed to optimize the dose of $1\alpha 25(\text{OH})_2\text{D}_3$ and BXL0124 to use in further assays. Treatment with $1\alpha 25(\text{OH})_2\text{D}_3$ (10nM, 100nM) or BXL0124 (1nM, 10nM, 100nM) significantly reduced the mammosphere forming efficiency (MFE) of MCF10DCIS mammospheres at all doses tested (Fig. 4.2). We selected a dose of 10nM for BXL0124 and a dose of 100nM for $1\alpha 25(\text{OH})_2\text{D}_3$ based on previous studies which showed that a dose of $1\alpha 25(\text{OH})_2\text{D}_3$ 10-fold higher than that of BXL0124 is typically need to achieve the same biological effects (202).

In mammosphere cultures, MCF10DCIS cells began to form colonies of 100 μm in size starting at day 3 (data not shown). The mammospheres continued to grow in size and number through days 4 and 5. Between days 5 and 7, the number of mammospheres began to decrease. We analyzed mammospheres at their peak of growth at days 4 and 5, as well as when their number began to decrease at day 7. Spheres that formed from MCF10DCIS cells were irregularly shaped and formless (Fig. 4.3A). When these spheres were grown in the presence of $1\alpha 25(\text{OH})_2\text{D}_3$ or BXL0124, they showed a more round and uniform shape (Fig. 4.3A). Spheres from the normal mammary epithelial cell line, MCF10A, appeared relatively round and uniform, and there was no significant change in the MCF10A mammosphere shape in the presence of $1\alpha 25(\text{OH})_2\text{D}_3$ or BXL0124 (Fig. 4.3A). As shown in Figure 4.3B, treatment of MCF10DCIS mammospheres with $1\alpha 25(\text{OH})_2\text{D}_3$ or BXL0124 for 4, 5, and 7 days resulted in an overall increase in the

roundness of spheres. Day 5 showed the most significant difference with an increase of 35.4% with $1\alpha25(\text{OH})_2\text{D}_3$ ($p < 0.01$) and an increase of 35.6% with BXL0124 ($p < 0.01$). Treatment with $1\alpha25(\text{OH})_2\text{D}_3$ or BXL0124 did not show significant changes in the roundness of spheres in MCF10A cells (Fig. 4.3B). The mammosphere forming efficiency (MFE) of MCF10DCIS was 0.12% and 0.12% at days 4 and 5 respectively, and by day 7 the MFE was reduced to 0.06% in the control. Treatment with $1\alpha25(\text{OH})_2\text{D}_3$ significantly reduced the MFE of MCF10DCIS mammospheres at day 4 (38.8% inhibition, $p < 0.01$), day 5 (58.0% inhibition, $p < 0.01$), and day 7 (47.1% inhibition, $p < 0.05$) (Fig. 4.3C). The treatment with BXL0124 also inhibited the MFE of MCF10DCIS mammospheres at day 4 (40.8% inhibition, $p < 0.01$), day 5 (53.8% inhibition, $p < 0.01$), and day 7 (48.6% inhibition, $p < 0.01$) (Fig. 4.3C). Although $1\alpha25(\text{OH})_2\text{D}_3$ and BXL0124 modestly affected the MFE in MCF10A cells, the changes were not statistically significant (Fig. 4.3C).

4.3.3. $1\alpha25(\text{OH})_2\text{D}_3$ and BXL0124 inhibit the proliferation and decrease the expression of putative stem cell markers in MCF10DCIS mammospheres

MCF10DCIS mammospheres treated with vitamin D compounds demonstrated decreased cellular proliferation, as indicated by the reduction of protein levels of cyclin D1 and proliferating cell nuclear antigen (PCNA) (Fig. 4.4A). However, treatment of MCF10DCIS mammospheres with $1\alpha25(\text{OH})_2\text{D}_3$ and BXL0124 did not induce apoptosis (Fig. 4.4B).

Putative stem cell markers were analyzed to further characterize the effects that were observed in mammospheres. As early as day 4, treatment with vitamin D compounds showed a reduction in the protein levels of markers of stem cell maintenance and stem cell signaling molecules, such as CD44s (standard form) and CD44v (variant form), CD49f, cleaved-Notch1 (c-Notch1; the activated form of Notch1), and phosphorylated NFκB (pNFκB) (Fig. 4.5A). The reduction of these markers by vitamin D compounds persisted through days 5 and 7 of treatment, with the exception of pNFκB at day 7, which did not change upon treatment. The levels of total Notch1, NFκB, and CD24 were unaffected by treatment with vitamin D compounds (Fig. 4.5A).

The mRNA levels of key markers associated with stem cell maintenance, such as *CD44*, *ITGA6*, *ITGB6*, *LAMA5*, and *CD24*, were assessed at day 5. The expression of these markers decreased upon treatment with vitamin D compounds (Fig. 4.6A). Cell surface receptor *CD44* expression was decreased by 65% and 73% with $1\alpha25(\text{OH})_2\text{D}_3$ ($p < 0.01$) and BXL0124 ($p < 0.01$), respectively. Integrin *ITGA6* expression was decreased by 63% and 72% with $1\alpha25(\text{OH})_2\text{D}_3$ ($p < 0.01$) and BXL0124 ($p < 0.01$), respectively. Expression of another integrin, *ITGB6*, was decreased by 48% and 56% with $1\alpha25(\text{OH})_2\text{D}_3$ ($p < 0.01$) and BXL0124 ($p < 0.01$), respectively. *LAMA5* expression was decreased by 66% and 70% with $1\alpha25(\text{OH})_2\text{D}_3$ ($p < 0.01$) and BXL0124 ($p < 0.01$), respectively. *CD24* expression was modestly decreased by 26% and 40% with $1\alpha25(\text{OH})_2\text{D}_3$ ($p < 0.01$) and BXL0124 ($p < 0.01$), respectively.

Treatment with vitamin D compounds also reduced the expression of key molecules involved in stem cell signaling such as *NOTCH1*, Jagged ligands, and *NFKB1*

(Fig. 4.6B). Receptor *NOTCH1* expression was decreased by 72% and 84% with $1\alpha25(\text{OH})_2\text{D}_3$ ($p < 0.01$) and BXL0124 ($p < 0.01$), respectively. Ligand *JAG1* expression was decreased by 54% and 65% with $1\alpha25(\text{OH})_2\text{D}_3$ ($p < 0.01$) and BXL0124 ($p < 0.01$), respectively. Another ligand, *JAG2* expression was decreased by 69% and 75% with $1\alpha25(\text{OH})_2\text{D}_3$ ($p < 0.01$) and BXL0124 ($p < 0.01$), respectively. *NFKB1* expression was decreased by 62% and 66% with $1\alpha25(\text{OH})_2\text{D}_3$ ($p < 0.01$) and BXL0124 ($p < 0.01$), respectively.

Genes involved in pluripotency and maintenance of the stem cell population were also suppressed, including *OCT4* by 74% and 79% with $1\alpha25(\text{OH})_2\text{D}_3$ ($p < 0.01$) and BXL0124 ($p < 0.01$), respectively (Fig. 4.6C). Expression of *GATA3*, a transcription factor regulating luminal-epithelial differentiation, was decreased by 76% and 78% with $1\alpha25(\text{OH})_2\text{D}_3$ ($p < 0.01$) and BXL0124 ($p < 0.01$), respectively. Transcription factor *KLF4* (Kruppel-like factor 4) expression was decreased by 53% and 53% with $1\alpha25(\text{OH})_2\text{D}_3$ ($p < 0.01$) and BXL0124 ($p < 0.01$), respectively. The expression of transcription factors *SOX2* and *MYC* were slightly decreased with $1\alpha25(\text{OH})_2\text{D}_3$ and BXL0124.

4.3.4. $1\alpha25(\text{OH})_2\text{D}_3$ and BXL0124 inhibits the self-renewal of MCF10DCIS mammospheres

Control spheres that formed from MCF10DCIS cells showed an irregular and formless shape in primary, secondary and tertiary mammospheres (Fig. 4.7A). When

MCF10DCIS spheres were grown in the presence of $1\alpha 25(\text{OH})_2\text{D}_3$ (100 nM) or BXL0124 (10 nM), they showed a more round and uniform shape (Fig. 4.7B). The mammosphere forming efficiency (MFE) of MCF10DCIS primary mammospheres was significantly reduced upon treatment with $1\alpha 25(\text{OH})_2\text{D}_3$ (37.2% inhibition, $p < 0.01$) or BXL0124 (48.0% inhibition, $p < 0.01$) (Fig. 4.7A). Importantly, the MFE of mammospheres was increased from primary (0.24%) to secondary (0.50%) passages. Similar to the results with primary mammospheres, the MFE of secondary mammospheres was significantly repressed with $1\alpha 25(\text{OH})_2\text{D}_3$ (52.6% inhibition, $p < 0.01$) or BXL0124 (50.6% inhibition, $p < 0.01$). Tertiary mammospheres had a MFE of 0.56% in the control, and MFE was inhibited by $1\alpha 25(\text{OH})_2\text{D}_3$ (46.5% inhibition, $p < 0.01$) or BXL0124 (41.7% inhibition, $p < 0.01$) (Fig. 4.7A).

4.3.5. Mammosphere cell culture enriches for putative breast cancer stem cell populations and markers of pluripotency in SUM159 and MCF-7 cell lines

To confirm the results observed in the MCF10DCIS cell line, we investigated the effects of $1\alpha 25(\text{OH})_2\text{D}_3$ or BXL0124 on two additional cell lines, SUM159 and MCF-7. To validate the use of mammosphere cell culture with SUM159 and MCF-7 we assessed markers of cancer stem cells in monolayer cell culture and compared this to mammosphere cell culture. Flow cytometry analysis of CD24/ESA was first examined. We observed an increase in the putative $\text{CD}24^{\text{low}}/\text{ESA}^+$ breast cancer stem cell population in mammosphere cell culture in SUM159 (Fig. 4.8). The $\text{CD}24^{\text{low}}/\text{ESA}^+$ subpopulation was increased from 1.6% in monolayer conditions to 10.8% in mammosphere cell culture ($p <$

0.05) (Fig. 4.8). Similarly, the CD24⁻/ESA⁺ subpopulation in MCF-7 cells was enriched in mammosphere conditions. CD24⁻/ESA⁺ increased from 0% in monolayer to 1.9% in mammosphere cell culture ($p < 0.05$) (Fig. 4.8).

4.3.6. $1\alpha 25(\text{OH})_2\text{D}_3$ and BXL0124 inhibits the mammosphere forming efficiency in SUM159 and MCF-7 cell lines

Initially a dose range finding assay was performed for SUM159 and MCF-7 to optimize the dose of $1\alpha 25(\text{OH})_2\text{D}_3$ and BXL0124 to be used in further assays. The MFE of SUM159 was significantly reduced upon treatment with $1\alpha 25(\text{OH})_2\text{D}_3$ at 10nM (44.7% inhibition, $p < 0.05$) and 100nM (46.3% inhibition, $p < 0.05$) (Fig. 4.9A). The MFE of SUM159 was also significantly reduced with BXL0124 at 1nM (50.4% inhibition, $p < 0.05$), 10nM (52.8% inhibition, $p < 0.05$) and 100nM (76.4% inhibition, $p < 0.05$) (Fig. 4.9A). The MFE of MCF-7 was significantly reduced upon treatment with $1\alpha 25(\text{OH})_2\text{D}_3$ at 100nM (58.7% inhibition, $p < 0.05$) (Fig. 4.9B). The MFE of MCF-7 was significantly reduced in a dose dependent manner with BXL0124 at 1nM (46.7% inhibition, $p < 0.05$), 10nM (64.7% inhibition, $p < 0.05$) and 100nM (78.7% inhibition, $p < 0.05$) (Fig. 4.9A). Based on these results and previous studies we selected a dose of 10nM for BXL0124 and a dose of 100nM for $1\alpha 25(\text{OH})_2\text{D}_3$ for further studies (202).

4.3.7. $1\alpha 25(\text{OH})_2\text{D}_3$ and BXL0124 decrease the self-renewal of SUM159 mammospheres

Primary SUM159 mammospheres were larger compared to secondary and tertiary mammospheres (Fig. 4.10B). When SUM159 mammospheres were grown in the presence of $1\alpha 25(\text{OH})_2\text{D}_3$ (100 nM) or BXL0124 (10 nM), the number of colonies was decreased (Fig. 4.10B). The mammosphere forming efficiency (MFE) of SUM159 primary mammospheres was significantly reduced upon treatment with $1\alpha 25(\text{OH})_2\text{D}_3$ (60.6% inhibition, $p < 0.01$) or BXL0124 (64.7% inhibition, $p < 0.01$) (Fig. 4.10A). The MFE was increased from primary (1.11%) to secondary (1.69%) passages, suggesting enrichment of a subpopulation with self-renewal capacity. Similar to the results with primary mammospheres, the MFE of secondary mammospheres was significantly repressed with $1\alpha 25(\text{OH})_2\text{D}_3$ (60.7% inhibition, $p < 0.01$) or BXL0124 (62.4% inhibition, $p < 0.01$). Tertiary mammospheres had a MFE of 2.87% in the control, again suggesting further enrichment of a subpopulation with self-renewal capacity. The MFE was inhibited by $1\alpha 25(\text{OH})_2\text{D}_3$ (69.7% inhibition, $p < 0.01$) or BXL0124 (71.6% inhibition, $p < 0.01$) (Fig. 4.10A).

4.3.8. $1\alpha 25(\text{OH})_2\text{D}_3$ and BXL0124 decrease the self-renewal of MCF-7 mammospheres

Primary MCF-7 mammosphere were larger compared to secondary and tertiary mammospheres (Fig. 4.11B). When MCF-7 spheres were grown in the presence of $1\alpha 25(\text{OH})_2\text{D}_3$ (100 nM) or BXL0124 (10 nM), the number of colonies were decreased (Fig. 4.10B). The mammosphere forming efficiency (MFE) of MCF-7 primary mammospheres was significantly reduced upon treatment with $1\alpha 25(\text{OH})_2\text{D}_3$ (64.4%

inhibition, $p < 0.01$) or BXL0124 (71.2% inhibition, $p < 0.01$) (Fig. 4.11A). Similarly the MFE of secondary mammospheres was significantly repressed with $1\alpha25(\text{OH})_2\text{D}_3$ (82.0% inhibition, $p < 0.01$) or BXL0124 (95.0% inhibition, $p < 0.01$). Tertiary MFE was inhibited by $1\alpha25(\text{OH})_2\text{D}_3$ (80.5% inhibition, $p < 0.01$) or BXL0124 (78.8% inhibition, $p < 0.01$) (Fig. 4.11A). The MFE was decreased from primary (5.3%) to secondary (2.5%) passages, and further decreased in tertiary passages (1.5%), suggesting a decreased self-renewal capacity during serial passage in MCF-7 cells (Fig. 4.11A).

4.3.9. $1\alpha25(\text{OH})_2\text{D}_3$ and BXL0124 decrease the self-renewal of MCF-7 mammospheres supplemented with estradiol

Since MCF-7 cells are strongly dependent on estradiol supplementation for optimal growth, we assessed MFE of MCF-7 in the presence of 17β -estradiol (E2) and vitamin D compounds. Primary and secondary MCF-7 mammospheres supplemented with E2 were larger compared to control spheres without E2 (Fig. 4.12B). We observed that $1\alpha25(\text{OH})_2\text{D}_3$ and BXL0124 inhibited the estrogen-induced MFE in MCF-7 secondary mammospheres. The mammosphere forming efficiency (MFE) of MCF-7 primary mammospheres was increased by 25% when supplemented with E2 (1nM) (Fig 4.12A). The MFE of E2 treated spheres was significantly reduced upon treatment with $1\alpha25(\text{OH})_2\text{D}_3$ (50.2% inhibition, $p < 0.01$) or BXL0124 (50.7% inhibition, $p < 0.01$) (Fig. 4.12A).

Untreated primary spheres were passed to secondary mammospheres. E2 (1nM) supplementation increased sphere formation by 55% from untreated secondary spheres.

This estrogen-induced increase was repressed with $1\alpha,25(\text{OH})_2\text{D}_3$ (30.3% inhibition, $p < 0.01$) or BXL0124 (29.5% inhibition, $p < 0.01$). The MFE of untreated spheres was decreased from primary (3.57%) to secondary (0.87%) passages. E2 treated primary spheres were also passed to secondary mammospheres. E2 (1nM) supplementation increased untreated secondary spheres by 88%. This estrogen-induced increase was repressed with $1\alpha,25(\text{OH})_2\text{D}_3$ (41.1% inhibition, $p < 0.01$) or BXL0124 (33.2% inhibition, $p < 0.01$). There was a decrease in MFE from E2 treated primary spheres (4.46%) to E2 treated secondary spheres (1.55%), again suggesting a decreased self-renewal capacity during serial passage, even in MCF-7 spheres supplemented with E2 (Fig. 4.12A).

4.3.10. Mammosphere cell culture did not show enhanced tumor initiating capacity when compared to monolayer cell culture *in vivo*

Animals were injected with 1×10^5 MCF10DCIS cells grown in either monolayer or mammosphere conditions. There was a difference in tumor initiation between monolayer (32 days) or mammosphere (28 days) cell culture, although this was not a significant statistically due to small sample size (Fig. 4.13A,C). Monolayer cell culture formed tumors in two of three injected mice and mammosphere cells formed tumors in three of three injected mice (Fig. 4.13C). This data suggests that there could be increased tumorigenic potential of mammosphere cells over monolayer conditions; however the sample set is three mice per group and this data should be reconfirmed with a larger number of animals. Tumors were allowed to grow for 65 days at which point animals were sacrificed and tumors analyzed. The growth rates of monolayer tumors were not

significantly different than mammosphere tumors (Fig. 4.13A). Final tumor weights were not significantly different from monolayer (0.53g) to mammosphere (0.65g) (Fig. 4.13B). Despite these results it should be noted that the sample size was small and should be increased to further confirm the results.

4.4. Discussion

Accumulating evidence has shown that breast cancer stem cells (BCSCs) are responsible for the initiation, maintenance, and progression of breast cancer (224). Mammosphere cell culture, which produces spherical colonies enriched in stem and progenitor cells, has also been widely used to study pathways and properties of stem and progenitor cells (131). Utilizing the mammosphere forming assay, we have shown that vitamin D compounds significantly decreased the putative BCSC population and reduced mammosphere formation. Our data, in part, contribute to the mechanism by which vitamin D compounds reduce breast tumor growth, and point to effects mediated at the level of putative breast cancer stem cells.

Treatment with vitamin D compounds suppressed mammosphere formation of MCF10DCIS, SUM159, and MCF-7 breast cancer cells (Fig. 4.2, 4.9A,B). Since the mammosphere forming assay enriches for stem and progenitor cells (Fig. 4.1, 4.8), the reduction of MFE with vitamin D compounds could partially be due to the ability to suppress the putative BCSC populations. Although mammosphere cell culture enriches for the putative BCSC population *in vitro*, *in vivo* pilot studies did not show significant differences between monolayer or mammosphere cells in xenografts. It is important to

note that this was a small sample size and further studies should be performed to confirm or disprove these results.

Treatment with vitamin D compounds reduced cell proliferation but did not induce apoptosis in MCF10DCIS mammospheres (Fig. 4.4A-B). The data suggest that the reduction of MFE is primarily due to reduced growth of mammospheres and regulation of putative stem cell signaling pathways, rather than the killing of the BCSC-like cells. The irregular shape formed from MCF10DCIS cells grown in mammospheres was altered to a more round appearance by $1\alpha25(\text{OH})_2\text{D}_3$ and BXL0124 treatment. This round shape is similar to the appearance of the normal MCF10A cell line. The shape and MFE of MCF10A remained unchanged with vitamin D compound treatment, suggesting the ineffectiveness of vitamin D on normal cell types. Although the change from irregular spheres to more round spheres has not traditionally been linked to stem cells phenotype, it has recently been reported with the chemotherapeutic drug, paclitaxel, in MCF-7 mammospheres (227). These phenotypic changes of sphere shape were not observed in SUM159 or MCF-7 mammospheres when treated with vitamin D compounds, suggesting that this phenotypic change is cell type specific to MCF10DCIS cells. This could be linked to the unique characteristics of this cell line, which can differentiate to multiple lineages, including myoepithelial and luminal lineages. If vitamin D compounds can affect this differentiation, then spheres could express different structural proteins, and hence change the phenotype of the mammospheres. The overall effects on mammospheres indicate that treatment with vitamin D compounds could alter the characteristics of the stem cell population to that of a less malignant cell type.

To further investigate the role of $1\alpha,25(\text{OH})_2\text{D}_3$ and BXL0124 in the inhibition of stem cells, we analyzed markers commonly associated with stem cell maintenance and signaling. CD44 is a transmembrane glycoprotein which is involved in malignant progression and metastasis of breast cancer (228). Knockdown of CD44 induces differentiation and drives the BCSC-like population toward a non-BCSC-like phenotype (229). Knock down of $\alpha 6$ -integrin/ITGA6, also known as CD49f, causes a loss of the ability of cells to form mammospheres in the MCF-7 cell line, as well as reduced tumorigenicity *in vivo*, suggesting that CD49f is essential for the growth and survival of a more tumorigenic subpopulation of tumor cells (184). The Notch proteins are transmembrane receptors which are involved in the developmental fate of tissues and interact with a variety of ligands including jagged 1 and jagged 2 (230). NF κ B has been implicated in cancer stem cell proliferation and has demonstrated a role in mammosphere formation and maintenance (136, 231, 232). Therefore, reduction of these markers by treatment with vitamin D compounds may contribute to the inhibition of tumorigenicity directed by putative stem cells. The basal levels of two markers critical in mammosphere formation, CD44s and c-Notch1, were expressed at higher levels at days 4 and 5 compared to day 7. The reduction of these markers at day 7 correlated with the reduction of the MFE of MCF10DCIS mammospheres at day 7 (Fig. 4.5). As expected, sustained levels of signaling molecules associated with stem cells were critical in the maintenance of mammospheres over long periods of time.

To study the self-renewal of stem cells, we analyzed the mammosphere formation of secondary and tertiary spheres. MCF10DCIS and SUM159 demonstrated a progressive increase in the MFE in secondary and tertiary spheres, suggesting that these cell lines

enrich for a subpopulation with increased self-renewal capacity. It is interesting to note that MCF-7 mammosphere formation was reduced at the secondary and tertiary level, which is consistent with decreased self-renewal capacity of luminal progenitors upon serial passage. These mammospheres could be derived from self-renewing lineage-restricted progenitors, which are thought to represent more-differentiated downstream progenitor cells that should not have regenerative potential (233). Secondary and tertiary mammosphere formation was significantly inhibited by vitamin D compounds in MCF10DCIS, SUM159, MCF-7, and MCF-7 with estradiol supplementation, suggesting that vitamin D compounds inhibit the self-renewal capacity of BCSCs (Fig. 4.7, 4.10, 4.11, 4.12). We further investigated the role of vitamin D compounds on key transcription factors involved in the self-renewal of stem cells. Oct4 is a transcription factor that forms a heterodimer with Sox2 and regulates stem cell self-renewal capacity, and the knockdown of Oct4 promotes differentiation (234, 235). The transcription factor, Gata3, has been established as a critical regulator of luminal differentiation (236). The repression of pluripotency markers, such as *OCT4*, *KLF-4*, and *GATA3*, indicate that MCF10DCIS mammospheres treated with vitamin D compounds could potentially induce the differentiation of putative BCSCs.

4.5. Conclusion

Cancer progression, metastasis, and recurrence are significant problems in managing breast cancer. A significant body of evidence indicates that breast cancer stem cells drive these processes, complicating treatment strategies. A better understanding of

how BCSCs drive breast cancer progression will aid in developing targeted therapies toward BCSCs. We assessed vitamin D compounds on breast cancer stem cells by utilizing the mammosphere cell culture system. We observed decreases in the mammosphere formation and self-renewal, proliferation, and repression of markers of the stem cell phenotype and pluripotency. These results suggest a potential treatment strategy to reduce the putative BCSC population, and therefore enhance the effectiveness of breast cancer prevention and treatment through the use of vitamin D compounds.

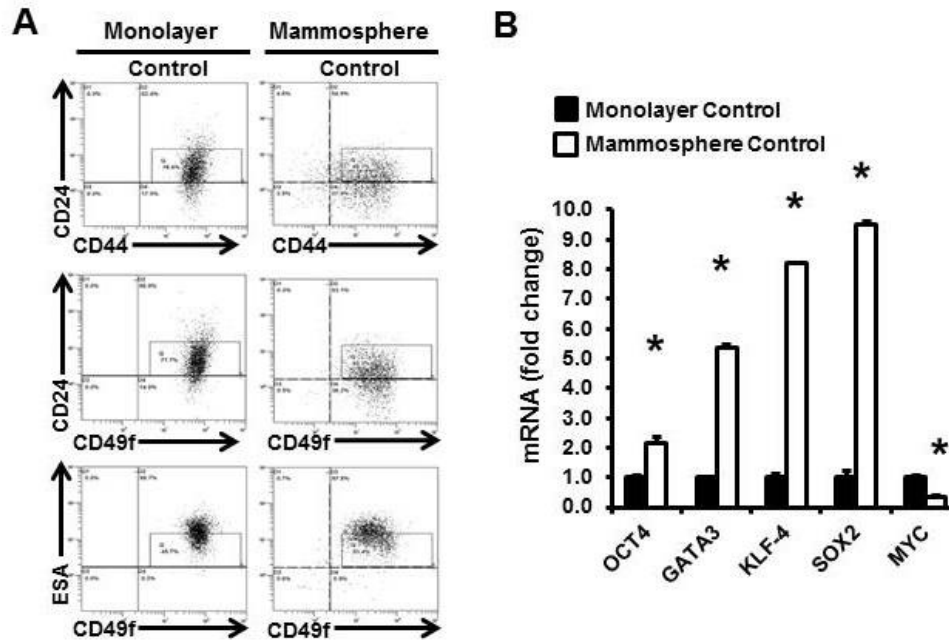


Figure 4.1 Mammosphere cell culture enriches for putative breast cancer stem cell subpopulations and markers of pluripotency in the MCF10DCIS cell line.

(A) Flow cytometry analysis of putative breast cancer stem cell markers, CD44, CD24, CD49f, and ESA were assessed in MCF10DCIS cells in monolayer and mammosphere cell culture conditions. (B) qPCR analysis of markers of pluripotency were assessed in MCF10DCIS cells in monolayer and mammosphere cell culture conditions. The data are presented as the mean \pm S.E.M. (n=4). * $p < 0.05$. Cycle numbers for qPCR are shown in parenthesis: *OCT4* (#29), *GATA3* (#26), *KLF4* (#28), *SOX2* (#34), and *MYC* (#24).

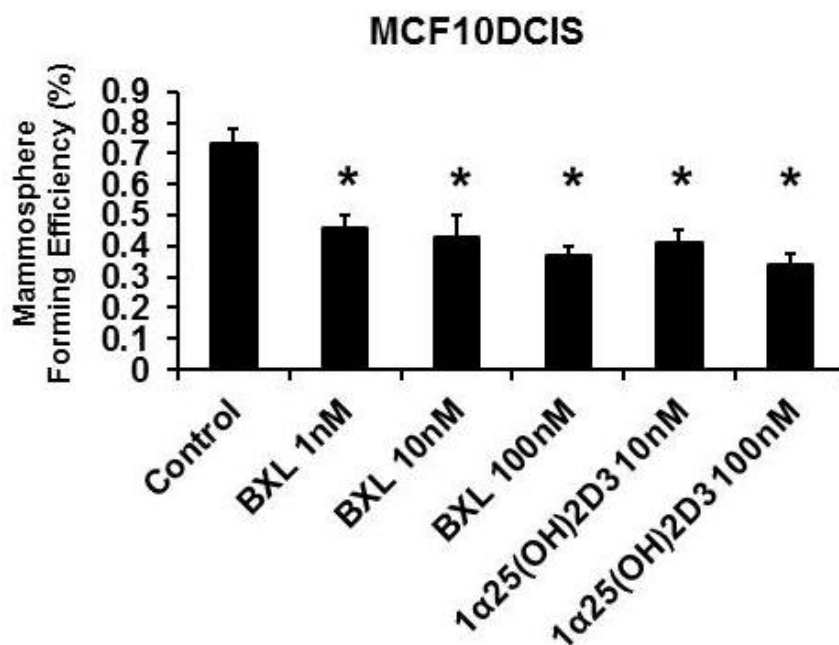


Figure 4.2 Dose optimization for the inhibition of mammosphere forming efficiency by $1\alpha25(\text{OH})_2\text{D}_3$ and BXL0124 in MCF10DCIS cells.

MCF10DCIS cells were plated at a density of 5,000 cells/mL in ultra-low attachment 24-well plates and grown for 5 days in the presence of $1\alpha25(\text{OH})_2\text{D}_3$ (10nM, 100nM) and BXL0124 (1nM, 10nM, and 100nM). Mammosphere forming efficiency (MFE) is shown. MFE was calculated by dividing the number of mammospheres ($\geq 100 \mu\text{m}$) formed by the number of cells seeded, presenting this as a percentage. The data are presented as the mean \pm S.E.M. (n=3). * $p < 0.05$.

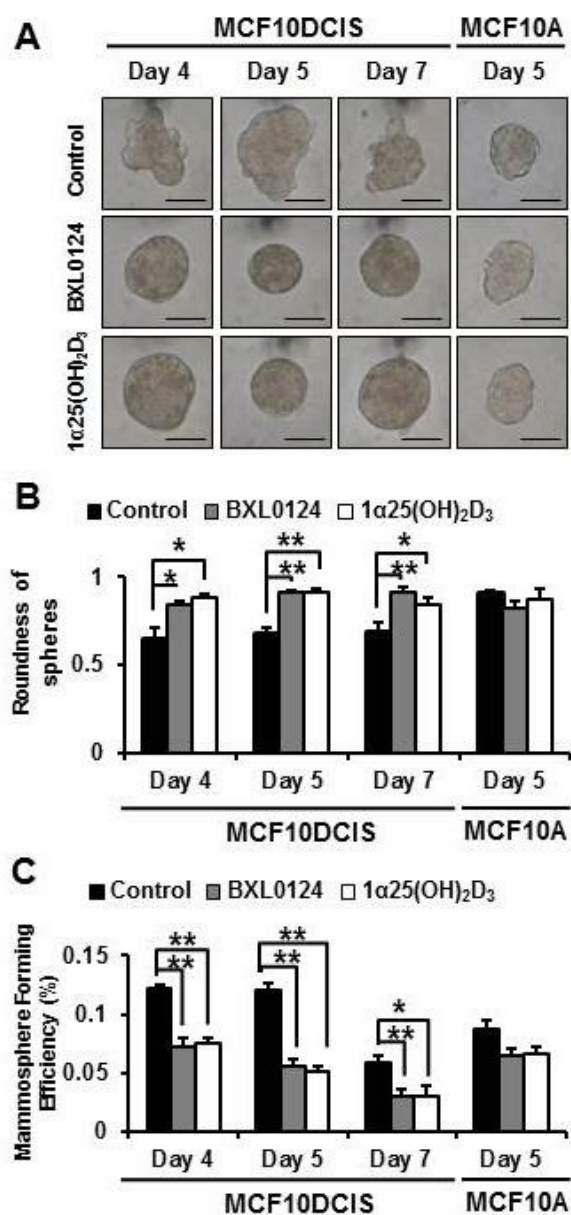


Figure 4.3 Repression of the mammosphere forming efficiency by 1 α 25(OH) $_2$ D $_3$ and BXL0124 in MCF10DCIS cells.

(A) MCF10DCIS cells were plated at a density of 10,000 cells/mL in ultra-low attachment 6-well plates and grown for 4, 5 and 7 days in the presence of 1 α 25(OH) $_2$ D $_3$ (100 nM) and BXL0124 (10 nM). MCF10A cells were plated at a density of 10,000

cells/mL in ultra-low attachment 6-well plates and growing them for 5 days. Representative pictures of MCF10DCIS and MCF10A mammospheres are shown for phenotypic comparison, scale bar 100 μ m. **(B)** Quantification of the roundness of the mammospheres is shown. A value of 1.0 represents an object that is perfectly round. A value of 0.0 represents an object that is formless. At least eight different mammospheres from three separate experiments were quantified to give the average measure of roundness. The data are presented as the mean \pm S.E.M. * $p < 0.05$, ** $p < 0.01$. **(C)** Mammosphere forming efficiency (MFE) is shown. MFE was calculated by dividing the number of mammospheres ($\geq 100 \mu$ m) formed by the number of cells seeded, presenting this as a percentage. The data are presented as the mean \pm S.E.M. (n=6). * $p < 0.05$, ** $p < 0.01$.

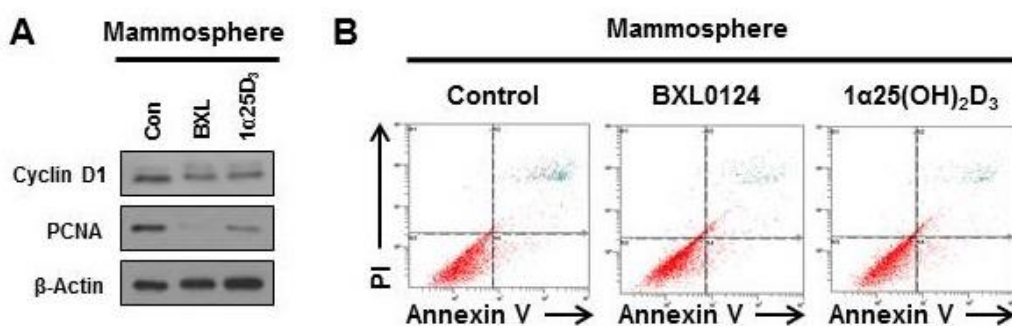


Figure 4.4 $1\alpha25(\text{OH})_2\text{D}_3$ and BXL0124 decrease proliferation but do not affect apoptosis in MCF10DCIS mammospheres.

(A) MCF10DCIS mammospheres were formed by plating 5,000 cells/mL in ultra-low attachment 6-well plates and growing them for 5 days. Western blot analysis was performed on mammospheres treated with DMSO control (Con), $1\alpha25(\text{OH})_2\text{D}_3$ ($1\alpha25\text{D}_3$, 100 nM) or BXL0124 (BXL, 10 nM), and analyzed for markers of proliferation, CyclinD1 and proliferating cell nuclear antigen (PCNA). Levels of β -actin were used as loading controls. (B) MCF10DCIS mammospheres were formed by plating 5,000 cells/mL. Mammospheres were collected after 5 days of treatment with DMSO control, $1\alpha25(\text{OH})_2\text{D}_3$ (100 nM), or BXL0124 (10 nM), and analyzed by flow cytometry after staining with Annexin V and propidium iodide (PI). Experiments were performed in duplicate and representative histograms from flow cytometry are shown.

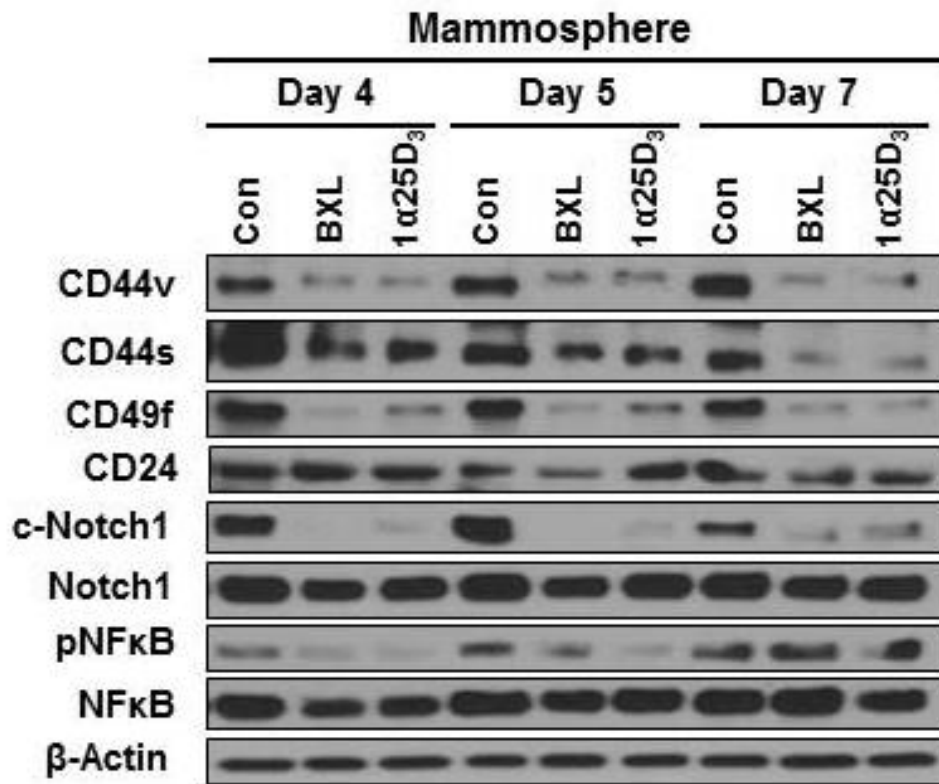


Figure 4.5 1 α 25(OH)₂D₃ and BXL0124 decrease the level of stem cell markers in MCF10DCIS mammospheres.

(A) Western blot analysis was performed on mammospheres collected from 4, 5, and 7 days of treatment with DMSO control (Con), 1 α 25(OH)₂D₃ (1 α 25D₃, 100 nM) or BXL0124 (BXL, 10 nM), and analyzed for markers associated with stem cell maintenance. Levels of β -actin were used as loading controls.

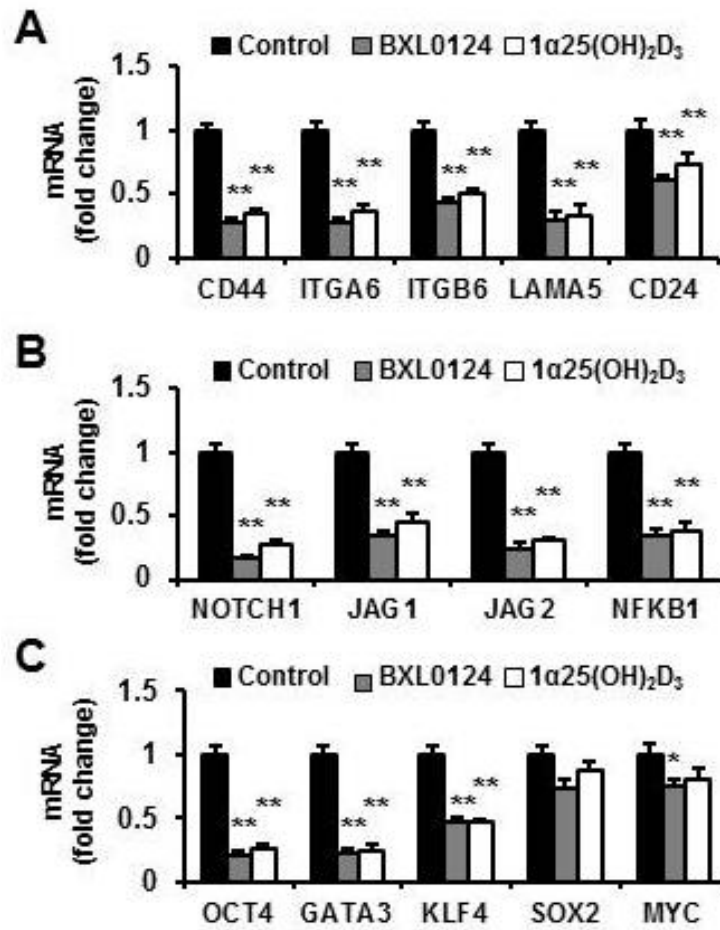


Figure 4.6 Repression of stem cell genes and markers of pluripotency by 1α25(OH)₂D₃ and BXL0124 in MCF10DCIS mammospheres.

qPCR analysis was performed on mammospheres harvested after 5 days of growth to assess the gene expression of markers associated with the stem cell phenotype (**A**), stem cell signaling (**B**), and genes related to pluripotency (**C**). The data are presented as the mean \pm S.E.M. (n=6). * $p < 0.05$, ** $p < 0.01$. Cycle numbers for qPCR are shown in parenthesis: *CD44* (#22), *ITGA6* (#23), *ITGB6* (#25), *LAMA5* (#24), *CD24* (#24), *NOTCH1* (#27), *JAG1* (#26), *JAG2* (#28), *NFKB1* (#26), *OCT4* (#29), *GATA3* (#26), *KLF4* (#28), *SOX2* (#34), and *MYC* (#24).

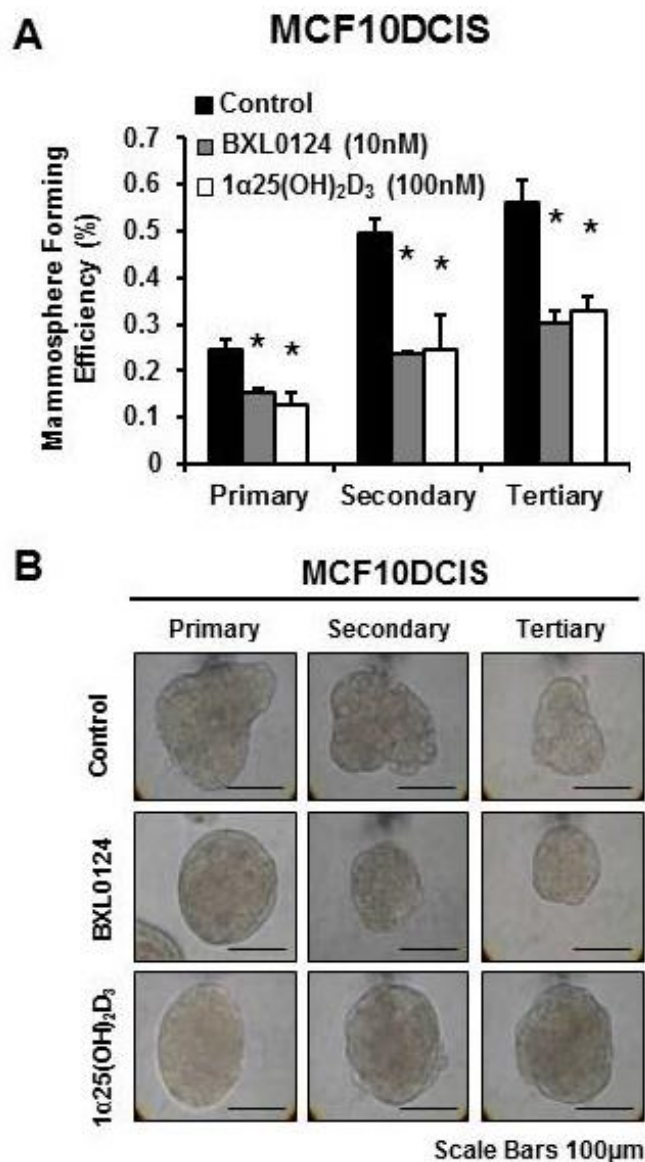


Figure 4.7 1α25(OH)₂D₃ and BXL0124 inhibit the self-renewal of MCF10DCIS mammospheres.

(A) MCF10DCIS cells were plated at a density of 5,000 cells/mL in ultra-low attachment 6-well plates and grown for 5 days with 1α25(OH)₂D₃ (100 nM) and BXL0124 (10 nM). Spheres were collected, dissociated, and re-plated at a density of 5,000 cells/mL for secondary and tertiary passages. Mammosphere forming efficiency (MFE) of primary,

secondary and tertiary passages of MCF10DCIS mammospheres is shown. MFE was calculated by dividing the number of mammospheres ($\geq 100 \mu\text{m}$) formed by the number of cells seeded presenting this as a percentage. Experiments were performed in triplicate and the data are presented as the mean \pm S.E.M. * $p < 0.01$. **(B)** Representative pictures of MCF10DCIS mammospheres from primary, secondary, and tertiary passages are shown for phenotypic comparison (scale bar $100 \mu\text{m}$).

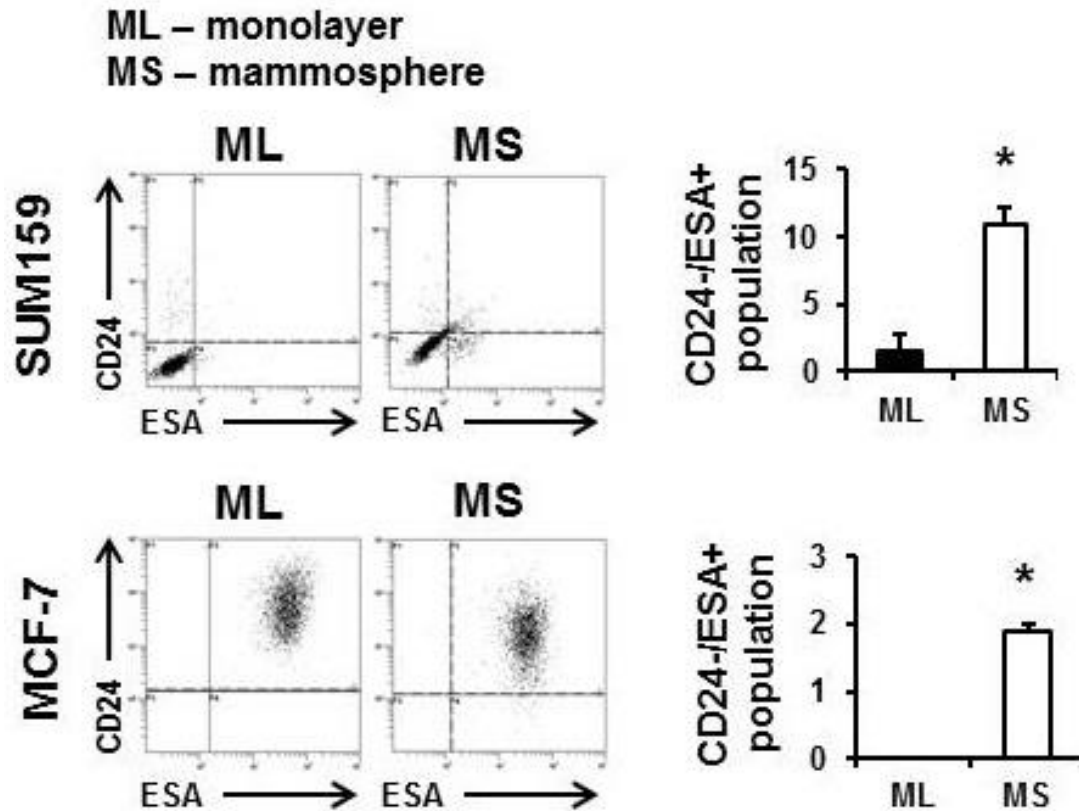


Figure 4.8 Mammosphere cell culture enriches for putative breast cancer stem cell subpopulations in SUM159 and MCF-7 breast cancer cell lines.

SUM159 and MCF-7 cells were grown in monolayer (ML) cell culture for 24 h or mammosphere (MS) cell culture for 5 days. Cells were stained with combinations of fluorophore labelled antibodies against CD24 and ESA, and then flow cytometry was performed. Representative histograms from flow cytometry are shown. The average percentage of putative breast cancer stem cell subpopulation, CD24⁻/ESA⁺ from three independent experiments are represented as a bar graph to show the difference between the monolayer and mammosphere cell culture. The data are presented as the mean \pm S.E.M. * $p < 0.05$.

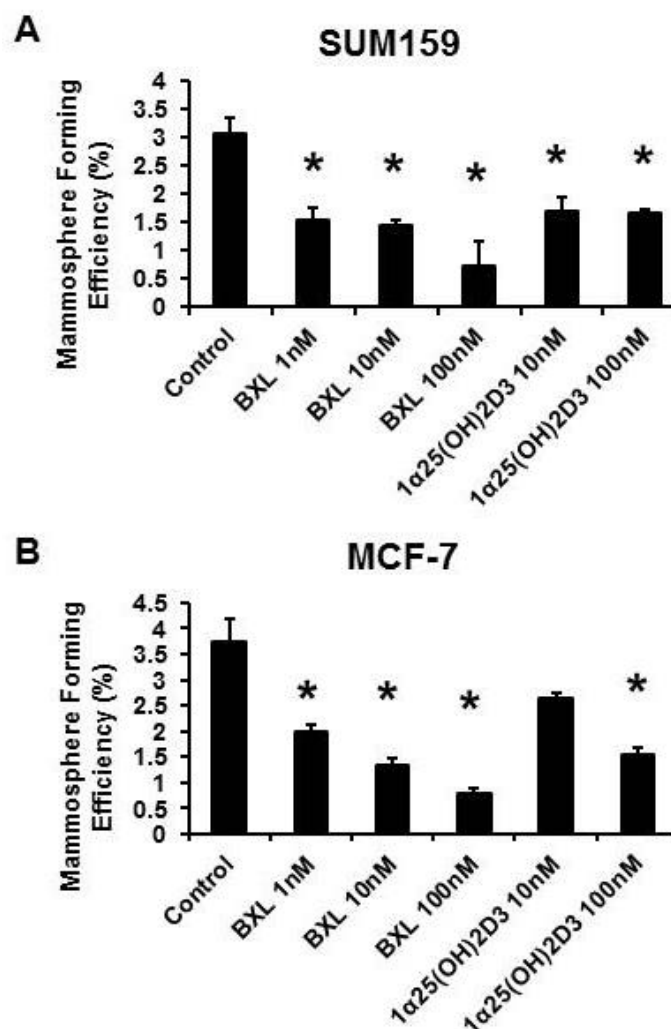


Figure 4.9 Dose optimization for the inhibition of mammosphere forming efficiency by $1\alpha25(\text{OH})_2\text{D}_3$ and BXL0124 in SUM159 and MCF-7 breast cancer cell lines.

SUM159 (**A**) or MCF-7 (**B**) cells were plated at a density of 2,000 cells/mL in ultra-low attachment 24-well plates and grown for 5 days in the presence of $1\alpha25(\text{OH})_2\text{D}_3$ (10nM, 100nM) and BXL0124 (1nM, 10nM, and 100nM). Mammosphere forming efficiency (MFE) is shown. MFE was calculated by dividing the number of mammospheres ($\geq 100 \mu\text{m}$) formed by the number of cells seeded, presenting this as a percentage. The data are presented as the mean \pm S.E.M. (n=3). * $p < 0.05$.

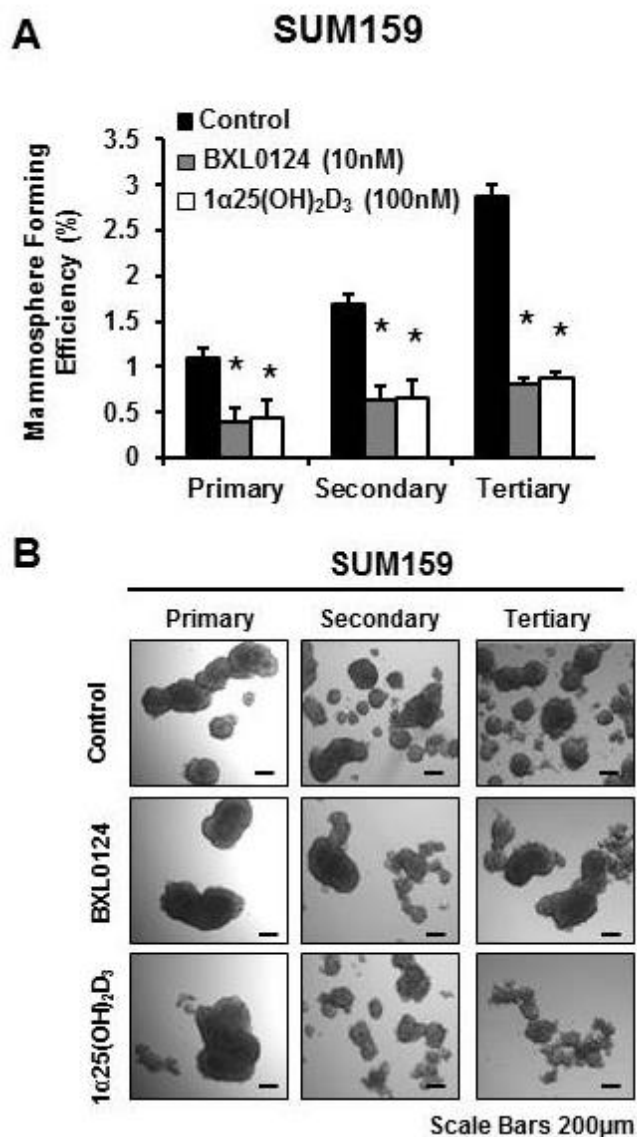


Figure 4.10 Inhibition of mammosphere self-renewal by 1 α 25(OH) $_2$ D $_3$ and BXL0124 in SUM159 mammospheres.

(A) SUM159 cells were plated at a density of 2,000 cells/mL in ultra-low attachment 6-well plates and grown for 5 days with 1 α 25(OH) $_2$ D $_3$ (100 nM) and BXL0124 (10 nM). Spheres were collected, dissociated, and re-plated at a density of 2,000 cells/mL for secondary and tertiary passages. Mammosphere forming efficiency (MFE) of primary,

secondary and tertiary passages of SUM159 mammospheres is shown. MFE was calculated by dividing the number of mammospheres ($\geq 100 \mu\text{m}$) formed by the number of cells seeded presenting this as a percentage. Experiments were performed in triplicate and the data are presented as the mean \pm S.E.M. * $p < 0.01$. **(B)** Representative pictures of SUM159 mammospheres from primary, secondary, and tertiary passages are shown for phenotypic comparison (scale bar $200 \mu\text{m}$).

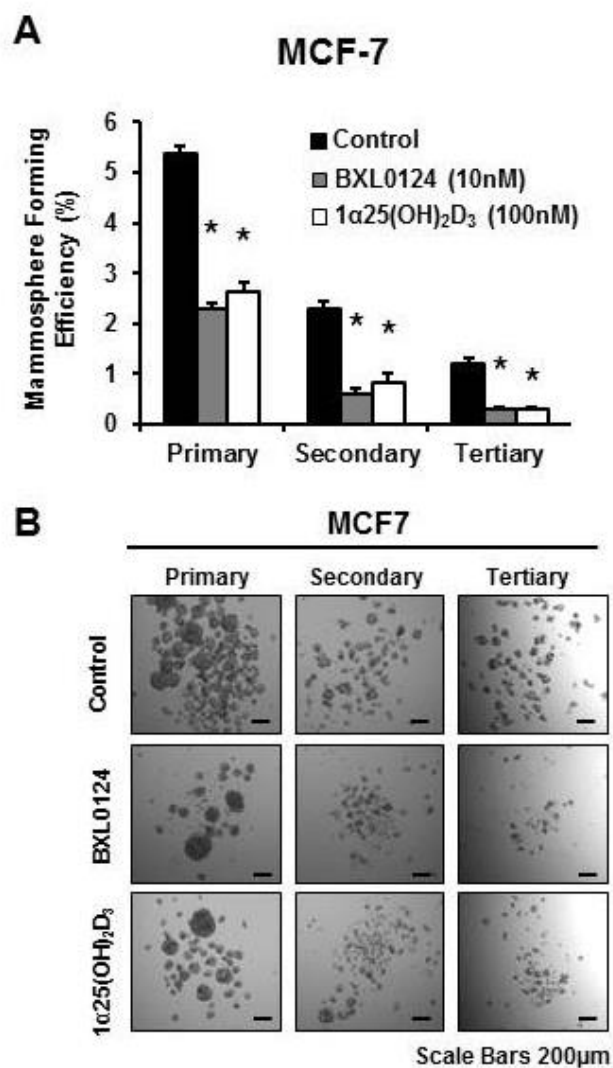


Figure 4.11 1 α 25(OH) $_2$ D $_3$ and BXL0124 inhibit the self-renewal of MCF-7 mammospheres.

(A) MCF-7 cells were plated at a density of 2,000 cells/mL in ultra-low attachment 6-well plates and grown for 5 days with 1 α 25(OH) $_2$ D $_3$ (100 nM) and BXL0124 (10 nM). Spheres were collected, dissociated, and re-plated at a density of 2,000 cells/mL for secondary and tertiary passages. Mammosphere forming efficiency (MFE) of primary, secondary and tertiary passages of MCF-7 mammospheres is shown. MFE was calculated

by dividing the number of mammospheres ($\geq 100 \mu\text{m}$) formed by the number of cells seeded presenting this as a percentage. Experiments were performed in triplicate and the data are presented as the mean \pm S.E.M. * $p < 0.01$. **(B)** Representative pictures of MCF-7 mammospheres from primary, secondary, and tertiary passages are shown for visual comparison of colony formation (scale bar $200 \mu\text{m}$).

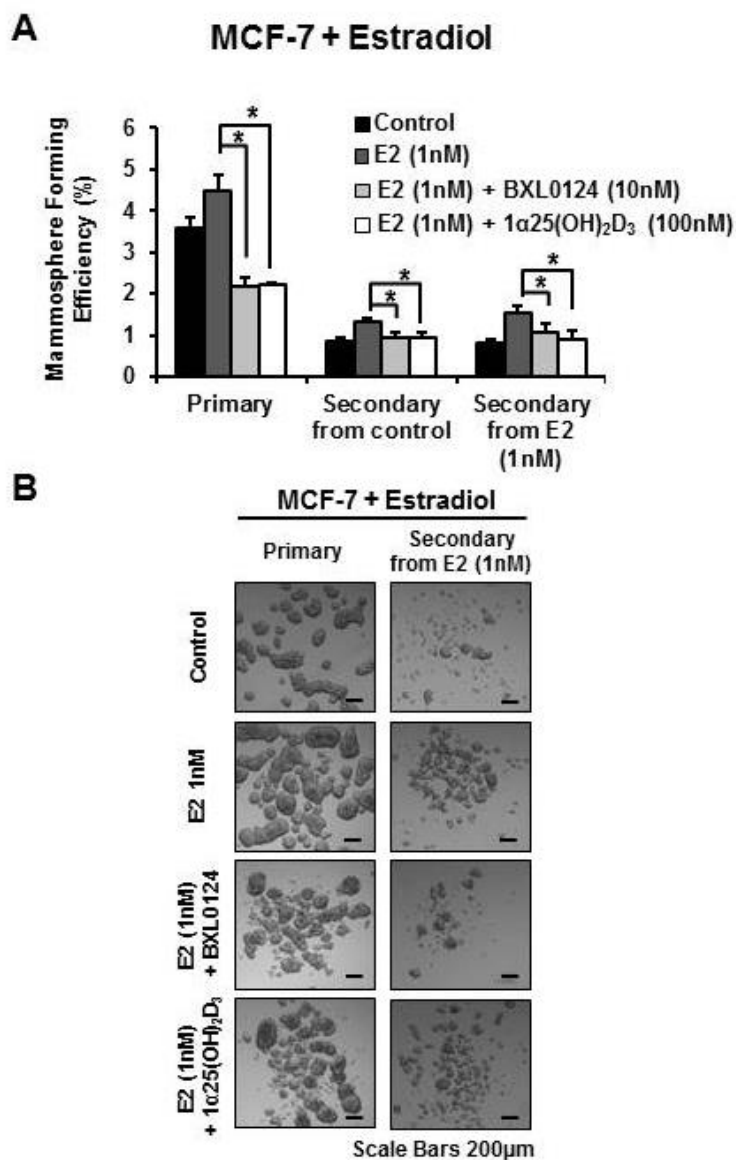


Figure 4.12 $1\alpha 25(\text{OH})_2\text{D}_3$ and BXL0124 inhibit the self-renewal of MCF-7 mammospheres supplemented with Estradiol.

(A) MCF-7 cells were plated at a density of 2,000 cells/mL in ultra-low attachment 6-well plates and grown for 5 days with Estradiol (1nM) or Estradiol (1nM) in the presence of $1\alpha 25(\text{OH})_2\text{D}_3$ (100 nM) and BXL0124 (10 nM). Primary spheres from control and Estradiol treatment were collected, dissociated, and re-plated at a density of 2,000

cells/mL for secondary passage. Mammosphere forming efficiency (MFE) of primary and secondary passages of MCF-7 mammospheres is shown. MFE was calculated by dividing the number of mammospheres ($\geq 100 \mu\text{m}$) formed by the number of cells seeded presenting this as a percentage. Experiments were performed in triplicate and the data are presented as the mean \pm S.E.M. * $p < 0.01$. **(B)** Representative pictures of MCF-7 mammospheres from primary and secondary passage from estradiol treated primary mammospheres are shown for visual comparison of colony formation (scale bar $200 \mu\text{m}$).

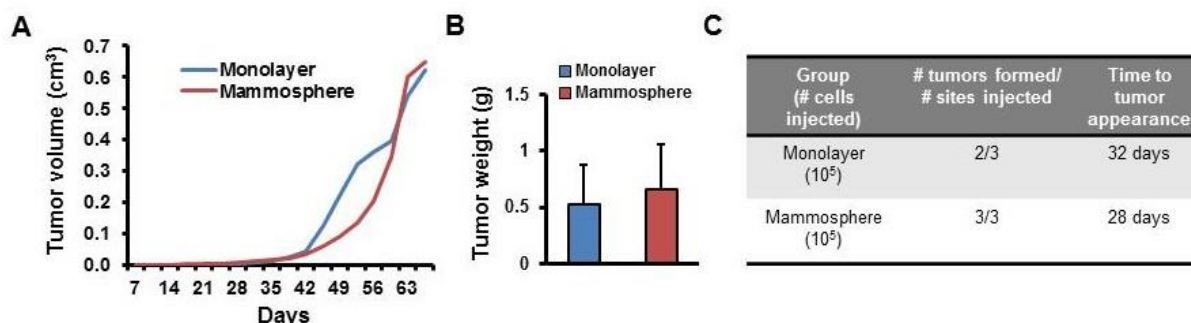


Figure 4.13 Comparison of xenograft growth from MCF10DCIS monolayer and mammosphere cell culture.

(A) Mammosphere (10⁵) and monolayer (10⁵) cells were injected into the mammary fat pad of nu/nu mice and tumor growth was assessed. Average tumor growth curves are shown. (monolayer n=2; mammospheres n=3). Tumor volume (V; cubed centimeters) was calculated using the equation $V = D \cdot d^2 / 2$ where D (centimeters) and d (centimeters) are the largest and smallest perpendicular diameters. (B) Average final tumor weights at necropsy are shown, monolayer (n=2) and mammosphere (n=3), mean \pm S.E.M. (C) A summary of the number of tumors formed and time to tumor formation for each cell culture condition is shown in a table.

Chapter 5: Inhibition of the breast cancer stem cell subpopulation by vitamin D and a Gemini vitamin D analog

5.1. Rationale

Based on data from the previous chapter, it is suggested that vitamin D compounds can inhibit the breast cancer stem cell (BCSC) population; however, effects on mammosphere cell do not directly address the BCSC-containing subpopulation. Our laboratory has previously demonstrated that BXL0124 was capable of decreasing the expression of CD44, which has been identified as a cancer stem cell marker (147). We have also shown that the CD44⁺/CD24⁻ subpopulation was reduced with BXL0124 treatment of MCF10DCIS cells (147). These studies have stimulated further investigation of the inhibitory effects of vitamin D and its analogs on the putative BCSC population.

Typically, fluorescence-activated cell sorting (FACS) has been used to identify populations of cancer cells that contain cancer stem cells (237). Different combinations of cell surface markers such as CD44, CD49f, CD24, and CD29 as well as the activity of certain enzymes such as aldehyde dehydrogenase isoform 1 (ALDH1) have been used to identify BCSCs (238). In this study we utilized the cell surface markers CD44 and CD24 to assess the role of vitamin D compounds on the putative CD44⁺/CD24^{-/low} breast cancer stem cell population *in vitro* and *in vivo*.

5.2. Materials and Methods

5.2.1. Reagents and Cell Culture

$1\alpha,25(\text{OH})_2\text{D}_3$ and a Gemini vitamin D analog [BXL0124; $1\alpha,25$ -dihydroxy-20R-21(3-hydroxy-3-deuteromethyl-4,4,4-trideuterobutyl)-23-yne-26,27-hexafluoro-cholecalciferol, >95% purity] (Figure 1) were provided by BioXell, Inc. (Nutley, NJ) and dissolved in dimethyl sulfoxide (DMSO). For *in vivo* animal experiments, BXL0124 was diluted in DMSO and PBS (Sigma, MO) for intraperitoneal administration. The MCF10DCIS human breast cell line was provided by Dr. Fred Miller at the Barbara Ann Karmanos Cancer Institute (Detroit, MI). The MCF10DCIS cell line was authenticated by short tandem repeat profiling at American Type Culture Collection (ATCC, Manassas, VA). MCF10DCIS human breast cancer cells were maintained in Dulbecco's Modified Eagle's Medium (DMEM)/F12 medium supplemented with 5% horse serum, 1% penicillin/streptomycin, and 1% HEPES solution at 37°C, 5% CO₂.

5.2.2. Flow Cytometry and FACS

In monolayer cell culture, MCF10DCIS cells were grown to 50% confluence and were subsequently treated with fresh medium containing the indicated concentrations of $1\alpha,25(\text{OH})_2\text{D}_3$ or BXL0124 for 24 h. Cells were harvested and processed for further analysis. The detailed procedure was described previously (147). MCF10DCIS cells were stained with antibodies against CD44-FITC (Cat. 555478), CD49f-FITC (Cat. 561893) and CD24-PE (Cat. 555428) from BD Biosciences (San Jose, CA). The stained MCF10DCIS cells were analyzed by flow cytometry using an FC500 Analyzer (Beckman Coulter) to determine the percentage of different CD44/CD24 and CD49f/CD24

subpopulations. The acquisition of $\geq 10,000$ cells per treatment was analyzed. FACS was performed by staining MCF10DCIS monolayer cells with CD44 and CD24 and sorting into three populations, CD44⁺/CD24⁻, CD44⁺/CD24^{low}, and CD44⁺/CD24^{high}. These subpopulations were then used for qPCR analysis and mammosphere cell culture.

5.2.3. Aldefluor Assay

The ALDEFLUOR kit (Cat. 01700, StemCell Technologies) was used to assess ALDH enzymatic activity. MCF10DCIS cells were harvested and stained according to the manufacturer's protocol. Briefly, cells (2×10^5 cells) were incubated in ALDEFLUOR assay buffer containing ALDH substrate (300 μ M) for 40 min. In each experiment, a sample of cells was stained under identical conditions with 1.5 mM of diethylaminobenzaldehyde (DEAB) reagent (Cat. 01705, StemCell Technologies) a specific ALDH inhibitor, as a negative control. The samples were assessed by flow cytometry by measuring ALDEFLUOR fluorescence vs. side scatter (SSC) histogram.

5.2.4. Quantitative Real-Time Polymerase Chain Reaction Analysis

These procedures have been reported previously (201, 202). The Taqman® probe-based gene expression system from Applied Biosystems (Foster City, CA) was used to detect the genes of interest. Labeled primers for *GAPDH* (Hs02758991), *CD44* (Hs01075861), *ITGA6* (Hs01041011), *ITGB6* (Hs00168458), *LAMA5* (Hs00966585), *CD24* (Hs03044178), *NOTCH1* (Hs01062014), *JAG1* (Hs01070032), *JAG2*

(Hs00171432), *NFKB1* (Hs00765730), *OCT4 (POU5F1)* (Hs00999634), *GATA3* (Hs00231122), *KLF4* (Hs00358836), *SOX2* (Hs01053049), and *MYC* (Hs00153108) *VDR* (Hs00172113), *MUC1* (Hs00159357), *ALDH1A1* (Hs00946916), *NANOG* (Hs04260366), and *BMP4* (Hs03676628) were used in analysis. *GAPDH* was used to normalize other genes for variations in RNA quality and amount of cDNA input.

5.2.5. Mammosphere Forming Assay

MCF10DCIS cells were grown to 50% confluence and cells were detached with StemPro Accutase (Life Technologies). Cells were then plated at 5,000 cells/mL in 6-well ultra-low attachment plates and maintained in Mammosphere serum-free medium supplemented with hydrocortisone and heparin (Stem Cell Technologies). Photos of mammospheres were taken, and the numbers of mammospheres were counted in order to determine the mammosphere forming efficiency (MFE). The MFE was calculated by dividing the number of mammospheres ($\geq 100 \mu\text{m}$) formed by the number of single cells seeded.

5.2.6. Xenograft Animal Studies and Tumor Dissociation

All animal studies were approved by the Institutional Review Board for the Animal Care and Facilities Committee of Rutgers University. Female nude mice (5-6 weeks old) were purchased from Charles River Laboratories (Wilmington, MA). They were allowed to acclimate for two weeks at which time they were injected (7-8 weeks

old) with human MCF10DCIS cells into the mammary fat pad or subcutaneously on the left dorsal flank at 10^6 cells per site and treatment beginning the following day. Mice were treated with DMSO control or BXL0124 ($0.1\mu\text{g/kg}$ Body Weight) via intraperitoneal injection six times per week for the experimental period. Animals were palpated twice each week to check for tumor formation and total body weights were measured weekly. Upon detection, tumors were measured with a vernier caliper and tumor volume (V; cubed centimeters) was calculated using the equation $V = D \cdot d^2 / 2$ where D (centimeters) and d (centimeters) are the largest and smallest perpendicular diameters, respectively. Upon termination of the experiment, animals were sacrificed, tumors were excised, snap frozen in liquid nitrogen for qPCR analysis and dissociated for further analysis. Xenografts were removed, weighed, and a section of tumor (weighing between 0.15-0.30g) was mechanically disaggregated using scalpels and tweezers in RPMI 1640 medium containing 2% FBS. This suspension was then enzymatically dissociated using StemPro Accutase (Life Technologies) at 37°C for three hours using mechanical dissociation by way of pipetting several times every 30 m. The resulting cell suspension is filtered through a $40\mu\text{m}$ cell strainer to remove clumps. This gives a single cell suspension which is stained with CD44 and CD24 and analyzed by flow cytometry to assess the CD44/CD24 subpopulations from tumors. Dead cells were excluded from analysis by staining with 7-actinoaminomycin-D (7-AAD) (Cat. 51-68981E, BD Biosciences, San Jose, CA). After dissociation, 10^6 cells were injected into the mammary fat pad of new batches of mice to form secondary xenografts. Secondary xenografts were allowed to grow for 28 days, at which time tumors were excised, weighed, dissociated, and analyzed by flow cytometry for CD44/CD24 expression.

5.2.7. Statistical analysis

Statistical significance was evaluated using the Student's t-test.

5.3. Results

5.3.1 CD44 and CD24 are markers for putative breast cancer stem cell subpopulations in MCF10DCIS cells

Fluorescence-activated cell sorting (FACS) or flow cytometry have been used to identify populations of cancer cells that contain cancer stem cells (237). Different combinations of cell surface markers such as CD44, CD49f, CD24, ESA, and CD29 as well as the activity of certain enzymes such as aldehyde dehydrogenase isoform 1 (ALDH1) have been used to identify BCSCs (238). We analyzed combinations of these markers by flow cytometry in MCF10DCIS cells to assess the optimal markers to use in this cell line for further analysis. Double staining with CD44/CD24 showed a population that was 100% CD44 positive and CD24 expression ranged from negative expression (approximately 41% of total population) to high expression (approximately 24% of total population). The putative breast cancer stem cell population $CD44^{+}/CD24^{-/low}$ population comprised approximately 68.7% of the total population (Fig. 5.1). Double staining of CD49f/CD24 showed that MCF10DCIS was 100% CD49f-positive and the putative $CD49f^{+}/CD24^{-/low}$ subpopulation was 69.0% (Fig. 5.1). By staining with CD24/ESA we observed that MCF10DCIS expressed ESA in all cells, suggesting that staining with ESA

will not further enrich for BCSCs in the MCF10DCIS cell line. We also utilized the Aldefluor assay to assess the enzymatic activity of ALDH. The putative BCSC population is believed to have enhanced ALDH activity. MCF10DCIS cells were 93.1% ALDH positive (Fig. 5.1). Due to this high level we did not further utilize ALDH as a marker to sort BCSCs in MCF10DCIS cells. Based on these results we utilized the cell surface markers, CD44, CD49f, and CD24 for further analysis of BCSCs in MCF10DCIS cells.

5.3.2. $1\alpha 25(\text{OH})_2\text{D}_3$ and BXL0124 decrease the breast cancer stem cell population in MCF10DCIS cells

MCF10DCIS cells represent a basal-like or claudin-low breast tumor subtype, which typically carries a poor prognosis (239). These cells are primarily CD44⁺ and CD49f⁺. We first examined the addition of CD24 as a marker to further define subpopulations within MCF10DCIS cells. Breast cancer stem cells are thought to reside in the CD44⁺/CD24^{-/low} and CD49f⁺/CD24^{-/low} subpopulations of cells (240, 241). These populations were decreased with $1\alpha 25(\text{OH})_2\text{D}_3$ (100 nM) and BXL0124 (10 nM) treatment (Fig. 5.2). The CD44⁺/CD24^{-/low} subpopulation was decreased from 68.7% in the control to 42.9% with $1\alpha 25(\text{OH})_2\text{D}_3$ ($p < 0.01$) and to 40.3% with BXL0124 treatment ($p < 0.01$). Similarly, the CD49f⁺/CD24^{-/low} population was decreased from 69.0% to 37.6% with $1\alpha 25(\text{OH})_2\text{D}_3$ ($p < 0.01$) and to 39.7% with BXL0124 treatment ($p < 0.05$). Concomitantly, the CD44⁺/CD24^{high} cell fraction was increased from 31.3% to 59.7% and 57.1% with $1\alpha 25(\text{OH})_2\text{D}_3$ and BXL0124 treatments, respectively, and the

CD49f⁺/CD24^{high} population was increased from 31.0% to 62.4% with 1 α 25(OH)₂D₃ and to 60.3% with BXL0124 treatment (Fig. 5.2). These data indicate that 1 α 25(OH)₂D₃ and BXL0124 treatments shift the CD44⁺/CD24^{-low} and CD49f⁺/CD24^{-low} subpopulations to populations that are more CD44⁺/CD24^{high} and CD49f⁺/CD24^{high}.

5.3.3. Fluorescently activated cell sorting (FACS) was used to sort the MCF10DCIS cells using CD44 and CD24

FACS analysis was used to sort MCF10DCIS cells into three subpopulations, CD44⁺/CD24⁻, CD44⁺/CD24^{low}, and CD44⁺/CD24^{high} (Fig. 5.3A). After FACS sorting, the three populations were assessed by flow cytometry to validate the cell sorting experiment (Fig. 5.3B). After flow analysis the CD44⁺/CD24⁻ subpopulation was 85.2% pure and observed to overlap into the CD44⁺/CD24^{low} population by 3.9%. The sorted CD44⁺/CD24^{low} population was 81.7% pure and overlapped into the CD44⁺/CD24⁻ by 18.3%. Finally, the CD44⁺/CD24^{high} subpopulation was 71.2% pure and overlapped into the CD44⁺/CD24^{low} subpopulation by 11.2%. These results suggest that FACS sorting is a sufficient method to sort subpopulations for assessment of these subpopulations and the effects of vitamin D compounds on these populations.

5.3.4. The CD44⁺/CD24^{-low} putative breast cancer stem cell population has higher expression of notch signaling ligands, Jag1 and Jag2

After FACS analysis cells were analyzed by qPCR to examine gene expression changes between the three sorted subpopulations. The $CD44^{+}/CD24^{high}$ subpopulation was set to 1 and the other subpopulations were assessed in relation to this. *CD24* expression was 74% and 82% lower in $CD44^{+}/CD24^{low}$ ($p < 0.01$) and $CD44^{+}/CD24^{-}$ ($p < 0.01$), respectively (Fig. 5.4A). Another luminal marker, *MUC1*, was lower by 68% and 81% in $CD44^{+}/CD24^{low}$ ($p < 0.01$) and $CD44^{+}/CD24^{-}$ ($p < 0.01$), respectively (Fig. 5.4D). Integrin *ITGA6* expression was increased by 32% and 23% in $CD44^{+}/CD24^{low}$ ($p < 0.01$) and $CD44^{+}/CD24^{-}$ ($p < 0.01$), respectively, compared to the $CD44^{+}/CD24^{high}$ population (Fig. 5.4A).

Key molecules involved in notch stem cell signaling were also regulated in the $CD44^{+}/CD24^{low}$ and $CD44^{+}/CD24^{-}$ subpopulations, suggesting enhanced stem cell signaling in these populations. Ligand *JAG1* expression was 32% and 10% higher in $CD44^{+}/CD24^{low}$ ($p < 0.01$) and $CD44^{+}/CD24^{-}$ ($p < 0.01$), respectively, compared to the $CD44^{+}/CD24^{high}$ population (Fig. 5.4B). Another notch ligand, *JAG2* expression was 50% and 66% greater in $CD44^{+}/CD24^{low}$ ($p < 0.01$) and $CD44^{+}/CD24^{-}$ ($p < 0.01$), respectively (Fig. 5.4B).

SOX2, a gene involved in pluripotency and maintenance of the stem cell population was 62% and 52% lower in $CD44^{+}/CD24^{low}$ ($p < 0.01$) and $CD44^{+}/CD24^{-}$ ($p < 0.01$), respectively (Fig. 5.4C). The expression of other transcription factors did not show significant differential expression between the three subpopulations assessed (Fig. 5.4C).

5.3.5. Vitamin D compounds repress the mammosphere formation of putative breast cancer stem cell subpopulations

MCF10DCIS cells were sorted and assessed in the mammosphere forming assay with vitamin D compound treatment. The putative breast cancer stem cell populations, CD44⁺/CD24^{low} and CD44⁺/CD24⁻ had a higher mammosphere forming efficiency compared to the CD44⁺/CD24^{high} population (Fig. 5.5 A). The CD44⁺/CD24^{high} population was 63.6% and 66% lower in the CD44⁺/CD24⁻ ($p < 0.01$) and CD44⁺/CD24^{low} ($p < 0.01$) populations, respectively (Fig. 5.5A). This data points toward the notion that these putative BCSC subpopulations have an enriched population capable of growth in non-adherent conditions, and hence stem cell activity. The MFE of CD44⁺/CD24⁻ spheres was significantly reduced upon treatment with $1\alpha 25(\text{OH})_2\text{D}_3$ (68.7% inhibition, $p < 0.01$) or BXL0124 (62% inhibition, $p < 0.05$) (Fig. 5.5A). Similarly the MFE of the CD44⁺/CD24^{low} subpopulation was repressed with $1\alpha 25(\text{OH})_2\text{D}_3$ (77.0% inhibition, $p < 0.01$) or BXL0124 (68.3% inhibition, $p < 0.01$). When CD44⁺/CD24^{high} spheres were grown in the presence of $1\alpha 25(\text{OH})_2\text{D}_3$ (100 nM) or BXL0124 (10 nM) there was not a significant decrease in the number of mammosphere colonies (Fig. 5.5A). Images of spheres visually reconfirmed the quantification of MFE in the three subpopulations with vitamin D treatments (Fig. 5.5B).

5.3.6. BXL0124 treatment of MCF10DCIS xenografts shifts the CD44/CD24 population to a CD24^{high} expressing population

BXL0124 was assessed in two separate experiments of MCF10DCIS mammary fat pad xenografts from mice injected with a different number of cells. Animals injected with 10^5 MCF10DCIS cells were assessed over 62 days. Tumors formed by day 21 in the control group and by day 25 in the BXL0124 treated group. BXL0124 treated animals showed a reduction in average tumor volume by day 62 with a 52.3% reduction in tumor size (Fig. 5.6A). Tumor weight was also reduced by 51.8% from control (1.68g) treated mice to BXL0124 (0.81g) treated mice (Fig. 5.6B). Tumors were excised, dissociated, and the CD44/CD24 subpopulations were analyzed by flow cytometry (Fig. 5.6D). There was a shift to a population that is more CD44⁺/CD24^{high} with BXL0124 treatment. There was an 81% increase in the average CD44⁺/CD24^{high} population shifting from 2.2% in the control group to 4% in the BXL0124 treatment group (Fig. 5.6C).

This assay was repeated in animals injected with 10^6 MCF10DCIS cells and assessed over 35 days. Tumors formed by day 5 in both the control and BXL0124 treated groups. BXL0124 showed a reduction in average tumor volume by day 35 with a 35% reduction in tumor size (Fig. 5.7A). Tumor weight was also reduced by 37.5% from control (0.64g) treated mice to BXL0124 (0.40g) treated mice (Fig. 5.7B). Tumors were excised, dissociated, and the CD44/CD24 subpopulations were analyzed by flow cytometry (Fig. 5.7D). The CD24^{high} subpopulation was gated to assess the levels of this population in tumors (Fig. 5.7D, green box). There was a shift to a population that is more CD44⁺/CD24^{high} with BXL0124 treatment. There was an 80% increase in the average CD44⁺/CD24^{high} population shifting from 10% in the control group to 18% in the BXL0124 treatment group (Fig. 5.7C).

5.3.7. BXL0124 reduces the expression of stem cell markers and markers of pluripotency in MCF10DCIS xenografts

BXL0124 treated tumors which showed a shift to a higher CD24 expressing population (Fig. 5.7), were assessed by qPCR for key markers associated with the cancer stem cell phenotype and pluripotency. Genes such as *CD44*, *CD24*, *SOX2*, *KLF4*, *OCT4*, *ALDH1A1*, and *MYC*, were assessed. Cell surface receptor *CD44* expression was decreased by 20% with BXL0124 ($p < 0.05$) (Fig. 5.8). *CD24* expression was modestly decreased by 23% with BXL0124. *ALDH1A1*, a putative cancer stem cell marker in breast cancer was decreased by 60% with BXL0124 ($p < 0.05$) (Fig. 5.8). The pluripotency marker *OCT4* was decreased by 30% with BXL0124 treatment in MCF10DCIS xenografts ($p < 0.05$) (Fig. 5.8). Treatment with BXL0124 also decreased *MYC* expression by 15%, although this result was not significant. The expression of transcription factors *SOX2* and *KLF4* were not significantly inhibited with BXL0124 treatment in MCF10DCIS xenograft tumors.

5.3.8. Effects of BXL0124 on re-established MCF10DCIS xenograft model

Cancer stem cells are defined by their ability to produce progressively growing tumors consisting of cells from the original tumor. To further assess the BCSC inhibiting potential of BXL0124, a limiting dilution transplant experiment was used with the MCF10DCIS xenograft model (Fig 5.9). For the primary assay mice were treated with BXL0124 (0.1 $\mu\text{g/kg}$ body weight/day) at day 1 after tumor implantation and observed over the course of 35 days. BXL0124 treatment showed a decrease in tumor volume and

weight (Fig 5.7A,B; 5.10A,B). The putative BCSC population was shifted to a population that is more CD24^{high} (Fig. 5.7C,D; 5.10C) and genes for putative BCSC markers, *CD44*, *ALDH1A1*, *OCT4* were reduced ($p < 0.05$) (Fig 5.8).

In the second serial passage in animals, primary tumors were excised, dissociated and then implanted into new mice (Fig. 5.9). Mice implanted with secondary tumor cells were not treated with vehicle control or BXL0124. Tumors formed by day 5 in both the control and BXL0124 treated groups. Control tumors reached a tumor volume of 1.70 cm³ and secondary tumors from BXL0124 reached a volume of 1.74 cm³ at 28 days (Fig 5.10D). Tumor weight was not significantly changed from secondary tumors from control (0.85g) or BXL0124 (1.17g) (Fig. 5.10E). Tumors were excised, dissociated, and the CD44/CD24 subpopulations were analyzed by flow cytometry. There was not a significant change in the CD44/CD24 subpopulations in secondary xenografts. CD44⁺/CD24^{high} subpopulations were 1.25% and 1.61% in secondary tumors from control or BXL0124, respectively (Fig. 5.10F).

It is also interesting to note that tumor growth was much more rapid in secondary xenografts when compared with the primary xenografts. Control tumors of primary xenografts reached a volume of 0.77 cm³ in 35 days, and the secondary xenografts reached 1.7 cm³ (2.2x larger than primary) in 28 days (Fig. 5.10A,D). The CD44⁺/CD24^{high} subpopulation was 10% in primary control tumors and decreased to 1.25% in secondary tumors, suggesting a shift to a population that is more CD24 negative. This would suggest that these tumors are more aggressive, as was observed.

5.3.9. Secondary xenografts from BXL0124 treated primary xenografts do not show a reduction of stem cell markers or markers of pluripotency

There was no change in CD24 expression in secondary tumors from either control or BXL0124 treated primary tumors (Fig. 5.10F). These tumors were assessed by qPCR for key markers associated with the cancer stem cell phenotype and pluripotency, such as *CD44*, *CD24*, *SOX2*, *KLF4*, *OCT4*, *ALDH1A1*, and *MYC*. Cell surface receptor *CD44* expression was modestly increased by 12% in secondary tumors from BXL0124 (Fig. 5.11). *CD24* expression was increased by 99% in secondary tumors from BXL0124 ($p < 0.01$) (Fig. 5.11). *ALDH1A1*, a putative cancer stem cell marker in breast cancer was unchanged in secondary tumors from BXL0124 (Fig. 5.11).

The pluripotency marker *OCT4* was increased by 21% in secondary tumors from BXL0124 treated primary tumors ($p < 0.01$) (Fig. 5.11). Transcription factor *KLF4* (Kruppel-like factor 4) expression was decreased by 45% in secondary tumors from BXL0124 treated primary tumors ($p < 0.01$) (Fig. 5.11). Levels of the gene *MYC* were increased by 63% in secondary tumors from BXL0124 treated primary tumors ($p < 0.01$) (Fig. 5.11). *SOX2* was not significantly altered in secondary tumors from BXL0124 treated primary tumors.

5.4. Discussion

Accumulating evidence has shown that breast cancer stem cells (BCSCs) are responsible for the initiation, maintenance, and progression of breast cancer (224). We have previously shown that vitamin D compounds can inhibit the formation of

mammosphere colonies, indicating their potential to inhibit the breast cancer stem cell (BCSC) population. Despite this the mammosphere assay is an indirect method to assess the role of therapeutic compounds on BCSCs. For this reason we utilized the specific cell surface markers, CD44, CD49f, and CD24 to further confirm the effects of vitamin D compounds on BCSCs.

MCF10DCIS falls under the basal-like or claudin-low breast tumor subtype, which consist primarily of a CD44⁺ population (242-244). For this reason we attempted to utilize ESA as a secondary marker to further enrich for BCSCs in the primarily CD44⁺ and CD49f⁺ MCF10DCIS cell line. However, the cells were entirely ESA positive, so this marker did not further enhance the ability to distinguish a stem cell-like population in this cell line (Fig 5.1). We isolated the putative CD44⁺/CD24^{-low} BCSC subpopulation by cell sorting. We characterized this subpopulation by qPCR analysis and, interestingly found that CD24^{-low} was correlated with an up-regulation of the Notch signaling pathway ligands, Jagged 1 and Jagged 2. This is consistent with a previous report by our laboratory demonstrating increased Jagged 2 levels, and in turn increased activation of Notch1 in CD44⁺/CD24⁻ and CD44⁺/CD24^{low} subpopulations (245). This implicates Notch1 signaling, which has been a well-established driver of BCSCs, in the putative BCSC subpopulation that we isolated (95, 133).

In this study, we found that the CD44⁺/CD24^{-low} stem cell enriched population of MCF10DCIS cells is shifted to a predominantly CD44⁺/CD24^{high} population upon treatment with 1 α 25(OH)₂D₃ or BXL0124 (Fig. 5.2). Supporting this finding, the CD49f⁺/CD24^{-low} population was shifted to a primarily CD49f⁺/CD24^{high} population upon treatment with 1 α 25(OH)₂D₃ or BXL0124 (Fig. 5.2). The shift to a CD24^{high}

population suggests that treatment with vitamin D compounds has the potential to specifically alter signaling or differentiation of the putative BCSC subpopulation.

The $CD44^+/CD24^-$, $CD44^+/CD24^{low}$, or $CD44^+/CD24^{high}$ subpopulations were utilized in mammosphere forming conditions. There was a significant increase in mammosphere formation of $CD44^+/CD24^-$, $CD44^+/CD24^{low}$ compared to the $CD44^+/CD24^{high}$ subpopulation, suggesting that these two subpopulations have an enriched cell population with self-renewal and BCSC properties. When the $CD44^+/CD24^-$ and $CD44^+/CD24^{low}$ spheres were grown in the presence of $1\alpha,25(OH)_2D_3$ or BXL0124, there was a significant reduction in mammosphere formation. However, this effect was not observed in the $CD44^+/CD24^{high}$ population, suggesting that vitamin D compounds have preferential inhibitory activity to the putative BCSC subpopulations.

Despite these results in the mammosphere assay, when MCF10DCIS cells were FACS sorted and separate populations were injected into nu/nu mice they failed to show a difference in tumor initiation or growth between the sorted subpopulations (Appendix 1). Insight into these results could be partially explained by the dynamics of cell sorting. Purified populations act as a snapshot and reflect the state of a population at a given moment in time. Common markers used for cancer stem cells change their expression with the cell cycle, during EMT, and during quiescent or activated states (246, 247). Consistent with this hypothesis, we observed a change in the tumor populations after tumors were excised (Appendix 2). Similarly we observed sorted subpopulations revert to the parental population after sorting and maintaining in cell culture for two or more passages (Appendix 3). This cell state transition was consistent with previous reports which showed that purified populations could reconstitute the proportions of populations

observed in the parental cell line, specifically in relation to CD44/CD24 sorted cells (248).

MCF10DCIS xenografts treated with BXL0124 showed a shift to a population that is more CD24^{high}. The shift to a higher CD24 expressing subpopulation observed in xenografts is also consistent with our findings *in vitro* which showed that $1\alpha,25(\text{OH})_2\text{D}_3$ or BXL0124 shifted the CD44⁺/CD24^{-low} to a predominantly CD44⁺/CD24^{high} population. This CD24 shift was correlated to the transcriptional repression of *CD44*, *OCT4*, and *ALDH1A1* by BXL0124 *in vivo* contributing to the reduced tumor burden (249). CD44 is a key regulator in extracellular matrix interactions and cancer stem cells, and correlates with the invasive and metastatic phenotype in breast cancer (182, 250). Previous data from our laboratory identified that CD44-STAT3 signaling is critical for MCF10DCIS cell invasion (202). Oct-4 is a transcription factor that forms a heterodimer with Sox2 and regulates stem cell self-renewal capacity, and the knockdown of Oct4 promotes differentiation (234, 235). Oct-4 is also expressed significantly higher in cancerous tissues than adjacent-tumor tissues and was expressed in CD44⁺/CD24⁻ tumor cells (249, 251). Bourguignon et al. demonstrated that the CD44 ligand, hyaluronic acid, initiates the interaction between CD44 and Nanog leading to the activation of the Nanog–Oct4 network (252). This process has also been associated with activation of multidrug-resistant genes and tumor progression in other cancer types (252). Aldehyde dehydrogenase 1 (ALDH1), is composed of six enzymes that are expressed at high levels in stem cells and are involved in the regulation of stem cell function. ALDH1A1 was correlated with a poor prognosis and reduced overall survival in breast cancer patients (253-255). Therefore, the shift to a CD24^{high} population and the down-regulation of these

three markers indicates potential BXL0124-mediated repression of a cancer stem cell population in MCF10DCIS xenografts.

Ideally, tumors that form initially in primary mice are again assessed for the content of cells with cancer stem cell activity, demonstrated through injection and re-established tumor formation in secondary mice (256). Primary xenografts from control and BXL0124 treated mice were excised dissociated and injected into a secondary set of mice without treatment to assess the long term effects of BXL0124 on the cancer stem cell subpopulation. We did not observe a significant shift to a higher CD24 expressing population in secondary tumors and markers that were correlated with a CD24^{high} shift, *CD44*, *OCT4*, and *ALDH1A*, were not reduced in secondary xenografts derived from primary BXL0124 treated xenografts. These factors suggest that the BCSC population is not regulated in secondary tumors, explaining the lack of reduction in tumor burden. These data suggest that reduction of the BCSC population by BXL0124 is a transient process and constant stimulation by BXL0124 or vitamin D compounds is required to sustain the reduced stemness of breast cancer cells.

5.5 Conclusion

We have provided evidence *in vitro* that vitamin D compounds repressed the BCSC population. We have also demonstrated that BXL0124 was effective at targeting the putative BCSC subpopulation and pluripotency genes *in vivo*. BXL0124 repressed the stem cell phenotype by regulating stemness genes including *CD44*, *OCT4*, and *ALDH1A1*. Our data, in part, contribute to the mechanism by which vitamin D

compounds reduce breast tumor growth, and point to effects mediated at the level of putative breast cancer stem cells.

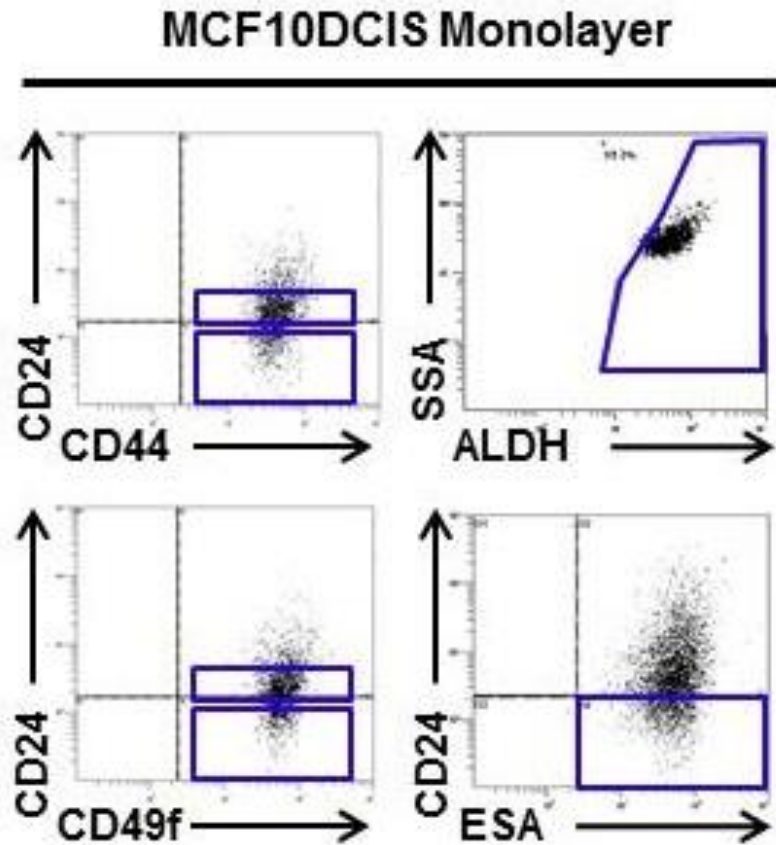


Figure 5.1 Levels of putative breast cancer stem cell markers in the MCF10DCIS cell line. MCF10DCIS cells were grown in monolayer cell culture for 24h without treatment

Cells were stained with combinations of antibodies against CD44, CD49f, CD24, ESA, as well as assessed for aldehyde dehydrogenase activity (ALDH) by using the Aldefluor assay. Flow cytometry analysis was performed. Representative histograms from flow cytometry are shown. Blue boxes highlight the putative breast cancer stem cell containing subpopulation for given markers. SSA - single-scattering albedo.

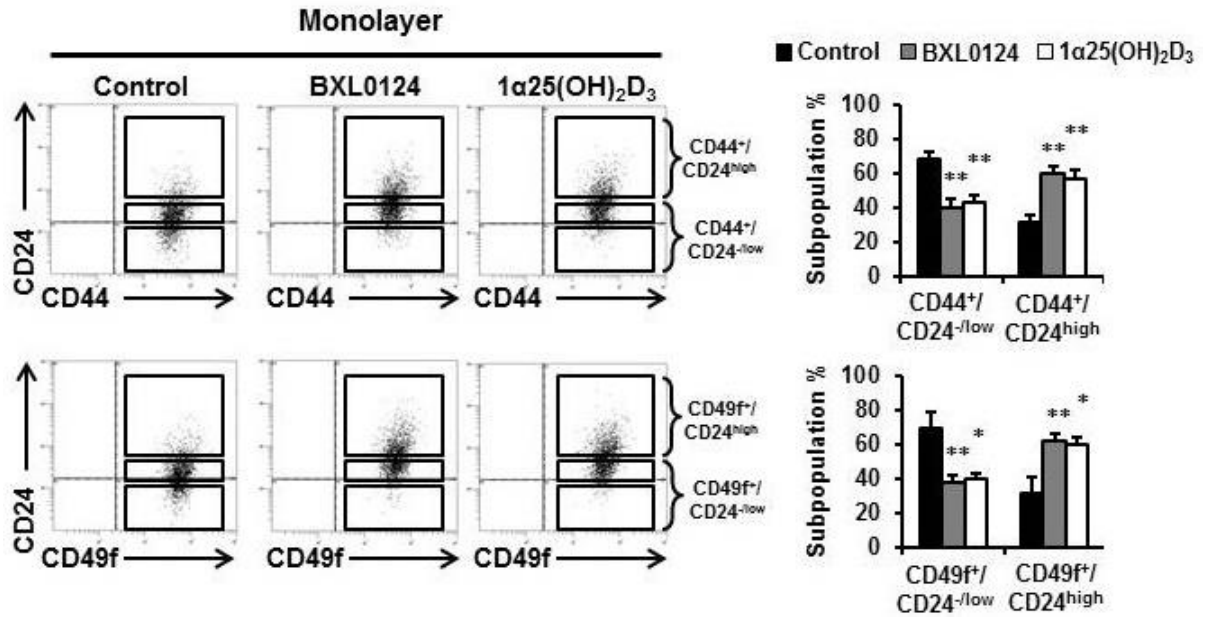


Figure 5.2 1α25(OH)₂D₃ and BXL0124 repress the breast cancer stem cell subpopulations in MCF10DCIS cells

MCF10DCIS cells were grown in monolayer cell culture and treated with 1α25(OH)₂D₃ (100 nM) and BXL0124 (10 nM) for 24 h. Cells were stained with combinations of antibodies against CD44 or CD49f and CD24, and then flow cytometry was performed. Representative histograms from flow cytometry of MCF10DCIS cells treated with vitamin D compounds are shown. Different subpopulations based on varying levels of CD24 are highlighted on the histograms with bold rectangles. The average percentage of CD44⁺/CD24^{low} and CD49f⁺/CD24^{low} subpopulations as well as the CD44⁺/CD24^{high} and CD49f⁺/CD24^{high} subpopulations from three independent experiments are represented as a bar graph to show the difference between the control and treatment groups. The data are presented as the mean ± S.E.M. * p < 0.05, ** p < 0.01.

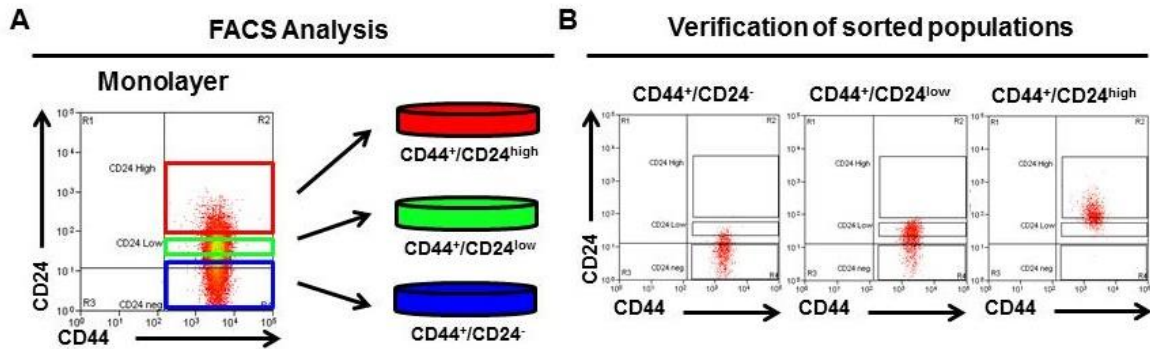


Figure 5.3 Flow cytometry verification of FACS sorted subpopulations of MCF10DCIS cells based on CD44 and CD24 cell sorting

(A) MCF10DCIS cells were grown in monolayer cell culture and harvested after 48h. Cells were stained with antibodies to CD44 and CD24, and then they were sorted into three subpopulations by fluorescently activated cell sorting (FACS), $CD44^{+}/CD24^{high}$, $CD44^{+}/CD24^{low}$, and $CD44^{+}/CD24^{-}$. (B) After FACS sorting the three subpopulations were immediately analyzed by flow cytometry to validate that the three subpopulations were sorted correctly and that there was little contamination between the three subpopulations.

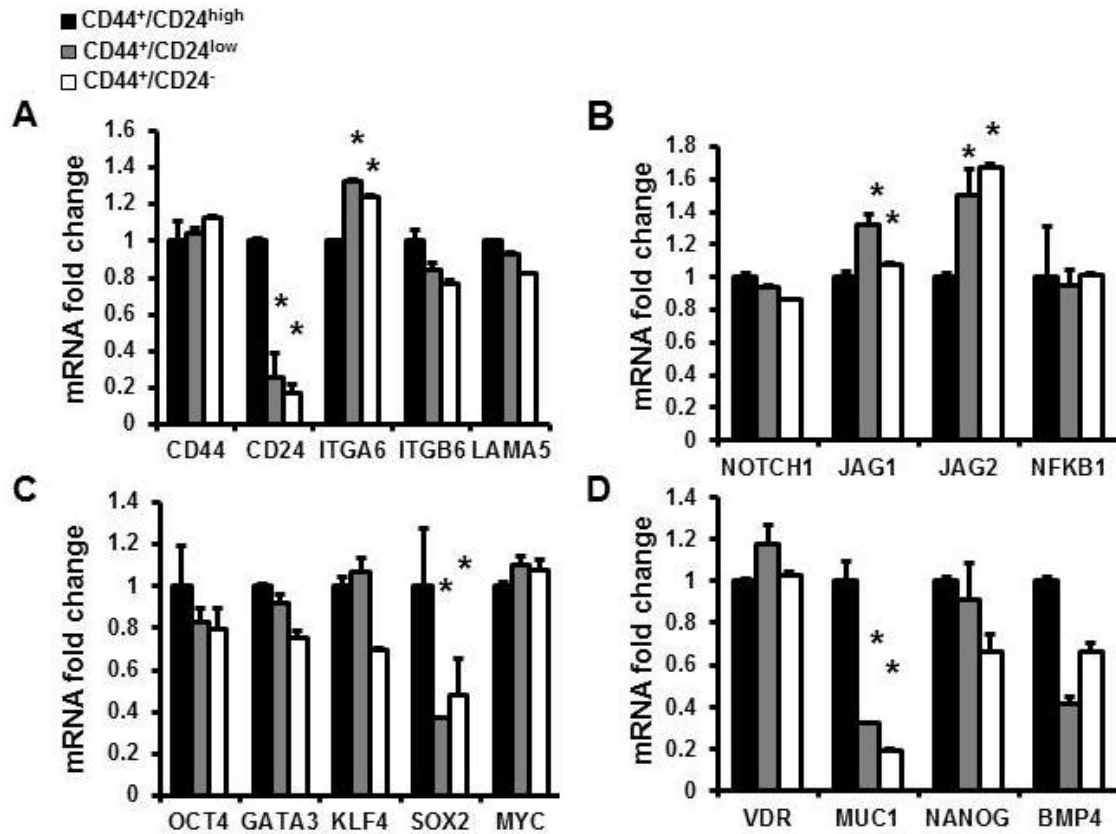


Figure 5.4 Gene expression of breast cancer stem cell markers in MCF10DCIS subpopulations

qPCR analysis was performed MCF10DCIS subpopulations after FACS sorting for genes associated with (A) surface markers, (B) stem cell signaling, (C) genes related to pluripotency, and (D) differentiation associated genes. The data are presented as the mean \pm S.E.M. (n=6). * $p < 0.05$. Cycle number averages for qPCR are shown in parenthesis: *CD44* (#2), *CD24* (#22), *ITGA6* (#21), *ITGB6* (#23), *LAMA5* (#22), *NOTCH1* (#23), *JAG1* (#22), *JAG2* (#24), *NFKB1* (#23), *OCT4* (#27), *GATA3* (#24), *KLF4* (#26), *SOX2* (#34), *MYC* (#22), *VDR* (#26), *MUC1* (#28), *NANOG* (#32), and *BMP4* (#33).

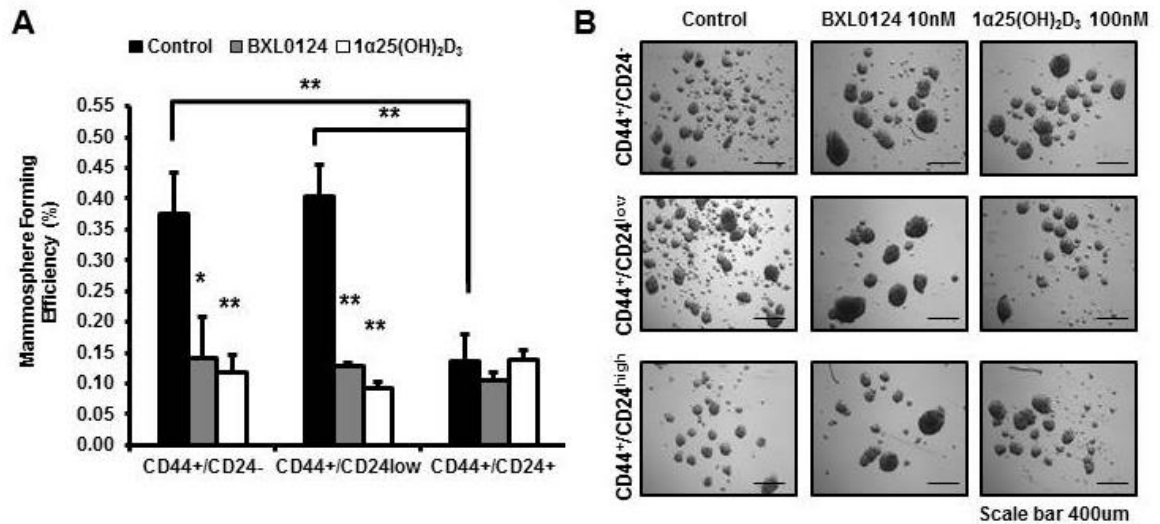


Figure 5.5 Vitamin D compounds repress the formation of putative breast cancer stem cell subpopulations in mammosphere cell culture

(A) MCF10DCIS cells were stained with antibodies to CD44 and CD24, they were sorted into three subpopulations by fluorescently activated cell sorting (FACS), CD44⁺/CD24^{high}, CD44⁺/CD24^{low}, and CD44⁺/CD24⁻. These subpopulations were plated at a density of 5,000 cells/mL into mammosphere cell conditions and grown for 5 days in the presence of 1α25(OH)₂D₃ (100 nM) and BXL0124 (10 nM). Mammosphere forming efficiency (MFE) of primary MCF10DCIS mammospheres from different subpopulations is shown. MFE was calculated by dividing the number of mammospheres (≥ 100 μm) formed by the number of cells seeded presenting this as a percentage. Experiments were performed in triplicate and the data are presented as the mean ± S.E.M. * $p < 0.05$, ** $p < 0.01$. **(B)** Representative pictures of primary MCF10DCIS mammospheres from different subpopulations is shown for visual comparison of colony formation (scale bar 400 μm).

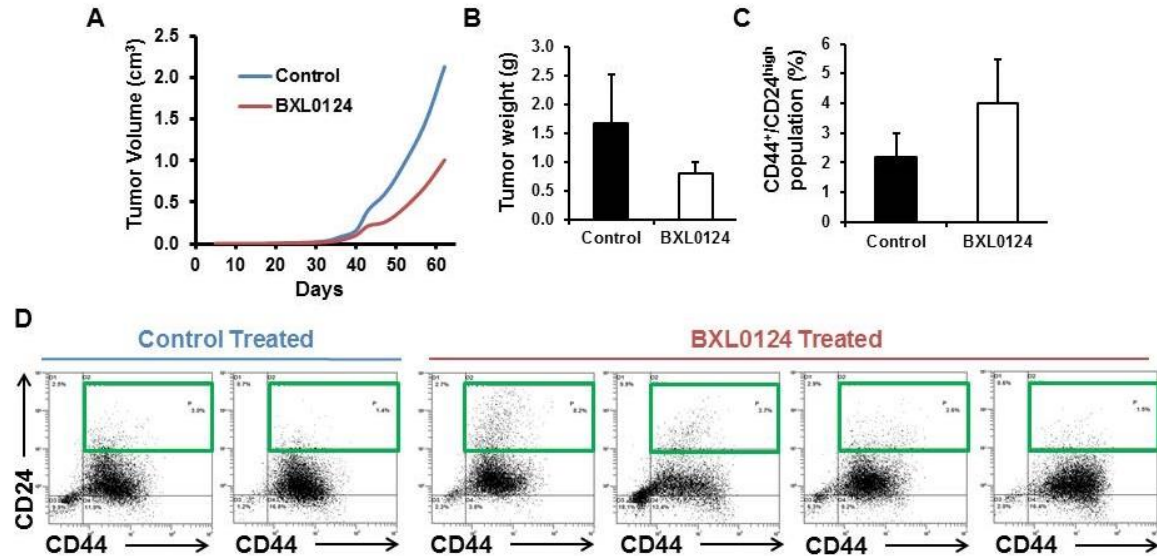


Figure 5.6 BXL0124 treatment of MCF10DCIS xenografts shifts the CD44⁺/CD24⁻ subpopulation to a population that is more CD24^{high}

(A) BXL0124 (0.1 $\mu\text{g/kg}$ body weight) was administered via intraperitoneal (i.p.) injection to MCF10DCIS (10^5 cells) xenografted nu/nu mice (n=3-4) once a day 6 times a week. Average tumor growth curves are shown. Tumor volume was measured twice a week. Tumor weight was measured at necropsy. (B) Average final tumor weights at necropsy are shown, control (n=3) and BXL0124 (n=4), mean \pm S.E.M. (C) Average percentage of the CD44⁺/CD24^{high} subpopulation in MCF10DCIS tumors treated with BXL0124 (0.1 $\mu\text{g/kg}$ body weight) is shown, control (n=3) and BXL0124 (n=4), mean \pm S.E.M. Tumors were excised and dissociated by mechanical and enzymatic digestion then analyzed by flow cytometry for CD44 and CD24 expression. (D) Histograms from flow cytometry analysis of CD44/CD24 staining of tumor samples are shown. Each histogram represents one xenografted MCF10DCIS tumor. Green boxes highlight the CD44⁺/CD24^{high} subpopulation.

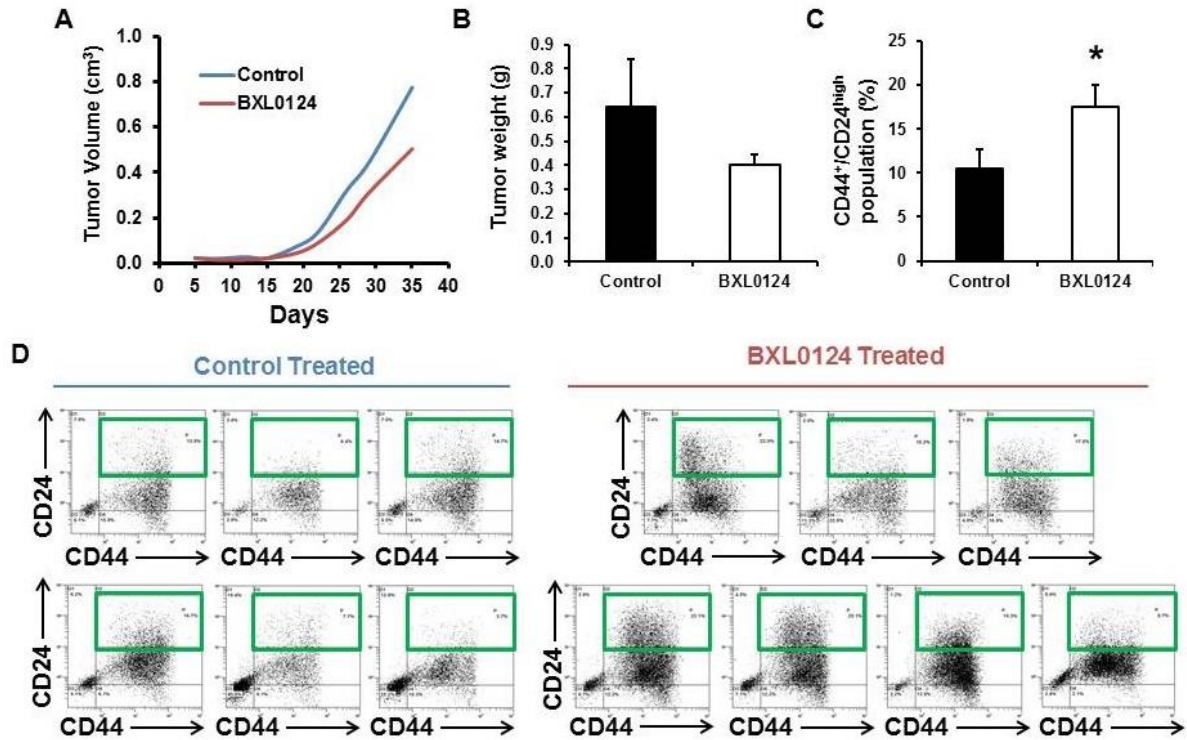


Figure 5.7 BXL0124 treatment of MCF10DCIS xenografts shifts the CD44⁺/CD24^{high} subpopulation to a population that is more CD24^{high}

(A) BXL0124 (0.1 $\mu\text{g/kg}$ body weight) was administered via intraperitoneal (i.p.) injection to MCF10DCIS (10^6 cells) xenografted nu/nu mice (n=6-7) once a day 6 times a week. Average tumor growth curves are shown. Tumor volume was measured twice a week. Tumor weight was measured at necropsy. (B) Average final tumor weights at necropsy are shown, control (n=6) and BXL0124 (n=7), mean \pm S.E.M. (C) Tumors were excised and dissociated by mechanical and enzymatic digestion then analyzed by flow cytometry for CD44 and CD24 expression. Average percentage of the CD44⁺/CD24^{high} subpopulation in MCF10DCIS tumors treated with BXL0124 (0.1 $\mu\text{g/kg}$ body weight) is shown, control (n=6) and BXL0124 (n=7), mean \pm S.E.M., * p < 0.05. (D) Histograms from flow cytometry analysis of CD44/CD24 staining of tumor samples are shown. Each

histogram represents one xenografted MCF10DCIS tumor. Green boxes highlight the $CD44^{+}/CD24^{\text{high}}$ subpopulation.

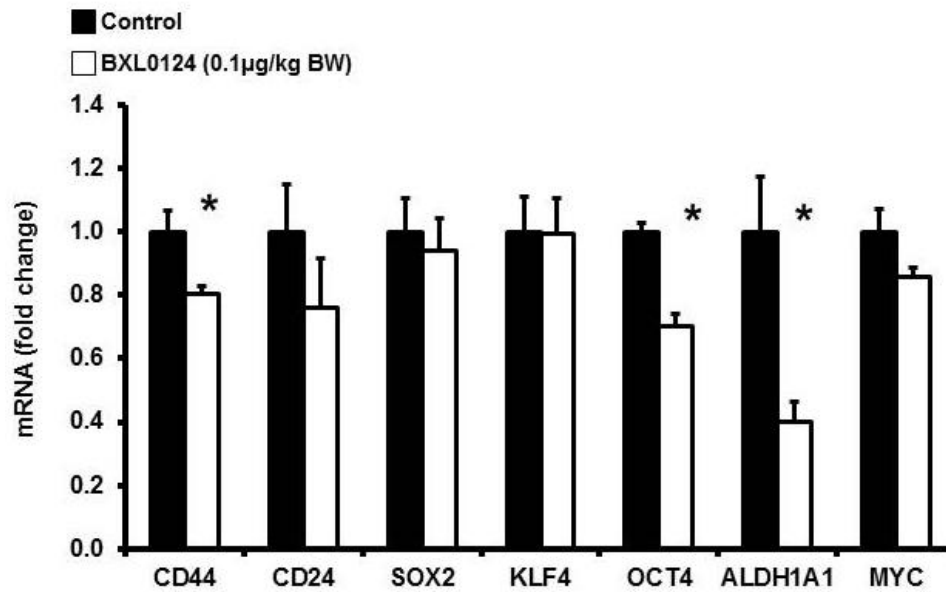


Figure 5.8 BXL0124 represses markers of pluripotency and cancer stem cell genes in MCF10DCIS xenografts

Tumors were excised and dissociated by mechanical and enzymatic digestion then analyzed by qPCR for genes associated with pluripotency and the stem cell phenotype. The data are presented as the mean \pm S.E.M. (n=6-7). * $p < 0.05$. Cycle number averages for qPCR are shown in parenthesis: *CD44* (#20), *CD24* (#26), *SOX2* (#34), *KLF4* (#29), *OCT4* (#27), *ALDH1A1* (#29), and *MYC* (#24).

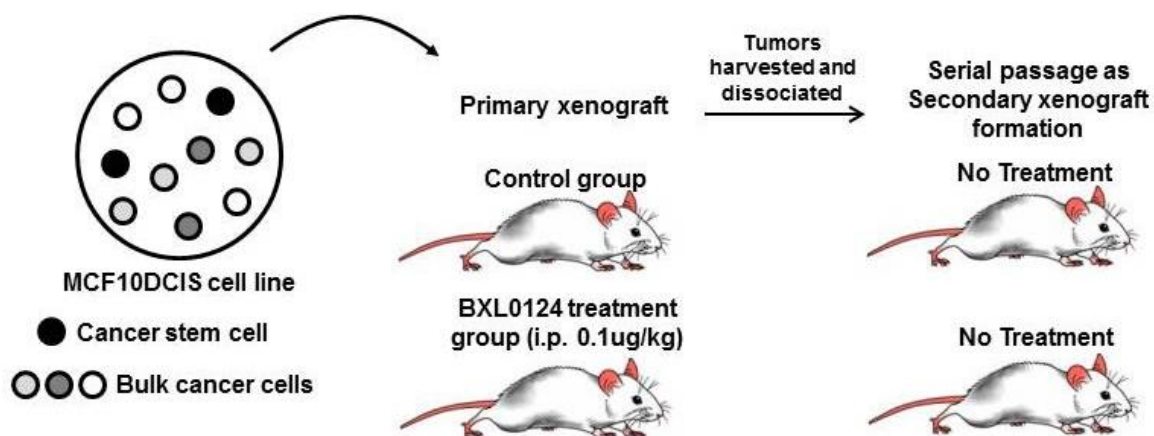


Figure 5.9 Schematic of MCF10DCIS xenograft tumorigenicity assay in nu/nu mice after BXL0124 treatment in primary xenografts and secondary xenografts

Cancer stem cells are defined by their ability to produce progressively growing tumors consisting of cells from the original tumor. For this reason they are implicated in tumor initiation and progression. Limiting-dilution or clonal tracking of tumor cells are classical strategies that are used to determine the tumor initiating capacity and frequency of breast cancer stem cells. Therefore MCF10DCIS tumors that form during vehicle (DMSO) and BXL0124 treatment (0.1 $\mu\text{g/kg}$ body weight by i.p. injections) in primary tumors are tested for their breast cancer stem cell content by harvesting then dissociating and serial passaging the primary xenografts into nude mice.

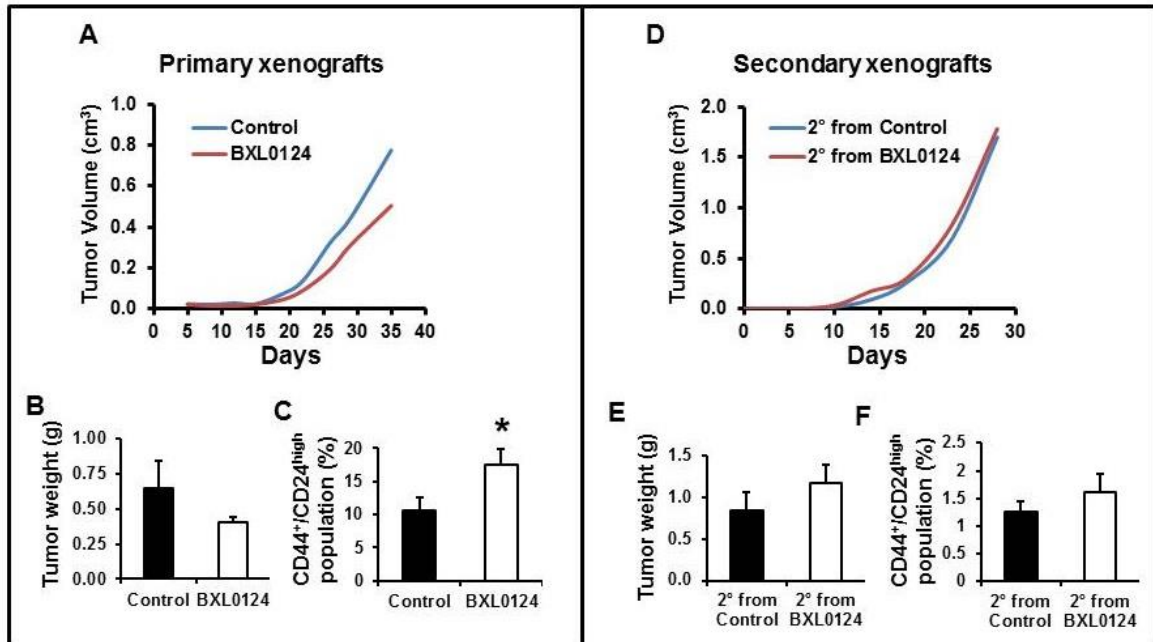


Figure 5.10 BXL0124 treatment does not result in long term effects on tumor growth in secondary MCF10DCIS xenografts relative to untreated mice.

(A) BXL0124 (0.1 $\mu\text{g/kg}$ body weight) was administered via intraperitoneal (i.p.) injection to nu/nu mice with mammary fat pad MCF10DCIS (10^6 cells) xenografts (n=6-7) once a day 6 times a week. Average tumor growth curves are shown. Tumor volume was measured twice a week. Tumor weight was measured at necropsy. (B) Average final tumor weights at necropsy are shown, control (n=6) and BXL0124 (n=7), mean \pm S.E.M. (C) Tumors were excised and dissociated by mechanical and enzymatic digestion then analyzed by flow cytometry for CD44 and CD24 expression. Average percentage of the CD44⁺/CD24^{high} subpopulation in MCF10DCIS tumors treated with BXL0124 (0.1 $\mu\text{g/kg}$ body weight) is shown, control (n=6) and BXL0124 (n=7), mean \pm S.E.M., * $p < 0.05$. (D) Primary xenografts from the control group and BXL0124 treated group were excised, dissociated and reinjected (10^6 cells) into the mammary fat pad of nu/nu mice (n=8 per

group). Average tumor growth curves are shown. Tumor volume was measured twice a week. Tumor weight was measured at necropsy. **(E)** Average final tumor weights at necropsy are shown, $n=8$, mean \pm S.E.M. **(F)** Tumors were excised and dissociated by mechanical and enzymatic digestion then analyzed by flow cytometry for CD44 and CD24 expression. The average percentage of the CD44⁺/CD24^{high} subpopulation in secondary untreated MCF10DCIS tumors from primary control and primary BXL0124 treated tumors is shown, $n=8$, mean \pm S.E.M.

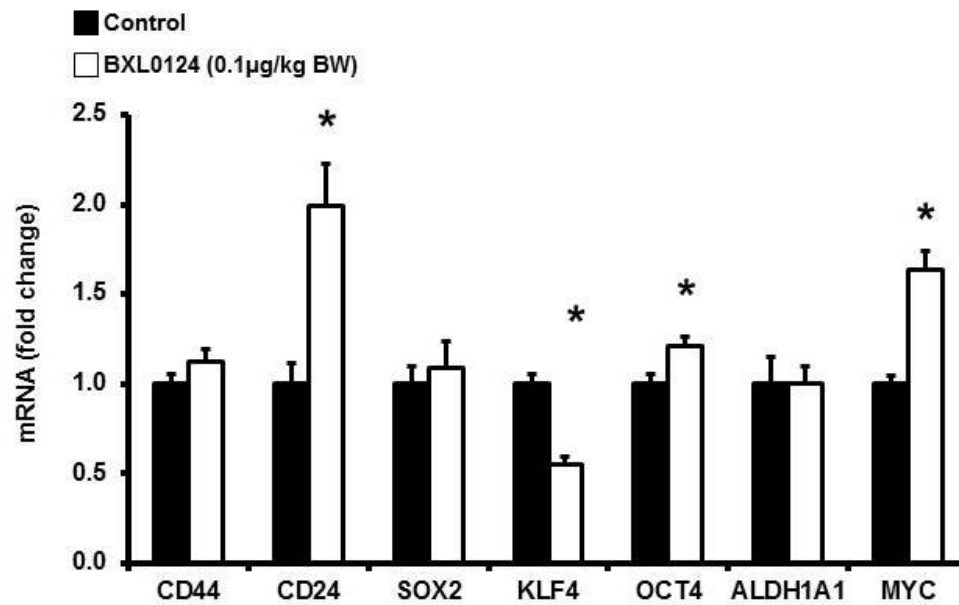


Figure 5.11 Secondary MCF10DCIS xenografts from BXL0124 treated primary xenografts do not show reductions in pluripotency genes

Tumors were excised and dissociated by mechanical and enzymatic digestion then analyzed by qPCR for genes associated with pluripotency and the stem cell phenotype. The data are presented as the mean \pm S.E.M. (n=5). * $p < 0.01$. Cycle number averages for qPCR are shown in parenthesis: *CD44* (#20), *CD24* (#26), *SOX2* (#34), *KLF4* (#29), *OCT4* (#27), *ALDH1A1* (#29), and *MYC* (#23)

Chapter 6: Conclusion

Breast cancer is a collection of genetically diverse diseases with distinct histopathological features progressing from pre-malignant hyperplasia to invasive and ultimately metastasis. With more advanced screening methods, the early stages of breast cancer are becoming more common but therapeutic agents for their treatment are limited. As such it is important to test potential therapeutics for their breast cancer preventive and inhibitory effects in the early stages of breast cancer. In this study we assessed vitamin D compounds for their inhibition of breast cancer progression and regulation of breast cancer stem cells (BCSCs).

In the MCF10DCIS model of breast cancer progression a vitamin D analog, BXL0124, inhibited ductal carcinoma *in situ* (DCIS) progression to IDC. BXL0124 treatment decreased cell proliferation and maintained vitamin D receptor (VDR) levels in tumors. BXL0124 treated cells maintained the critical myoepithelial cell layer and basement membrane involved in DCIS structures. In addition, BXL0124 treatment reduced the mRNA levels of matrix metalloproteinases (MMPs), contributing to the inhibition of invasive transition.

Breast cancer stem cells (BCSCs) are a subset of tumor cells that are believed to be the cells responsible for the establishment and maintenance of tumors. Moreover, BCSCs are suggested to be the main cause of progression to metastasis and recurrence of cancer because of their tumor-initiating abilities and resistance to conventional therapies.

Since BCSCs are a major factor involved in breast cancer progression we assessed the role of vitamin D compounds on this population. These studies showed that the

mammosphere formation and self-renewal of mammospheres was inhibited by treatment with vitamin D compounds ($1\alpha,25(\text{OH})_2\text{D}_3$ or BXL0124). These effects were attributed to the repression of markers associated with the stem cell-like phenotype and signaling, such as CD44, CD49f, c-Notch1, and pNF κ B *in vitro*. In turn the repression of pluripotency genes, *OCT4* and *KLF-4*, and *CD44* were also observed in mammospheres, contributing to the inhibition of stem cell self-renewal. This data suggests that a regulatory loop of these signaling markers and transcription factors likely plays a role in the inhibition of BCSCs by vitamin D compounds.

The putative CD44⁺/CD24^{-/low} breast cancer stem cell population was reduced *in vitro*, suggesting the inhibition or repression of the BCSC population. Vitamin D compounds specifically inhibited the mammosphere formation of BCSC subpopulations and did not have significant effects on the CD44⁺/CD24^{high} subpopulation. MCF10DCIS xenografts treated with BXL0124 showed a shift to a population that is more CD24^{high}. The shift to a higher CD24 expressing subpopulation observed in xenografts is consistent with our findings *in vitro* and points to the regulation of the BCSC subpopulation *in vivo*. The CD44⁺/CD24^{high} subpopulation in MCF10DCIS expresses lower levels of notch signaling, which contribute to the reduced tumor burden observed in these xenografts (245). Supporting this, BXL0124 has been shown to decrease notch signaling both *in vitro* and in mammosphere cell culture (245, 257). Also consistent with our previous findings *in vitro* we observed the repression of *CD44* and *OCT4*, as well as *ALDH1A1* in xenografts.

The wide range of biological activities of vitamin D and its analogs have suggested their potential as therapeutic agents in breast cancer (258). However the

investigation of VDR levels in clinical samples of breast cancer suggested that vitamin D supplementation would be most beneficial as a preventative agent due to higher VDR levels in normal mammary tissue. We demonstrated the preventive potential of the Gemini vitamin D analog, BXL0124 on the inhibition of breast cancer progression, and inhibitory effects of vitamin D compounds on the breast cancer stem cell population *in vitro* and *in vivo*. Overall these results contribute to the understanding of vitamin D mediated reduction in tumor growth and progression in breast cancer.

Chapter 7: Future Directions

Our studies show that vitamin D compounds could be effective treatment options to inhibit the progression of pre-malignant lesions of the breast due to regulation of the breast cancer stem cell (BCSC) population. These studies have prompted novel questions as to the mechanistic understanding of stem cell regulation by vitamin D, as well as other roles that vitamin D compounds might play in the inhibition of breast cancer.

From the results in these studies we hypothesize that BXL0124 treatment affects BCSCs leading to a more differentiated tumor cell type with a greater ability to form organized structures and maintain cell polarity. DCIS is now seen as a diverse stage of breast cancer where the degree of differentiation within the DCIS lesion has a significant impact on the outcome of the tumor (259). DCIS cases exhibiting low differentiation most often progress to invasive carcinoma, whereas cases of high differentiation are less likely to do so (259). Based on our data we hypothesize that BXL0124 treatment can maintain the differentiated state of progenitors and stem cells. Signals from the stromal environment could induce the de-differentiation of myoepithelial cells back to a progenitor or stem-like state in normal progression. As a consequence, the myoepithelial cell layer is gradually lost transiting to an invasive phenotype.

We observed a correlation of increased CD24 expression with a decrease in transcription of *CD44*, *OCT4*, and *ALDH1A1* with the gemini vitamin D analog, BXL0124, in MCF10DCIS xenografts. Vitamin D mediated reduction of pluripotency markers, such as *OCT4*, *KLF-4*, and *GATA3*, *in vitro* was also detected. The activation of Oct4 has been shown to promote de-differentiation and induce a cancer stem cell

phenotype (260). Similarly, the knockdown of Oct4 promotes differentiation (234, 235). A study by Bourguignon and colleagues linked the activation of CD44 with downstream stimulation of the Nanog-Oct4 network (252). Therefore it is possible that BXL0124 is exerting its stem cell inhibitory effects by down-regulation of CD44 with downstream effects on the stem cell markers, Oct4, and ALDH1A1, leading to differentiation of stem cells to more mature "normal" cancer cells. To study this we would utilize the mammosphere assay which allows the differentiation of stem cells to multiple lineages. Such lineage markers (Table 1.3) would be assessed in MCF10DCIS, MCF-7, and SUM159 primary, secondary, and tertiary spheres in the presence of vitamin D compounds to see if the markers are altered. These markers would also be assessed during breast cancer progression using xenografts of the MCF10DCIS cell line at the critical DCIS to IDC transition observed at weeks 3 and 4. These studies would provide a unique mechanism by which vitamin D compounds could maintain the differentiated state of BCSCs along a specific lineage to impede the progression of breast cancer.

Since we observed a shift of the $CD44^{+}/CD24^{-/low}$ subpopulation to a population that is more $CD44^{+}/CD24^{high}$ that was correlated to a repression of *OCT4* transcription *in vitro* and *in vivo*, we propose to assess the role of CD24 and OCT4 on tumor progression. We will utilize RNA interference as well as gene overexpression in the nonmalignant cell line MCF10A in comparison to the malignant cell line MCF10DCIS. Xenograft transplantation using the nonmalignant MCF10A and malignant MCF10DCIS cell line will be conducted. Upon establishment of tumors, inhibition of CD24 and OCT4 expression can be achieved using short interfering RNA. These markers can then be assessed on the basis of tumor burden, breast cancer progression and the levels of BCSCs

within the tumors. Utilizing the nonmalignant cell line MCF10A will help determine the role of these markers in malignant transformation, and assess whether their regulation is sufficient to induce a tumorigenic cell line.

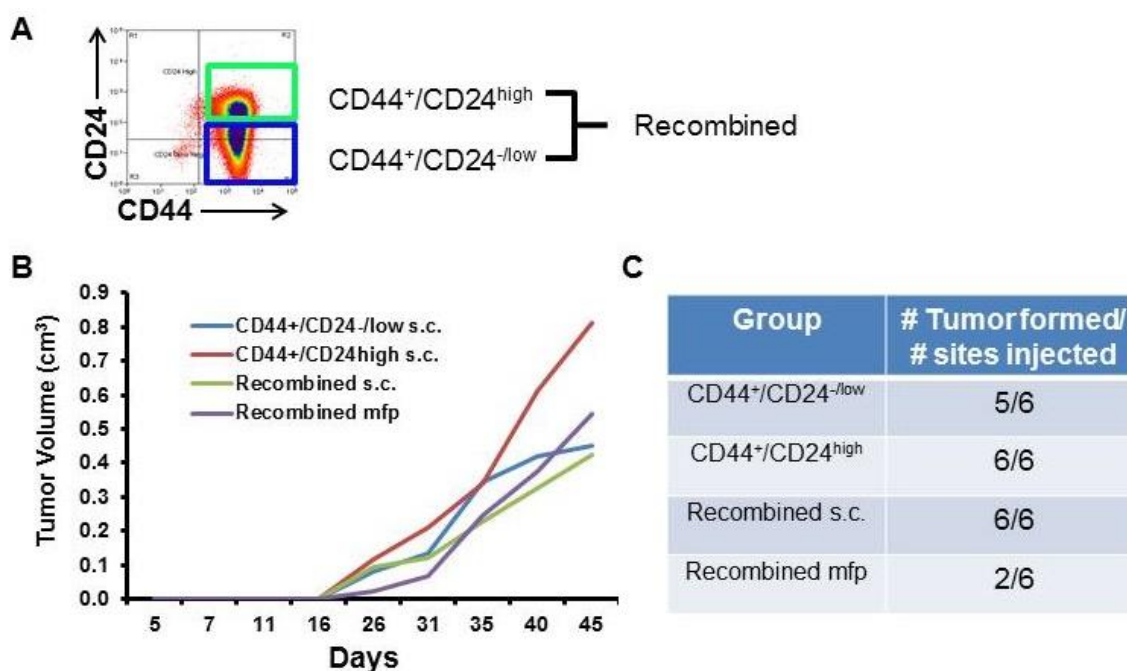
Studies have shown that cells that survive chemotherapy are enriched for putative BCSCs and these cells were capable of increased colony formation and enrichment of the $CD44^{+}/CD24^{-/low}$ population (89, 90, 261). Therefore the combination of stem cell targeting therapies with chemotherapy or traditional therapies may target the whole cancer cell population and offer a strategy for more effective treatments (262). Based on experiments in future directions we suggest that vitamin D compounds might differentiate BCSCs to a bulk population that would be more susceptible to chemotherapy. Vitamin D treatment may be a useful adjuvant therapy used prior to or in conjunction with other treatment modalities. In order to study this vitamin D would be administered in combination with a variety of first line therapeutics, such as docetaxel and cisplatin in an animal model of breast cancer progression. Xenograft transplantation experiments using cell lines from multiple subtypes of breast cancer would be treated with monotherapy of each agent and in combination with vitamin D compounds, to assess their therapeutic effects. To further assess the effects of the treatments on BCSC and regulation of differentiation, tumors would be evaluated for the amount of remaining stem cell subpopulations as well as differentiated cell populations.

We have suggested that vitamin D compounds inhibit breast cancer progression from DCIS to IDC by way of BCSC regulation. CSCs are believed to compose a subpopulation in tumors which are responsible for drug resistance, tumor recurrence, and metastasis (85-88). The prevalence of $CD44^{+}/CD24^{-/low}$ cells in breast cancer has been

implicated in distant metastases (263). Since vitamin D compounds are capable of shifting this population to a higher CD24 expressing population we hypothesize that vitamin D compounds might further inhibit metastasis as breast tumors progress. The metastatic MDA-MB-231 cell line, an estrogen-independent breast cancer cell line derived from the pleural effusion of a cancer patient, can be used in a mouse model of metastasis via intravenous injection of the cells into immunodeficient mice. Xenografts using the MCF10CA1a cell line injected subcutaneously into mice could investigate this hypothesis. Treatment of these two models with vitamin D compounds and analysis of sites of metastasis in breast cancer, such as lung, brain, and bone would give new insights into the mechanistic role of vitamin D. Although the implantation of established cell lines derived from human breast cancer is relatively simple and allows the genetic or pharmacological manipulation of the implanted cells, there are clear limitations to such models. First, immune responses, which have a key role during tumor development, are impaired in immunocompromised mice. Second, stromal components are not of tumor origin.

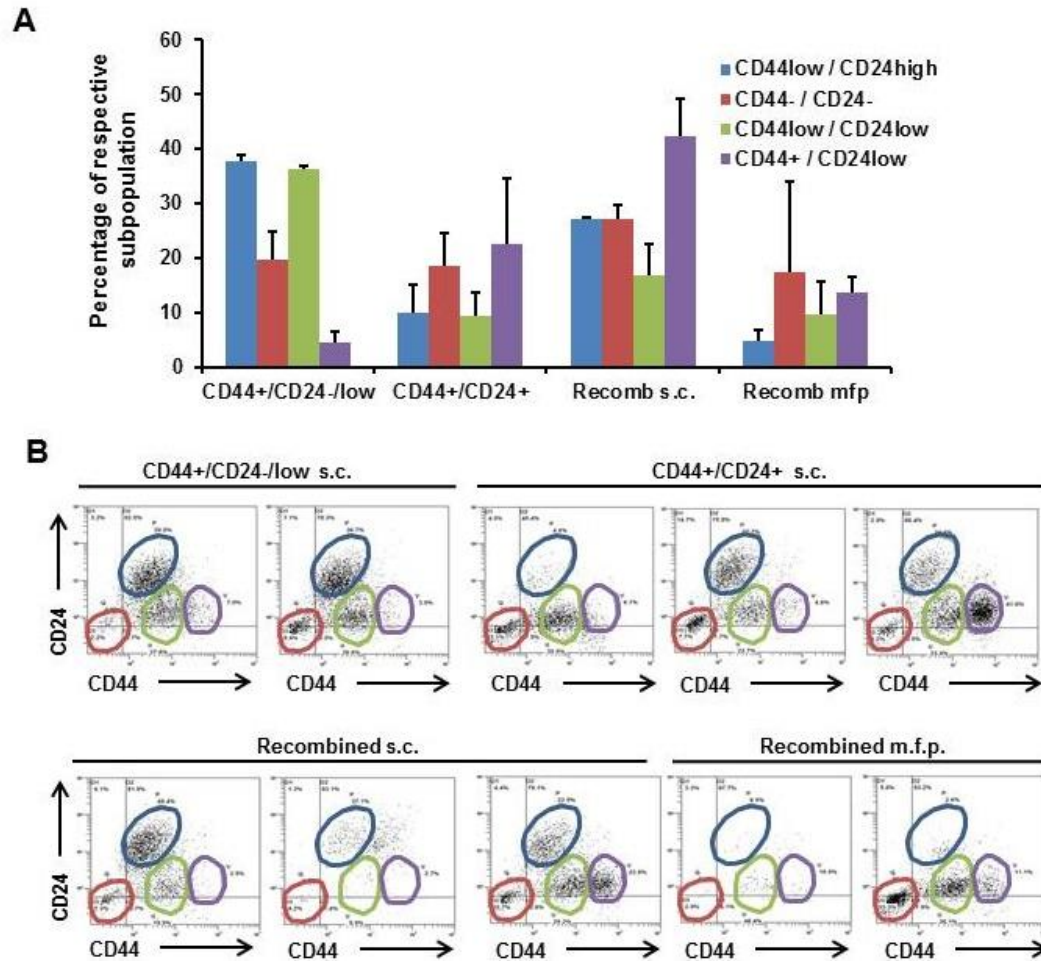
Vitamin D compounds might have other anti-cancer effects in addition to their proposed role in the inhibition of breast cancer progression and effects on the BCSC subpopulation. This makes them desirable preventive and therapeutic candidates for breast cancer. Future studies will elucidate mechanisms by which these compounds inhibit breast cancer progression and provide a better understanding of how to best utilize them clinically.

Appendix

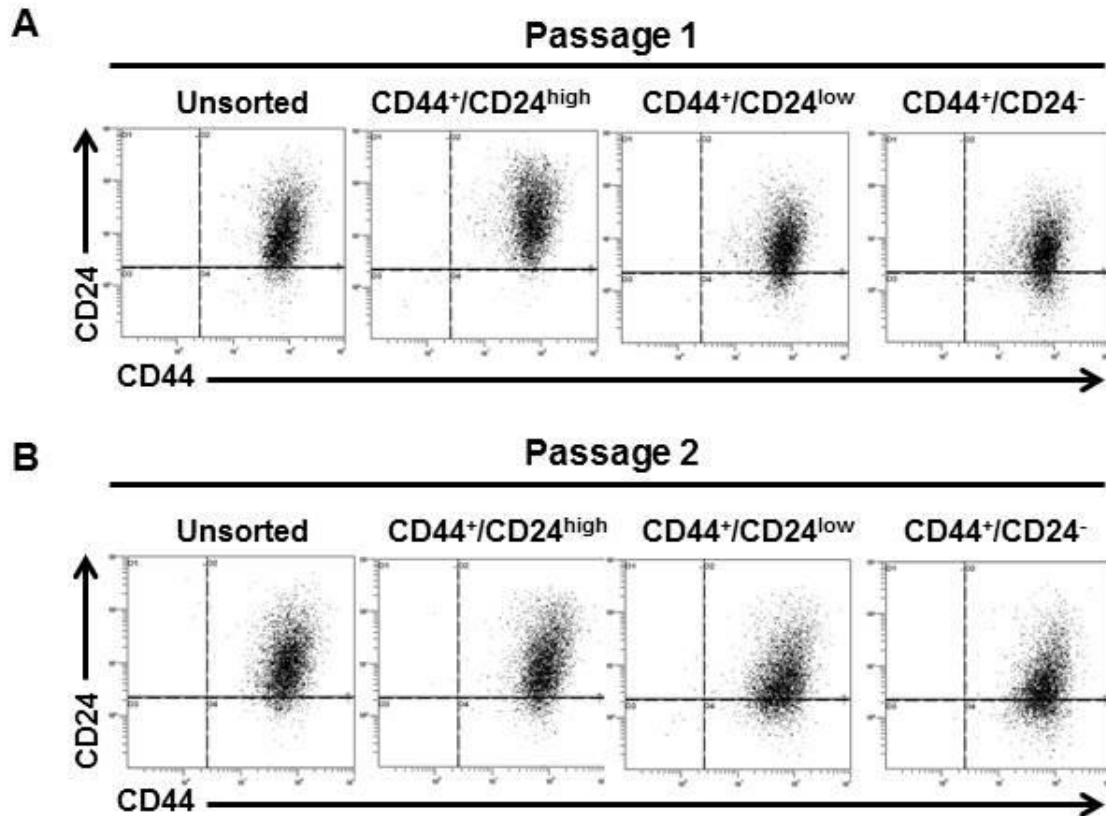


Appendix 1. Tumorigenicity of FACS sorted MCF10DCIS subpopulations *in vivo*.

(A) MCF10DCIS cells were FACS sorted by CD44 and CD24 into two subpopulations, CD44⁺/CD24^{high} and CD44⁺/CD24^{low}, these two populations were then recombined to reform the whole tumor cell population (B) Average tumor growth curves are shown. The two FACS sorted subpopulations were injected to subcutaneous xenografts (10⁵ cells). The recombined population was injected subcutaneously (10⁵ cells) and into the mammary fat pad (10⁵ cells) of nu/nu mice. (C) A summary of tumor formation for each subpopulation is shown.



Appendix 2. Flow cytometry analysis of CD44 and CD24 levels in MCF10DCIS subpopulation subcutaneous xenografts. (A) Tumors from subpopulations (CD44⁺/CD24^{high} and CD44⁺/CD24^{low}) and recombined populations were excised, dissociated, and analyzed by flow cytometry for CD44 and CD24 expression. The average of each subpopulation is represented in a bar graph as the mean \pm S.E.M., n=2-3 (B) Histograms from flow cytometry analysis of CD44/CD24 staining of tumor samples are shown. Each histogram represents one xenografted tumor. Colored boxes highlight the gating used for different subpopulations. Blue - CD44^{low}/CD24^{high}, Red - CD44⁻/CD24⁻, Green - CD44^{low}/CD24^{low} and Purple - CD44⁺/CD24^{low}.



Appendix 3. Passage of MCF10DCIS subpopulations in monolayer cell culture after FACS sorting. (A) MCF10DCIS were FACS sorted based on CD44 and CD24 expression. These sorted cells were then plated in monolayer cell culture. After 48h of growth they were assessed by flow cytometry for CD44 and CD24. Histograms for each subpopulation are shown. (B) After 48h of growth in the primary passage cells were harvested and passed to a second passage. After 72h of growth in secondary passage the cells were assessed by flow cytometry for CD44 and CD24. Histograms for each subpopulation are shown.

References

1. Siegel RL, Miller KD, Jemal A. Cancer statistics, 2015. *CA Cancer J Clin*. 2015;65:5-29.
2. Amir E, Freedman OC, Seruga B, Evans DG. Assessing women at high risk of breast cancer: a review of risk assessment models. *J Natl Cancer Inst*. 2010;102:680-91.
3. Troester MA, Swift-Scanlan T. Challenges in studying the etiology of breast cancer subtypes. *Breast Cancer Res*. 2009;11:104.
4. Almendro V, Fuster G. Heterogeneity of breast cancer: etiology and clinical relevance. *Clin Transl Oncol*. 2011;13:767-73.
5. Pare R, Yang T, Shin JS, Tan PH, Lee CS. Breast cancer precursors: diagnostic issues and current understanding on their pathogenesis. *Pathology*. 2013;45:209-13.
6. Hu X, Stern HM, Ge L, O'Brien C, Haydu L, Honchell CD, et al. Genetic alterations and oncogenic pathways associated with breast cancer subtypes. *Mol Cancer Res*. 2009;7:511-22.
7. Walsh T, Lee MK, Casadei S, Thornton AM, Stray SM, Pennil C, et al. Detection of inherited mutations for breast and ovarian cancer using genomic capture and massively parallel sequencing. *Proc Natl Acad Sci U S A*. 2010;107:12629-33.
8. Prat A, Perou CM. Deconstructing the molecular portraits of breast cancer. *Mol Oncol*. 2011;5:5-23.
9. Perou CM, Sorlie T, Eisen MB, van de Rijn M, Jeffrey SS, Rees CA, et al. Molecular portraits of human breast tumours. *Nature*. 2000;406:747-52.
10. Sorlie T, Perou CM, Tibshirani R, Aas T, Geisler S, Johnsen H, et al. Gene expression patterns of breast carcinomas distinguish tumor subclasses with clinical implications. *Proc Natl Acad Sci U S A*. 2001;98:10869-74.
11. Hu Z, Fan C, Oh DS, Marron JS, He X, Qaqish BF, et al. The molecular portraits of breast tumors are conserved across microarray platforms. *BMC Genomics*. 2006;7:96.
12. Carey LA, Perou CM, Livasy CA, Dressler LG, Cowan D, Conway K, et al. Race, breast cancer subtypes, and survival in the Carolina Breast Cancer Study. *JAMA*. 2006;295:2492-502.
13. Voduc KD, Cheang MC, Tyldesley S, Gelmon K, Nielsen TO, Kennecke H. Breast cancer subtypes and the risk of local and regional relapse. *J Clin Oncol*. 2010;28:1684-91.
14. Metzger-Filho O, Sun Z, Viale G, Price KN, Crivellari D, Snyder RD, et al. Patterns of Recurrence and outcome according to breast cancer subtypes in lymph node-negative disease: results from international breast cancer study group trials VIII and IX. *J Clin Oncol*. 2013;31:3083-90.
15. Potemski P, Kusinska R, Watala C, Pluciennik E, Bednarek AK, Kordek R. Prognostic relevance of basal cytokeratin expression in operable breast cancer. *Oncology*. 2005;69:478-85.

16. Dowsett M, Cuzick J, Wale C, Forbes J, Mallon EA, Salter J, et al. Prediction of risk of distant recurrence using the 21-gene recurrence score in node-negative and node-positive postmenopausal patients with breast cancer treated with anastrozole or tamoxifen: a TransATAC study. *J Clin Oncol*. 2010;28:1829-34.
17. Troester MA, Herschkowitz JI, Oh DS, He X, Hoadley KA, Barbier CS, et al. Gene expression patterns associated with p53 status in breast cancer. *BMC Cancer*. 2006;6:276.
18. Gradishar WJ. Adjuvant endocrine therapy for early breast cancer: the story so far. *Cancer Invest*. 2010;28:433-42.
19. Dunnwald LK, Rossing MA, Li CI. Hormone receptor status, tumor characteristics, and prognosis: a prospective cohort of breast cancer patients. *Breast Cancer Res*. 2007;9:R6.
20. Effects of chemotherapy and hormonal therapy for early breast cancer on recurrence and 15-year survival: an overview of the randomised trials. *Lancet*. 2005;365:1687-717.
21. Gibson L, Lawrence D, Dawson C, Bliss J. Aromatase inhibitors for treatment of advanced breast cancer in postmenopausal women. *Cochrane database of systematic reviews*. 2009:CD003370.
22. Ross JS, Slodkowska EA, Symmans WF, Pusztai L, Ravdin PM, Hortobagyi GN. The HER-2 receptor and breast cancer: ten years of targeted anti-HER-2 therapy and personalized medicine. *Oncologist*. 2009;14:320-68.
23. Yang XR, Sherman ME, Rimm DL, Lissowska J, Brinton LA, Peplonska B, et al. Differences in risk factors for breast cancer molecular subtypes in a population-based study. *Cancer Epidemiol Biomarkers Prev*. 2007;16:439-43.
24. Millikan RC, Newman B, Tse CK, Moorman PG, Conway K, Dressler LG, et al. Epidemiology of basal-like breast cancer. *Breast Cancer Res Treat*. 2008;109:123-39.
25. Yang XR, Chang-Claude J, Goode EL, Couch FJ, Nevanlinna H, Milne RL, et al. Associations of breast cancer risk factors with tumor subtypes: a pooled analysis from the Breast Cancer Association Consortium studies. *J Natl Cancer Inst*. 2011;103:250-63.
26. Hynes NE, Lane HA. ERBB receptors and cancer: the complexity of targeted inhibitors. *Nat Rev Cancer*. 2005;5:341-54.
27. Yarden Y, Sliwkowski MX. Untangling the ErbB signalling network. *Nat Rev Mol Cell Biol*. 2001;2:127-37.
28. Arteaga CL, Sliwkowski MX, Osborne CK, Perez EA, Puglisi F, Gianni L. Treatment of HER2-positive breast cancer: current status and future perspectives. *Nat Rev Clin Oncol*. 2012;9:16-32.
29. Alimandi M, Romano A, Curia MC, Muraro R, Fedi P, Aaronson SA, et al. Cooperative signaling of ErbB3 and ErbB2 in neoplastic transformation and human mammary carcinomas. *Oncogene*. 1995;10:1813-21.

30. Wallasch C, Weiss FU, Niederfellner G, Jallal B, Issing W, Ullrich A. Heregulin-dependent regulation of HER2/neu oncogenic signaling by heterodimerization with HER3. *EMBO J*. 1995;14:4267-75.
31. Nahta R, Hung MC, Esteva FJ. The HER-2-targeting antibodies trastuzumab and pertuzumab synergistically inhibit the survival of breast cancer cells. *Cancer Res*. 2004;64:2343-6.
32. Hudis CA. Trastuzumab--mechanism of action and use in clinical practice. *N Engl J Med*. 2007;357:39-51.
33. Tevaarwerk AJ, Kolesar JM. Lapatinib: a small-molecule inhibitor of epidermal growth factor receptor and human epidermal growth factor receptor-2 tyrosine kinases used in the treatment of breast cancer. *Clin Ther*. 2009;31 Pt 2:2332-48.
34. Romond EH, Perez EA, Bryant J, Suman VJ, Geyer CE, Jr., Davidson NE, et al. Trastuzumab plus adjuvant chemotherapy for operable HER2-positive breast cancer. *N Engl J Med*. 2005;353:1673-84.
35. Gori S, Montemurro F, Spazzapan S, Metro G, Foglietta J, Bisagni G, et al. Retreatment with trastuzumab-based therapy after disease progression following lapatinib in HER2-positive metastatic breast cancer. *Ann Oncol*. 2012;23:1436-41.
36. Montemurro F, Donadio M, Clavarezza M, Redana S, Jacomuzzi ME, Valabrega G, et al. Outcome of patients with HER2-positive advanced breast cancer progressing during trastuzumab-based therapy. *Oncologist*. 2006;11:318-24.
37. Berns K, Horlings HM, Hennessy BT, Madiredjo M, Hijmans EM, Beelen K, et al. A functional genetic approach identifies the PI3K pathway as a major determinant of trastuzumab resistance in breast cancer. *Cancer Cell*. 2007;12:395-402.
38. Eichhorn PJ, Gili M, Scaltriti M, Serra V, Guzman M, Nijkamp W, et al. Phosphatidylinositol 3-kinase hyperactivation results in lapatinib resistance that is reversed by the mTOR/phosphatidylinositol 3-kinase inhibitor NVP-BEZ235. *Cancer Res*. 2008;68:9221-30.
39. Serra V, Markman B, Scaltriti M, Eichhorn PJ, Valero V, Guzman M, et al. NVP-BEZ235, a dual PI3K/mTOR inhibitor, prevents PI3K signaling and inhibits the growth of cancer cells with activating PI3K mutations. *Cancer Res*. 2008;68:8022-30.
40. Andre F, Campone M, O'Regan R, Manlius C, Massacesi C, Sahmoud T, et al. Phase I study of everolimus plus weekly paclitaxel and trastuzumab in patients with metastatic breast cancer pretreated with trastuzumab. *J Clin Oncol*. 2010;28:5110-5.
41. Burness ML, Grushko TA, Olopade OI. Epidermal growth factor receptor in triple-negative and basal-like breast cancer: promising clinical target or only a marker? *Cancer J*. 2010;16:23-32.
42. Seal MD, Chia SK. What is the difference between triple-negative and basal breast cancers? *Cancer J*. 2010;16:12-6.
43. Dent R, Trudeau M, Pritchard KI, Hanna WM, Kahn HK, Sawka CA, et al. Triple-negative breast cancer: clinical features and patterns of recurrence. *Clin Cancer Res*. 2007;13:4429-34.

44. Nofech-Mozes S, Trudeau M, Kahn HK, Dent R, Rawlinson E, Sun P, et al. Patterns of recurrence in the basal and non-basal subtypes of triple-negative breast cancers. *Breast Cancer Res Treat.* 2009;118:131-7.
45. Cancer Genome Atlas N. Comprehensive molecular portraits of human breast tumours. *Nature.* 2012;490:61-70.
46. Collins LC, Martyniak A, Kandel MJ, Stadler ZK, Masciari S, Miron A, et al. Basal cytokeratin and epidermal growth factor receptor expression are not predictive of BRCA1 mutation status in women with triple-negative breast cancers. *Am J Surg Pathol.* 2009;33:1093-7.
47. Bombonati A, Sgroi DC. The molecular pathology of breast cancer progression. *J Pathol.* 2011;223:307-17.
48. Brinton LA, Sherman ME, Carreon JD, Anderson WF. Recent trends in breast cancer among younger women in the United States. *J Natl Cancer Inst.* 2008;100:1643-8.
49. Gudjonsson T, Adriance MC, Sternlicht MD, Petersen OW, Bissell MJ. Myoepithelial cells: their origin and function in breast morphogenesis and neoplasia. *J Mammary Gland Biol Neoplasia.* 2005;10:261-72.
50. Virnig BA, Tuttle TM, Shamliyan T, Kane RL. Ductal carcinoma in situ of the breast: a systematic review of incidence, treatment, and outcomes. *J Natl Cancer Inst.* 2010;102:170-8.
51. Hu M, Yao J, Carroll DK, Weremowicz S, Chen H, Carrasco D, et al. Regulation of in situ to invasive breast carcinoma transition. *Cancer Cell.* 2008;13:394-406.
52. Pandey PR, Saidou J, Watabe K. Role of myoepithelial cells in breast tumor progression. *Front Biosci (Landmark Ed).* 2010;15:226-36.
53. Virnig BA, Tuttle TM, Shamliyan T, Kane RL. Ductal carcinoma in situ of the breast: a systematic review of incidence, treatment, and outcomes. *Journal of the National Cancer Institute.* 2010;102:170-8.
54. Fowble B, Hanlon AL, Fein DA, Hoffman JP, Sigurdson ER, Patchefsky A, et al. Results of conservative surgery and radiation for mammographically detected ductal carcinoma in situ (DCIS). *Int J Radiat Oncol Biol Phys.* 1997;38:949-57.
55. Page DL, Dupont WD, Rogers LW, Jensen RA, Schuyler PA. Continued local recurrence of carcinoma 15-25 years after a diagnosis of low grade ductal carcinoma in situ of the breast treated only by biopsy. *Cancer.* 1995;76:1197-200.
56. Collins LC, Tamimi RM, Baer HJ, Connolly JL, Colditz GA, Schnitt SJ. Outcome of patients with ductal carcinoma in situ untreated after diagnostic biopsy: results from the Nurses' Health Study. *Cancer.* 2005;103:1778-84.
57. Sanders ME, Schuyler PA, Dupont WD, Page DL. The natural history of low-grade ductal carcinoma in situ of the breast in women treated by biopsy only revealed over 30 years of long-term follow-up. *Cancer.* 2005;103:2481-4.
58. Zahl P-H, Mæhlen J, Welch HG. The natural history of invasive breast cancers detected by screening mammography. *Archives of Internal Medicine.* 2008;168:2311.

59. Solin LJ, Gray R, Baehner FL, Butler SM, Hughes LL, Yoshizawa C, et al. A multigene expression assay to predict local recurrence risk for ductal carcinoma in situ of the breast. *J Natl Cancer Inst.* 2013;105:701-10.
60. Chapman JA, Miller NA, Lickley HL, Qian J, Christens-Barry WA, Fu Y, et al. Ductal carcinoma in situ of the breast (DCIS) with heterogeneity of nuclear grade: prognostic effects of quantitative nuclear assessment. *BMC Cancer.* 2007;7:174.
61. Axelrod DE, Miller NA, Lickley HL, Qian J, Christens-Barry WA, Yuan Y, et al. Effect of quantitative nuclear image features on recurrence of Ductal Carcinoma In Situ (DCIS) of the breast. *Cancer Inform.* 2008;6:99-109.
62. Silverstein MJ, Barth A, Poller DN, Gierson ED, Colburn WJ, Waisman JR, et al. Ten-year results comparing mastectomy to excision and radiation therapy for ductal carcinoma in situ of the breast. *Eur J Cancer.* 1995;31A:1425-7.
63. Burstein HJ, Polyak K, Wong JS, Lester SC, Kaelin CM. Ductal carcinoma in situ of the breast. *N Engl J Med.* 2004;350:1430-41.
64. Bissell MJ, Radisky D. Putting tumours in context. *Nat Rev Cancer.* 2001;1:46-54.
65. Elenbaas B, Weinberg RA. Heterotypic signaling between epithelial tumor cells and fibroblasts in carcinoma formation. *Exp Cell Res.* 2001;264:169-84.
66. Allinen M, Beroukhi R, Cai L, Brennan C, Lahti-Domenici J, Huang H, et al. Molecular characterization of the tumor microenvironment in breast cancer. *Cancer Cell.* 2004;6:17-32.
67. Lyons TR, O'Brien J, Borges VF, Conklin MW, Keely PJ, Eliceiri KW, et al. Postpartum mammary gland involution drives progression of ductal carcinoma in situ through collagen and COX-2. *Nat Med.* 2011;17:1109-15.
68. Hu M, Peluffo G, Chen H, Gelman R, Schnitt S, Polyak K. Role of COX-2 in epithelial-stromal cell interactions and progression of ductal carcinoma in situ of the breast. *Proc Natl Acad Sci U S A.* 2009;106:3372-7.
69. Barker HE, Chang J, Cox TR, Lang G, Bird D, Nicolau M, et al. LOXL2-mediated matrix remodeling in metastasis and mammary gland involution. *Cancer Res.* 2011;71:1561-72.
70. Levental KR, Yu H, Kass L, Lakins JN, Egeblad M, Erler JT, et al. Matrix crosslinking forces tumor progression by enhancing integrin signaling. *Cell.* 2009;139:891-906.
71. Vargas AC, McCart Reed AE, Waddell N, Lane A, Reid LE, Smart CE, et al. Gene expression profiling of tumour epithelial and stromal compartments during breast cancer progression. *Breast Cancer Res Treat.* 2012;135:153-65.
72. Tait LR, Pauley RJ, Santner SJ, Heppner GH, Heng HH, Rak JW, et al. Dynamic stromal-epithelial interactions during progression of MCF10DCIS.com xenografts. *Int J Cancer.* 2007;120:2127-34.

73. Porcile C, Bajetto A, Barbieri F, Barbero S, Bonavia R, Biglieri M, et al. Stromal cell-derived factor-1alpha (SDF-1alpha/CXCL12) stimulates ovarian cancer cell growth through the EGF receptor transactivation. *Exp Cell Res*. 2005;308:241-53.
74. Ahr B, Denizot M, Robert-Hebmann V, Brelot A, Biard-Piechaczyk M. Identification of the cytoplasmic domains of CXCR4 involved in Jak2 and STAT3 phosphorylation. *J Biol Chem*. 2005;280:6692-700.
75. Zhao M, Discipio RG, Wimmer AG, Schraufstatter IU. Regulation of CXCR4-mediated nuclear translocation of extracellular signal-related kinases 1 and 2. *Mol Pharmacol*. 2006;69:66-75.
76. Chu H, Zhou H, Liu Y, Liu X, Hu Y, Zhang J. Functional expression of CXC chemokine receptor-4 mediates the secretion of matrix metalloproteinases from mouse hepatocarcinoma cell lines with different lymphatic metastasis ability. *Int J Biochem Cell Biol*. 2007;39:197-205.
77. Leivonen SK, Ala-Aho R, Koli K, Grenman R, Peltonen J, Kahari VM. Activation of Smad signaling enhances collagenase-3 (MMP-13) expression and invasion of head and neck squamous carcinoma cells. *Oncogene*. 2006;25:2588-600.
78. McDermott SP, Wicha MS. Targeting breast cancer stem cells. *Mol Oncol*. 2010;4:404-19.
79. Sanguinetti A, Bistoni G, Avenia N. Stem cells and breast cancer, where we are? A concise review of literature. *G Chir*. 2011;32:438-46.
80. Wicha MS. Targeting self-renewal, an Achilles' heel of cancer stem cells. *Nat Med*. 2014;20:14-5.
81. Reya T, Morrison SJ, Clarke MF, Weissman IL. Stem cells, cancer, and cancer stem cells. *Nature*. 2001;414:105-11.
82. Al-Hajj M, Wicha MS, Benito-Hernandez A, Morrison SJ, Clarke MF. Prospective identification of tumorigenic breast cancer cells. *Proc Natl Acad Sci U S A*. 2003;100:3983-8.
83. Herschkowitz JI, Zhao W, Zhang M, Usary J, Murrow G, Edwards D, et al. Comparative oncogenomics identifies breast tumors enriched in functional tumor-initiating cells. *Proc Natl Acad Sci U S A*. 2012;109:2778-83.
84. Gangopadhyay S, Nandy A, Hor P, Mukhopadhyay A. Breast cancer stem cells: a novel therapeutic target. *Clin Breast Cancer*. 2013;13:7-15.
85. Sampieri K, Fodde R. Cancer stem cells and metastasis. *Semin Cancer Biol*. 2012;22:187-93.
86. Fridriksdottir AJ, Petersen OW, Ronnov-Jessen L. Mammary gland stem cells: current status and future challenges. *Int J Dev Biol*. 2011;55:719-29.
87. Badve S, Nakshatri H. Breast-cancer stem cells-beyond semantics. *Lancet Oncol*. 2012;13:e43-8.
88. Eyler CE, Rich JN. Survival of the fittest: cancer stem cells in therapeutic resistance and angiogenesis. *J Clin Oncol*. 2008;26:2839-45.

89. Li X, Lewis MT, Huang J, Gutierrez C, Osborne CK, Wu MF, et al. Intrinsic resistance of tumorigenic breast cancer cells to chemotherapy. *J Natl Cancer Inst.* 2008;100:672-9.
90. Yu F, Yao H, Zhu P, Zhang X, Pan Q, Gong C, et al. let-7 regulates self renewal and tumorigenicity of breast cancer cells. *Cell.* 2007;131:1109-23.
91. Hennessy BT, Gonzalez-Angulo AM, Stemke-Hale K, Gilcrease MZ, Krishnamurthy S, Lee JS, et al. Characterization of a naturally occurring breast cancer subset enriched in epithelial-to-mesenchymal transition and stem cell characteristics. *Cancer Res.* 2009;69:4116-24.
92. Mani SA, Guo W, Liao MJ, Eaton EN, Ayyanan A, Zhou AY, et al. The epithelial-mesenchymal transition generates cells with properties of stem cells. *Cell.* 2008;133:704-15.
93. Korkaya H, Liu S, Wicha MS. Breast cancer stem cells, cytokine networks, and the tumor microenvironment. *J Clin Invest.* 2011;121:3804-9.
94. Takebe N, Harris PJ, Warren RQ, Ivy SP. Targeting cancer stem cells by inhibiting Wnt, Notch, and Hedgehog pathways. *Nat Rev Clin Oncol.* 2011;8:97-106.
95. Pannuti A, Foreman K, Rizzo P, Osipo C, Golde T, Osborne B, et al. Targeting Notch to target cancer stem cells. *Clin Cancer Res.* 2010;16:3141-52.
96. Reedijk M. Notch signaling and breast cancer. *Adv Exp Med Biol.* 2012;727:241-57.
97. Reedijk M, Pinnaduwege D, Dickson BC, Mulligan AM, Zhang H, Bull SB, et al. JAG1 expression is associated with a basal phenotype and recurrence in lymph node-negative breast cancer. *Breast Cancer Res Treat.* 2008;111:439-48.
98. Hassan KA, Wang L, Korkaya H, Chen G, Maillard I, Beer DG, et al. Notch pathway activity identifies cells with cancer stem cell-like properties and correlates with worse survival in lung adenocarcinoma. *Clin Cancer Res.* 2013;19:1972-80.
99. Harrison H, Farnie G, Howell SJ, Rock RE, Stylianou S, Brennan KR, et al. Regulation of breast cancer stem cell activity by signaling through the Notch4 receptor. *Cancer Res.* 2010;70:709-18.
100. McAuliffe SM, Morgan SL, Wyant GA, Tran LT, Muto KW, Chen YS, et al. Targeting Notch, a key pathway for ovarian cancer stem cells, sensitizes tumors to platinum therapy. *Proc Natl Acad Sci U S A.* 2012;109:E2939-48.
101. Xing F, Okuda H, Watabe M, Kobayashi A, Pai SK, Liu W, et al. Hypoxia-induced Jagged2 promotes breast cancer metastasis and self-renewal of cancer stem-like cells. *Oncogene.* 2011;30:4075-86.
102. Bao B, Wang Z, Ali S, Kong D, Li Y, Ahmad A, et al. Notch-1 induces epithelial-mesenchymal transition consistent with cancer stem cell phenotype in pancreatic cancer cells. *Cancer Lett.* 2011;307:26-36.
103. Kondratyev M, Kreso A, Hallett RM, Girgis-Gabardo A, Barcelon ME, Ilieva D, et al. Gamma-secretase inhibitors target tumor-initiating cells in a mouse model of ERBB2 breast cancer. *Oncogene.* 2012;31:93-103.

104. Qiu M, Peng Q, Jiang I, Carroll C, Han G, Rymer I, et al. Specific inhibition of Notch1 signaling enhances the antitumor efficacy of chemotherapy in triple negative breast cancer through reduction of cancer stem cells. *Cancer Lett.* 2013;328:261-70.
105. Fan X, Khaki L, Zhu TS, Soules ME, Talsma CE, Gul N, et al. NOTCH pathway blockade depletes CD133-positive glioblastoma cells and inhibits growth of tumor neurospheres and xenografts. *Stem Cells.* 2010;28:5-16.
106. Sharma A, Paranjape AN, Rangarajan A, Dighe RR. A monoclonal antibody against human Notch1 ligand-binding domain depletes subpopulation of putative breast cancer stem-like cells. *Mol Cancer Ther.* 2012;11:77-86.
107. Dievart A, Beaulieu N, Jolicoeur P. Involvement of Notch1 in the development of mouse mammary tumors. *Oncogene.* 1999;18:5973-81.
108. Dontu G, Jackson KW, McNicholas E, Kawamura MJ, Abdallah WM, Wicha MS. Role of Notch signaling in cell-fate determination of human mammary stem/progenitor cells. *Breast Cancer Res.* 2004;6:R605-15.
109. Khramtsov AI, Khramtsova GF, Tretiakova M, Huo D, Olopade OI, Goss KH. Wnt/beta-catenin pathway activation is enriched in basal-like breast cancers and predicts poor outcome. *Am J Pathol.* 2010;176:2911-20.
110. Ayyanan A, Civenni G, Ciarloni L, Morel C, Mueller N, Lefort K, et al. Increased Wnt signaling triggers oncogenic conversion of human breast epithelial cells by a Notch-dependent mechanism. *Proc Natl Acad Sci U S A.* 2006;103:3799-804.
111. Rijsewijk F, Schuermann M, Wagenaar E, Parren P, Weigel D, Nusse R. The *Drosophila* homolog of the mouse mammary oncogene *int-1* is identical to the segment polarity gene *wingless*. *Cell.* 1987;50:649-57.
112. Tsukamoto AS, Grosschedl R, Guzman RC, Parslow T, Varmus HE. Expression of the *int-1* gene in transgenic mice is associated with mammary gland hyperplasia and adenocarcinomas in male and female mice. *Cell.* 1988;55:619-25.
113. Anastas JN, Moon RT. WNT signalling pathways as therapeutic targets in cancer. *Nat Rev Cancer.* 2013;13:11-26.
114. Clevers H, Nusse R. Wnt/beta-catenin signaling and disease. *Cell.* 2012;149:1192-205.
115. Nelson WJ, Nusse R. Convergence of Wnt, beta-catenin, and cadherin pathways. *Science.* 2004;303:1483-7.
116. Takahashi-Yanaga F, Kahn M. Targeting Wnt signaling: can we safely eradicate cancer stem cells? *Clin Cancer Res.* 2010;16:3153-62.
117. Gurney A, Axelrod F, Bond CJ, Cain J, Chartier C, Donigan L, et al. Wnt pathway inhibition via the targeting of Frizzled receptors results in decreased growth and tumorigenicity of human tumors. *Proc Natl Acad Sci U S A.* 2012;109:11717-22.
118. Ingham PW, McMahon AP. Hedgehog signaling in animal development: paradigms and principles. *Genes Dev.* 2001;15:3059-87.
119. Briscoe J, Therond PP. The mechanisms of Hedgehog signalling and its roles in development and disease. *Nat Rev Mol Cell Biol.* 2013;14:416-29.

120. Beachy PA, Karhadkar SS, Berman DM. Tissue repair and stem cell renewal in carcinogenesis. *Nature*. 2004;432:324-31.
121. Stanton BZ, Peng LF. Small-molecule modulators of the Sonic Hedgehog signaling pathway. *Mol Biosyst*. 2010;6:44-54.
122. Pola R, Ling LE, Silver M, Corbley MJ, Kearney M, Blake Pepinsky R, et al. The morphogen Sonic hedgehog is an indirect angiogenic agent upregulating two families of angiogenic growth factors. *Nat Med*. 2001;7:706-11.
123. O'Toole SA, Machalek DA, Shearer RF, Millar EK, Nair R, Schofield P, et al. Hedgehog overexpression is associated with stromal interactions and predicts for poor outcome in breast cancer. *Cancer Res*. 2011;71:4002-14.
124. Yang L, Xie G, Fan Q, Xie J. Activation of the hedgehog-signaling pathway in human cancer and the clinical implications. *Oncogene*. 2010;29:469-81.
125. Dreesen O, Brivanlou AH. Signaling pathways in cancer and embryonic stem cells. *Stem Cell Rev*. 2007;3:7-17.
126. Horbelt D, Denkis A, Knaus P. A portrait of Transforming Growth Factor beta superfamily signalling: Background matters. *Int J Biochem Cell Biol*. 2012;44:469-74.
127. Ikushima H, Miyazono K. TGFbeta signalling: a complex web in cancer progression. *Nat Rev Cancer*. 2010;10:415-24.
128. Drabsch Y, ten Dijke P. TGF-beta signalling and its role in cancer progression and metastasis. *Cancer Metastasis Rev*. 2012;31:553-68.
129. Buijs JT, van der Horst G, van den Hoogen C, Cheung H, de Rooij B, Kroon J, et al. The BMP2/7 heterodimer inhibits the human breast cancer stem cell subpopulation and bone metastases formation. *Oncogene*. 2012;31:2164-74.
130. Reynolds BA, Weiss S. Generation of neurons and astrocytes from isolated cells of the adult mammalian central nervous system. *Science*. 1992;255:1707-10.
131. Dontu G, Abdallah WM, Foley JM, Jackson KW, Clarke MF, Kawamura MJ, et al. In vitro propagation and transcriptional profiling of human mammary stem/progenitor cells. *Genes Dev*. 2003;17:1253-70.
132. Ponti D, Costa A, Zaffaroni N, Pratesi G, Petrangolini G, Coradini D, et al. Isolation and in vitro propagation of tumorigenic breast cancer cells with stem/progenitor cell properties. *Cancer Res*. 2005;65:5506-11.
133. Farnie G, Clarke RB, Spence K, Pinnock N, Brennan K, Anderson NG, et al. Novel cell culture technique for primary ductal carcinoma in situ: role of Notch and epidermal growth factor receptor signaling pathways. *J Natl Cancer Inst*. 2007;99:616-27.
134. Shaw FL, Harrison H, Spence K, Ablett MP, Simoes BM, Farnie G, et al. A detailed mammosphere assay protocol for the quantification of breast stem cell activity. *J Mammary Gland Biol Neoplasia*. 2012;17:111-7.
135. Grimshaw MJ, Cooper L, Papazisis K, Coleman JA, Bohnenkamp HR, Chiapero-Stanke L, et al. Mammosphere culture of metastatic breast cancer cells enriches for tumorigenic breast cancer cells. *Breast cancer research : BCR*. 2008;10:R52.

136. Cioce M, Gherardi S, Viglietto G, Strano S, Blandino G, Muti P, et al. Mammosphere-forming cells from breast cancer cell lines as a tool for the identification of CSC-like- and early progenitor-targeting drugs. *Cell Cycle*. 2010;9:2878-87.
137. Dawson PJ, Wolman SR, Tait L, Heppner GH, Miller FR. MCF10AT: a model for the evolution of cancer from proliferative breast disease. *Am J Pathol*. 1996;148:313-9.
138. Miller FR, Soule HD, Tait L, Pauley RJ, Wolman SR, Dawson PJ, et al. Xenograft model of progressive human proliferative breast disease. *J Natl Cancer Inst*. 1993;85:1725-32.
139. Miller FR. Xenograft models of premalignant breast disease. *J Mammary Gland Biol Neoplasia*. 2000;5:379-91.
140. Miller FR, Santner SJ, Tait L, Dawson PJ. MCF10DCIS.com xenograft model of human comedo ductal carcinoma in situ. *Journal of the National Cancer Institute*. 2000;92:1185-6.
141. So JY, Lee HJ, Kramata P, Minden A, Suh N. Differential Expression of Key Signaling Proteins in MCF10 Cell Lines, a Human Breast Cancer Progression Model. *Mol Cell Pharmacol*. 2012;4:31-40.
142. Santner SJ, Dawson PJ, Tait L, Soule HD, Eliason J, Mohamed AN, et al. Malignant MCF10CA1 cell lines derived from premalignant human breast epithelial MCF10AT cells. *Breast Cancer Res Treat*. 2001;65:101-10.
143. Worsham MJ, Pals G, Schouten JP, Miller F, Tiwari N, van Spaendonk R, et al. High-resolution mapping of molecular events associated with immortalization, transformation, and progression to breast cancer in the MCF10 model. *Breast Cancer Res Treat*. 2006;96:177-86.
144. Ma XJ, Salunga R, Tuggle JT, Gaudet J, Enright E, McQuary P, et al. Gene expression profiles of human breast cancer progression. *Proc Natl Acad Sci U S A*. 2003;100:5974-9.
145. Rhee DK, Park SH, Jang YK. Molecular signatures associated with transformation and progression to breast cancer in the isogenic MCF10 model. *Genomics*. 2008;92:419-28.
146. Kim SH, Miller FR, Tait L, Zheng J, Novak RF. Proteomic and phosphoproteomic alterations in benign, premalignant and tumor human breast epithelial cells and xenograft lesions: biomarkers of progression. *Int J Cancer*. 2009;124:2813-28.
147. So JY, Lee HJ, Smolarek AK, Paul S, Wang CX, Maehr H, et al. A novel Gemini vitamin D analog represses the expression of a stem cell marker CD44 in breast cancer. *Molecular pharmacology*. 2011;79:360-7.
148. Holick MF. Vitamin D: evolutionary, physiological and health perspectives. *Curr Drug Targets*. 2011;12:4-18.
149. Jones G, Prosser DE, Kaufmann M. Cytochrome P450-mediated metabolism of vitamin D. *J Lipid Res*. 2014;55:13-31.

150. Zhu J, DeLuca HF. Vitamin D 25-hydroxylase - Four decades of searching, are we there yet? *Arch Biochem Biophys*. 2012;523:30-6.
151. Carlberg C. Current understanding of the function of the nuclear vitamin D receptor in response to its natural and synthetic ligands. *Recent Results Cancer Res*. 2003;164:29-42.
152. Feldman D, Krishnan AV, Swami S, Giovannucci E, Feldman BJ. The role of vitamin D in reducing cancer risk and progression. *Nature reviews Cancer*. 2014;14:342-57.
153. Lopes N, Sousa B, Martins D, Gomes M, Vieira D, Veronese LA, et al. Alterations in Vitamin D signalling and metabolic pathways in breast cancer progression: a study of VDR, CYP27B1 and CYP24A1 expression in benign and malignant breast lesions. *BMC Cancer*. 2010;10:483.
154. Hobaus J, Thiem U, Hummel DM, Kallay E. Role of calcium, vitamin D, and the extrarenal vitamin D hydroxylases in carcinogenesis. *Anticancer Agents Med Chem*. 2013;13:20-35.
155. Deeb KK, Trump DL, Johnson CS. Vitamin D signalling pathways in cancer: potential for anticancer therapeutics. *Nature reviews Cancer*. 2007;7:684-700.
156. Evans RM. The steroid and thyroid hormone receptor superfamily. *Science*. 1988;240:889-95.
157. Carlberg C. Current understanding of the function of the nuclear vitamin D receptor in response to its natural and synthetic ligands. *Recent Results Cancer Res*. 2003;164:29-42.
158. Holick MF. Vitamin D deficiency. *The New England journal of medicine*. 2007;357:266-81.
159. Haussler MR, Jurutka PW, Mizwicki M, Norman AW. Vitamin D receptor (VDR)-mediated actions of 1 α ,25(OH)₂vitamin D₃: genomic and non-genomic mechanisms. *Best Pract Res Clin Endocrinol Metab*. 2011;25:543-59.
160. Wali RK, Baum CL, Sitrin MD, Brasitus TA. 1,25(OH)₂ vitamin D₃ stimulates membrane phosphoinositide turnover, activates protein kinase C, and increases cytosolic calcium in rat colonic epithelium. *J Clin Invest*. 1990;85:1296-303.
161. Morelli S, Buitrago C, Boland R, de Boland AR. The stimulation of MAP kinase by 1,25(OH)₂-vitamin D₃ in skeletal muscle cells is mediated by protein kinase C and calcium. *Mol Cell Endocrinol*. 2001;173:41-52.
162. Grant WB. An ecologic study of dietary and solar ultraviolet-B links to breast carcinoma mortality rates. *Cancer*. 2002;94:272-81.
163. Garland CF, Garland FC, Gorham ED, Lipkin M, Newmark H, Mohr SB, et al. The role of vitamin D in cancer prevention. *Am J Public Health*. 2006;96:252-61.
164. Garland CF, Garland FC. Do sunlight and vitamin D reduce the likelihood of colon cancer? *Int J Epidemiol*. 1980;9:227-31.

165. Garland CF, Gorham ED, Mohr SB, Grant WB, Giovannucci EL, Lipkin M, et al. Vitamin D and prevention of breast cancer: pooled analysis. *The Journal of steroid biochemistry and molecular biology*. 2007;103:708-11.
166. Garland FC, Garland CF, Gorham ED, Young JF. Geographic variation in breast cancer mortality in the United States: a hypothesis involving exposure to solar radiation. *Prev Med*. 1990;19:614-22.
167. El Abdaimi K, Dion N, Papavasiliou V, Cardinal PE, Binderup L, Goltzman D, et al. The vitamin D analogue EB 1089 prevents skeletal metastasis and prolongs survival time in nude mice transplanted with human breast cancer cells. *Cancer Res*. 2000;60:4412-8.
168. Krishnan AV, Feldman D. Mechanisms of the anti-cancer and anti-inflammatory actions of vitamin D. *Annu Rev Pharmacol Toxicol*. 2011;51:311-36.
169. Matthews D, LaPorta E, Zinser GM, Narvaez CJ, Welsh J. Genomic vitamin D signaling in breast cancer: Insights from animal models and human cells. *J Steroid Biochem Mol Biol*. 2010;121:362-7.
170. Swami S, Krishnan AV, Wang JY, Jensen K, Horst R, Albertelli MA, et al. Dietary vitamin D(3) and 1,25-dihydroxyvitamin D(3) (calcitriol) exhibit equivalent anticancer activity in mouse xenograft models of breast and prostate cancer. *Endocrinology*. 2012;153:2576-87.
171. Colston KW, Hansen CM. Mechanisms implicated in the growth regulatory effects of vitamin D in breast cancer. *Endocr Relat Cancer*. 2002;9:45-59.
172. Koli K, Keski-Oja J. 1 α ,25-dihydroxyvitamin D₃ and its analogues down-regulate cell invasion-associated proteases in cultured malignant cells. *Cell Growth Differ*. 2000;11:221-9.
173. Krishnan AV, Swami S, Peng L, Wang J, Moreno J, Feldman D. Tissue-selective regulation of aromatase expression by calcitriol: implications for breast cancer therapy. *Endocrinology*. 2010;151:32-42.
174. James SY, Mackay AG, Binderup L, Colston KW. Effects of a new synthetic vitamin D analogue, EB1089, on the oestrogen-responsive growth of human breast cancer cells. *The Journal of endocrinology*. 1994;141:555-63.
175. Stoica A, Saceda M, Fakhro A, Solomon HB, Fenster BD, Martin MB. Regulation of estrogen receptor- α gene expression by 1, 25-dihydroxyvitamin D in MCF-7 cells. *J Cell Biochem*. 1999;75:640-51.
176. Lee HJ, Paul S, Atalla N, Thomas PE, Lin X, Yang I, et al. Gemini vitamin D analogues inhibit estrogen receptor-positive and estrogen receptor-negative mammary tumorigenesis without hypercalcemic toxicity. *Cancer Prev Res (Phila)*. 2008;1:476-84.
177. Smith DC, Johnson CS, Freeman CC, Muindi J, Wilson JW, Trump DL. A Phase I trial of calcitriol (1,25-dihydroxycholecalciferol) in patients with advanced malignancy. *Clin Cancer Res*. 1999;5:1339-45.
178. Trump DL, Hersherberger PA, Bernardi RJ, Ahmed S, Muindi J, Fakih M, et al. Anti-tumor activity of calcitriol: pre-clinical and clinical studies. *J Steroid Biochem Mol Biol*. 2004;89-90:519-26.

179. Jones G. Vitamin D analogs. *Endocrinol Metab Clin North Am.* 2010;39:447-72.
180. So JY, Wahler JE, Yoon T, Smolarek AK, Lin Y, Shih WJ, et al. Oral Administration of a Gemini Vitamin D Analog, a Synthetic Triterpenoid and the Combination Prevents Mammary Tumorigenesis Driven by ErbB2 Overexpression. *Cancer prevention research.* 2013;6:959-70.
181. Anzano MA, Smith JM, Uskokovic MR, Peer CW, Mullen LT, Letterio JJ, et al. 1 alpha,25-Dihydroxy-16-ene-23-yne-26,27-hexafluorocholecalciferol (Ro24-5531), a new deltanoid (vitamin D analogue) for prevention of breast cancer in the rat. *Cancer Res.* 1994;54:1653-6.
182. Gotte M, Yip GW. Heparanase, hyaluronan, and CD44 in cancers: a breast carcinoma perspective. *Cancer Res.* 2006;66:10233-7.
183. Godar S, Ince TA, Bell GW, Feldser D, Donaher JL, Bergh J, et al. Growth-inhibitory and tumor- suppressive functions of p53 depend on its repression of CD44 expression. *Cell.* 2008;134:62-73.
184. Cariati M, Naderi A, Brown JP, Smalley MJ, Pinder SE, Caldas C, et al. Alpha-6 integrin is necessary for the tumourigenicity of a stem cell-like subpopulation within the MCF7 breast cancer cell line. *Int J Cancer.* 2008;122:298-304.
185. Vieira AF, Ricardo S, Ablett MP, Dionisio MR, Mendes N, Albergaria A, et al. P-cadherin is coexpressed with CD44 and CD49f and mediates stem cell properties in basal-like breast cancer. *Stem Cells.* 2012;30:854-64.
186. Eirew P, Stingl J, Raouf A, Turashvili G, Aparicio S, Emerman JT, et al. A method for quantifying normal human mammary epithelial stem cells with in vivo regenerative ability. *Nat Med.* 2008;14:1384-9.
187. Gudjonsson T, Villadsen R, Nielsen HL, Ronnov-Jessen L, Bissell MJ, Petersen OW. Isolation, immortalization, and characterization of a human breast epithelial cell line with stem cell properties. *Genes Dev.* 2002;16:693-706.
188. Velasco-Velazquez MA, Homsí N, De La Fuente M, Pestell RG. Breast cancer stem cells. *Int J Biochem Cell Biol.* 2012;44:573-7.
189. Khoury T, Ademuyiwa FO, Chandrasekhar R, Jabbour M, Deleo A, Ferrone S, et al. Aldehyde dehydrogenase 1A1 expression in breast cancer is associated with stage, triple negativity, and outcome to neoadjuvant chemotherapy. *Mod Pathol.* 2012;25:388-97.
190. Ginestier C, Hur MH, Charafe-Jauffret E, Monville F, Dutcher J, Brown M, et al. ALDH1 is a marker of normal and malignant human mammary stem cells and a predictor of poor clinical outcome. *Cell Stem Cell.* 2007;1:555-67.
191. Croker AK, Goodale D, Chu J, Postenka C, Hedley BD, Hess DA, et al. High aldehyde dehydrogenase and expression of cancer stem cell markers selects for breast cancer cells with enhanced malignant and metastatic ability. *Journal of Cellular and Molecular Medicine.* 2009;13:2236-52.
192. Wright MH, Calcagno AM, Salcido CD, Carlson MD, Ambudkar SV, Varticovski L. Brca1 breast tumors contain distinct CD44+/CD24- and CD133+ cells with cancer stem cell characteristics. *Breast Cancer Res.* 2008;10:R10.

193. Shackleton M, Vaillant F, Simpson KJ, Stingl J, Smyth GK, Asselin-Labat ML, et al. Generation of a functional mammary gland from a single stem cell. *Nature*. 2006;439:84-8.
194. Malhotra GK, Zhao X, Band H, Band V. Shared signaling pathways in normal and breast cancer stem cells. *J Carcinog*. 2011;10:38.
195. Ronchini C, Capobianco AJ. Induction of cyclin D1 transcription and CDK2 activity by Notch(ic): implication for cell cycle disruption in transformation by Notch(ic). *Mol Cell Biol*. 2001;21:5925-34.
196. Oswald F, Liptay S, Adler G, Schmid RM. NF-kappaB2 is a putative target gene of activated Notch-1 via RBP-Jkappa. *Mol Cell Biol*. 1998;18:2077-88.
197. Katoh Y, Katoh M. Hedgehog signaling, epithelial-to-mesenchymal transition and miRNA (review). *Int J Mol Med*. 2008;22:271-5.
198. Schmierer B, Hill CS. TGFbeta-SMAD signal transduction: molecular specificity and functional flexibility. *Nat Rev Mol Cell Biol*. 2007;8:970-82.
199. Zavadil J, Bitzer M, Liang D, Yang YC, Massimi A, Kneitz S, et al. Genetic programs of epithelial cell plasticity directed by transforming growth factor-beta. *Proc Natl Acad Sci U S A*. 2001;98:6686-91.
200. Lee HJ, Ju J, Paul S, So JY, DeCastro A, Smolarek A, et al. Mixed tocopherols prevent mammary tumorigenesis by inhibiting estrogen action and activating PPAR-gamma. *Clin Cancer Res*. 2009;15:4242-9.
201. Lee HJ, Liu H, Goodman C, Ji Y, Maehr H, Uskokovic M, et al. Gene expression profiling changes induced by a novel Gemini Vitamin D derivative during the progression of breast cancer. *Biochemical pharmacology*. 2006;72:332-43.
202. So JY, Smolarek AK, Salerno DM, Maehr H, Uskokovic M, Liu F, et al. Targeting CD44-STAT3 signaling by Gemini vitamin D analog leads to inhibition of invasion in basal-like breast cancer. *PloS one*. 2013;8:e54020.
203. Kessenbrock K, Plaks V, Werb Z. Matrix metalloproteinases: regulators of the tumor microenvironment. *Cell*. 2010;141:52-67.
204. Westermarck J, Kahari VM. Regulation of matrix metalloproteinase expression in tumor invasion. *FASEB J*. 1999;13:781-92.
205. Cathcart J, Pulkoski-Gross A, Cao J. Targeting Matrix Metalloproteinases in Cancer: Bringing New Life to Old Ideas. *Genes Dis*. 2015;2:26-34.
206. Saarialho-Kere UK, Chang ES, Welgus HG, Parks WC. Distinct localization of collagenase and tissue inhibitor of metalloproteinases expression in wound healing associated with ulcerative pyogenic granuloma. *J Clin Invest*. 1992;90:1952-7.
207. Brew K, Nagase H. The tissue inhibitors of metalloproteinases (TIMPs): an ancient family with structural and functional diversity. *Biochim Biophys Acta*. 2010;1803:55-71.
208. Pechoux C, Gudjonsson T, Ronnov-Jessen L, Bissell MJ, Petersen OW. Human mammary luminal epithelial cells contain progenitors to myoepithelial cells. *Dev Biol*. 1999;206:88-99.

209. Smalley MJ, Titley J, O'Hare MJ. Clonal characterization of mouse mammary luminal epithelial and myoepithelial cells separated by fluorescence-activated cell sorting. *In Vitro Cell Dev Biol Anim.* 1998;34:711-21.
210. Duffy MJ, Maguire TM, Hill A, McDermott E, O'Higgins N. Metalloproteinases: role in breast carcinogenesis, invasion and metastasis. *Breast Cancer Res.* 2000;2:252-7.
211. Radisky ES, Radisky DC. Matrix metalloproteinase-induced epithelial-mesenchymal transition in breast cancer. *J Mammary Gland Biol Neoplasia.* 2010;15:201-12.
212. Giannelli G, Falk-Marzillier J, Schiraldi O, Stetler-Stevenson WG, Quaranta V. Induction of cell migration by matrix metalloproteinase-2 cleavage of laminin-5. *Science.* 1997;277:225-8.
213. Sato H, Takino T, Okada Y, Cao J, Shinagawa A, Yamamoto E, et al. A matrix metalloproteinase expressed on the surface of invasive tumour cells. *Nature.* 1994;370:61-5.
214. Hotary K, Li XY, Allen E, Stevens SL, Weiss SJ. A cancer cell metalloprotease triad regulates the basement membrane transmigration program. *Genes Dev.* 2006;20:2673-86.
215. Schnitt SJ. The transition from ductal carcinoma in situ to invasive breast cancer: the other side of the coin. *Breast Cancer Res.* 2009;11:101.
216. Zinser G, Packman K, Welsh J. Vitamin D(3) receptor ablation alters mammary gland morphogenesis. *Development.* 2002;129:3067-76.
217. Welsh J. Vitamin D and prevention of breast cancer. *Acta Pharmacol Sin.* 2007;28:1373-82.
218. Wahler J, So JY, Kim YC, Liu F, Maehr H, Uskokovic M, et al. Inhibition of the transition of ductal carcinoma in situ to invasive ductal carcinoma by a Gemini vitamin D analog. *Cancer Prev Res (Phila).* 2014;7:617-26.
219. Jones G, Strugnell SA, DeLuca HF. Current understanding of the molecular actions of vitamin D. *Physiol Rev.* 1998;78:1193-231.
220. Berger U, Wilson P, McClelland RA, Colston K, Haussler MR, Pike JW, et al. Immunocytochemical detection of 1,25-dihydroxyvitamin D receptors in normal human tissues. *J Clin Endocrinol Metab.* 1988;67:607-13.
221. Johnson CE, Gorringer KL, Thompson ER, Opekin K, Boyle SE, Wang Y, et al. Identification of copy number alterations associated with the progression of DCIS to invasive ductal carcinoma. *Breast Cancer Res Treat.* 2012;133:889-98.
222. Lee S, Stewart S, Nagtegaal I, Luo J, Wu Y, Colditz G, et al. Differentially expressed genes regulating the progression of ductal carcinoma in situ to invasive breast cancer. *Cancer Res.* 2012;72:4574-86.
223. Moelans CB, de Wegers RA, Monsuurs HN, Maess AH, van Diest PJ. Molecular differences between ductal carcinoma in situ and adjacent invasive breast carcinoma: a multiplex ligation-dependent probe amplification study. *Cell Oncol (Dordr).* 2011;34:475-82.

224. Li Q, Yao Y, Eades G, Liu Z, Zhang Y, Zhou Q. Downregulation of miR-140 promotes cancer stem cell formation in basal-like early stage breast cancer. *Oncogene*. 2014;33:2589-600.
225. Rota LM, Lazzarino DA, Ziegler AN, LeRoith D, Wood TL. Determining mammosphere-forming potential: application of the limiting dilution analysis. *J Mammary Gland Biol Neoplasia*. 2012;17:119-23.
226. So JY, Lin JJ, Wahler J, Liby KT, Sporn MB, Suh N. A Synthetic Triterpenoid CDDO-Im Inhibits Tumorsphere Formation by Regulating Stem Cell Signaling Pathways in Triple-Negative Breast Cancer. *PLoS One*. 2014;9:e107616.
227. de la Mare JA, Sterrenberg JN, Sukhthankar MG, Chiwakata MT, Beukes DR, Blatch GL, et al. Assessment of potential anti-cancer stem cell activity of marine algal compounds using an in vitro mammosphere assay. *Cancer Cell Int*. 2013;13:39.
228. Ponta H, Sherman L, Herrlich PA. CD44: from adhesion molecules to signalling regulators. *Nat Rev Mol Cell Biol*. 2003;4:33-45.
229. Pham PV, Phan NL, Nguyen NT, Truong NH, Duong TT, Le DV, et al. Differentiation of breast cancer stem cells by knockdown of CD44: promising differentiation therapy. *J Transl Med*. 2011;9:209.
230. Dontu G, Al-Hajj M, Abdallah WM, Clarke MF, Wicha MS. Stem cells in normal breast development and breast cancer. *Cell Prolif*. 2003;36 Suppl 1:59-72.
231. Shostak K, Chariot A. NF-kappaB, stem cells and breast cancer: the links get stronger. *Breast Cancer Res*. 2011;13:214.
232. Liu M, Sakamaki T, Casimiro MC, Willmarth NE, Quong AA, Ju X, et al. The canonical NF-kappaB pathway governs mammary tumorigenesis in transgenic mice and tumor stem cell expansion. *Cancer Res*. 2010;70:10464-73.
233. Moraes RC, Zhang X, Harrington N, Fung JY, Wu MF, Hilsenbeck SG, et al. Constitutive activation of smoothened (SMO) in mammary glands of transgenic mice leads to increased proliferation, altered differentiation and ductal dysplasia. *Development*. 2007;134:1231-42.
234. Zaehres H, Lensch MW, Daheron L, Stewart SA, Itskovitz-Eldor J, Daley GQ. High-efficiency RNA interference in human embryonic stem cells. *Stem Cells*. 2005;23:299-305.
235. Rodda DJ, Chew JL, Lim LH, Loh YH, Wang B, Ng HH, et al. Transcriptional regulation of nanog by OCT4 and SOX2. *J Biol Chem*. 2005;280:24731-7.
236. Asselin-Labat ML, Sutherland KD, Barker H, Thomas R, Shackleton M, Forrest NC, et al. Gata-3 is an essential regulator of mammary-gland morphogenesis and luminal-cell differentiation. *Nat Cell Biol*. 2007;9:201-9.
237. Stingl J, Eaves CJ, Zandieh I, Emerman JT. Characterization of bipotent mammary epithelial progenitor cells in normal adult human breast tissue. *Breast Cancer Res Treat*. 2001;67:93-109.
238. Ablett MP, Singh JK, Clarke RB. Stem cells in breast tumours: are they ready for the clinic? *Eur J Cancer*. 2012;48:2104-16.

239. Rakha EA, Reis-Filho JS, Ellis IO. Basal-like breast cancer: a critical review. *J Clin Oncol*. 2008;26:2568-81.
240. Atkinson RL, Yang WT, Rosen DG, Landis MD, Wong H, Lewis MT, et al. Cancer stem cell markers are enriched in normal tissue adjacent to triple negative breast cancer and inversely correlated with DNA repair deficiency. *Breast Cancer Res*. 2013;15:R77.
241. Meyer MJ, Fleming JM, Lin AF, Hussnain SA, Ginsburg E, Vonderhaar BK. CD44posCD49fhiCD133/2hi defines xenograft-initiating cells in estrogen receptor-negative breast cancer. *Cancer Res*. 2010;70:4624-33.
242. Fillmore CM, Kuperwasser C. Human breast cancer cell lines contain stem-like cells that self-renew, give rise to phenotypically diverse progeny and survive chemotherapy. *Breast Cancer Res*. 2008;10:R25.
243. Honeth G, Bendahl PO, Ringner M, Saal LH, Gruvberger-Saal SK, Lovgren K, et al. The CD44+/CD24- phenotype is enriched in basal-like breast tumors. *Breast Cancer Res*. 2008;10:R53.
244. Ricardo S, Vieira AF, Gerhard R, Leitao D, Pinto R, Cameselle-Teijeiro JF, et al. Breast cancer stem cell markers CD44, CD24 and ALDH1: expression distribution within intrinsic molecular subtype. *J Clin Pathol*. 2011;64:937-46.
245. So JY, Wahler J, Das Gupta S, Salerno DM, Maehr H, Uskokovic M, et al. HES1-mediated inhibition of Notch1 signaling by a Gemini vitamin D analog leads to decreased CD44(+)/CD24(-/low) tumor-initiating subpopulation in basal-like breast cancer. *J Steroid Biochem Mol Biol*. 2015;148:111-21.
246. Pastrana E, Silva-Vargas V, Doetsch F. Eyes wide open: a critical review of sphere-formation as an assay for stem cells. *Cell Stem Cell*. 2011;8:486-98.
247. Antoniou A, Hebrant A, Dom G, Dumont JE, Maenhaut C. Cancer stem cells, a fuzzy evolving concept: a cell population or a cell property? *Cell Cycle*. 2013;12:3743-8.
248. Meyer MJ, Fleming JM, Ali MA, Pesesky MW, Ginsburg E, Vonderhaar BK. Dynamic regulation of CD24 and the invasive, CD44posCD24neg phenotype in breast cancer cell lines. *Breast Cancer Res*. 2009;11:R82.
249. Wang D, Lu P, Zhang H, Luo M, Zhang X, Wei X, et al. Oct-4 and Nanog promote the epithelial-mesenchymal transition of breast cancer stem cells and are associated with poor prognosis in breast cancer patients. *Oncotarget*. 2014;5:10803-15.
250. Kaufmann M, Heider KH, Sinn HP, von Minckwitz G, Ponta H, Herrlich P. CD44 variant exon epitopes in primary breast cancer and length of survival. *Lancet*. 1995;345:615-9.
251. Liu CG, Lu Y, Wang BB, Zhang YJ, Zhang RS, Lu Y, et al. Clinical implications of stem cell gene Oct-4 expression in breast cancer. *Ann Surg*. 2011;253:1165-71.
252. Bourguignon LY, Peyrollier K, Xia W, Gilad E. Hyaluronan-CD44 interaction activates stem cell marker Nanog, Stat-3-mediated MDR1 gene expression, and ankyrin-regulated multidrug efflux in breast and ovarian tumor cells. *J Biol Chem*. 2008;283:17635-51.

253. Liu Y, Lv DL, Duan JJ, Xu SL, Zhang JF, Yang XJ, et al. ALDH1A1 expression correlates with clinicopathologic features and poor prognosis of breast cancer patients: a systematic review and meta-analysis. *BMC Cancer*. 2014;14:444.
254. Wu S, Xue W, Huang X, Yu X, Luo M, Huang Y, et al. Distinct prognostic values of ALDH1 isoenzymes in breast cancer. *Tumour Biol*. 2015;36:2421-6.
255. Charafe-Jauffret E, Ginestier C, Iovino F, Tarpin C, Diebel M, Esterni B, et al. Aldehyde dehydrogenase 1-positive cancer stem cells mediate metastasis and poor clinical outcome in inflammatory breast cancer. *Clin Cancer Res*. 2010;16:45-55.
256. Nguyen LV, Vanner R, Dirks P, Eaves CJ. Cancer stem cells: an evolving concept. *Nat Rev Cancer*. 2012;12:133-43.
257. Wahler J, So JY, Cheng LC, Maehr H, Uskokovic M, Suh N. Vitamin D compounds reduce mammosphere formation and decrease expression of putative stem cell markers in breast cancer. *J Steroid Biochem Mol Biol*. 2015;148:148-55.
258. Brown AJ, Slatopolsky E. Vitamin D analogs: therapeutic applications and mechanisms for selectivity. *Mol Aspects Med*. 2008;29:433-52.
259. Jogi A, Vaapil M, Johansson M, Pahlman S. Cancer cell differentiation heterogeneity and aggressive behavior in solid tumors. *Ups J Med Sci*. 2012;117:217-24.
260. Liu A, Yu X, Liu S. Pluripotency transcription factors and cancer stem cells: small genes make a big difference. *Chin J Cancer*. 2013;32:483-7.
261. Creighton CJ, Li X, Landis M, Dixon JM, Neumeister VM, Sjolund A, et al. Residual breast cancers after conventional therapy display mesenchymal as well as tumor-initiating features. *Proc Natl Acad Sci U S A*. 2009;106:13820-5.
262. Economopoulou P, Kaklamani VG, Siziopikou K. The role of cancer stem cells in breast cancer initiation and progression: potential cancer stem cell-directed therapies. *Oncologist*. 2012;17:1394-401.
263. Abraham BK, Fritz P, McClellan M, Hauptvogel P, Athelougou M, Brauch H. Prevalence of CD44+/CD24-/low cells in breast cancer may not be associated with clinical outcome but may favor distant metastasis. *Clin Cancer Res*. 2005;11:1154-9.